Vibrational spectroscopy as a powerful tool for stratifying patients using minimal amounts of blood

Dissertation

zur Erlangung des akademischen Grades doctor rerum naturalium (Dr. rer. nat)

vorgelegt dem Rat der Chemisch-Geowissenschaftlichen Fakultät

der Friedrich-Schiller-Universität Jena von

M.S.-Optics Jing Huang

geboren am 04.03.1990 in Guangdong, China

Gutachter:

1. Prof. Dr. Jürgen Popp
2. Prof. Dr. Ute Neugebauer

Tag der Verteidigung: den 08.01.2020

Selbstständigkeitserklärung

Ich erkläre, dass ich die vorliegende Arbeit selbstständig und unter Verwendung der angegebenen Hilfsmittel, persönlichen Mitteilungen und Quellen angefertigt habe.

Jena, den 25.07.2019 Jing Huang

Erklärung gemäß § 5 (1) Punkt 3 der Promotionsordnung der Chemisch-Geowissenschaftlichen Fakultät

Erklärung

Ich erkläre,

dass mir die geltende Promotionsordnung der Fakultät bekannt ist;

dass ich die Dissertation selbst angefertigt, keine Textabschnitte eines Dritten oder eigener Prüfungsarbeiten ohne Kennzeichnung übernommen und alle von mir benutzten Hilfsmittel, persönlichen Mitteilungen und Quellen in meiner Arbeit angegeben habe;

dass mich ausschließlich die folgenden Personen bei der Auswahl und Auswertung des Materials sowie bei der Herstellung des Manuskripts unterstützt haben: Dr. Anuradha Ramoji, Prof. Dr. Ute Neugebauer, Prof. Dr. Jürgen Popp.

dass die Hilfe einer kommerziellen Promotionsvermittlung nicht in Anspruch genommen wurde und dass Dritte weder unmittelbar noch mittelbar geldwerte Leistungen von mir für Arbeiten erhalten haben, die im Zusammenhang mit dem Inhalt der vorgelegten Dissertation stehen;

dass ich die Dissertation noch nicht als Prüfungsarbeit für eine staatliche oder andere wissenschaftliche Prüfung eingereicht habe;

dass ich nicht die gleiche, eine in wesentlichen Teilen ähnliche oder eine andere Abhandlung bei einer anderen Hochschule als Dissertation eingereicht habe.

Jena, den 25.07.2019 Jing Huang

Abbreviations

AS	after surgery
BMI	body mass index
BS	before surgery
CABG	coronary artery bypass grafting
CAD	coronary artery disease
CCD	charge-coupled device
CRP	C-reactive protein
CV	cross-validation
CVD	cardiovascular disease
DCDR	drop coating deposition Raman
DCM	dilated cardiomyopathy
DM	diabetes mellitus
EDTA	Ethylenediaminetetraacetic acid
FPA	focal plane array
FPG	fasting plasma glucose
FT-IR	Fourier transform infrared
GA	glycated albumin
HbA1c	glycated haemoglobin
HF	heart failure
HLM	heart-lung machine
HPLC	high performance liquid chromatography
IA	immunoadsorption
IgG	immunoglobulin G
IL6	interleukin 6
LDA	linear discriminant analysis
LVEF	left ventricular ejection fraction
MCT	mercury cadmium telluride
MLR	monocytes to lymphocytes ratio
NLR	neutrophils to lymphocytes ratio
OGTT	oral glucose tolerance test
PBS	phosphate buffered saline
PC	principal component
PCA	principal component analysis

PCT	procalcitonin
PLR	platelets to lymphocytes ratio
PLSR	partial least squares regression
RBC	red blood cells
RMSEP	root mean squared error of prediction
RT	room temperature
SOP	standard operating procedure
SVM	support vector machine
TTC	Takotsubo cardiomyopathy
WBC	white blood cell
2h-PG	2h plasma glucose

Contents

List of figures

List of tables

Abstract

In 2017, it was reported that a number of 962 million people were 60 years old or older globally. In other words, nowadays we are already facing an aging society. The increase aging population will bring an increase number for those age-related body disorders which result from lifelong molecular and cellular impairments. Common age-related body disorders are cardiovascular disease, cancer, diabetes mellitus and chronic respiratory disease. In addition, aging people are easier to suffer multimorbidity, for example, 10% cardiovascular disease is reported to be caused by diabetes mellitus. Multimorbidity brings more difficulties to treat the aging people more properly and effectively. Besides, clinicians have realized that the response of different patients to the same medical treatment can differ. Above all, individual characterisation of one's unique condition is in higher demanded than ever before. Personalized medicine, an emerging and rapidly developing field beneficial from human Genome project, is potential to offer a molecular or genomic diagnosis and to realise early disease detection, targeted disease prevention, accelerated diagnosis, and targeted therapies. Personalized medicine crucially depends on the identification of biomarkers and the development of accurate and reliable diagnostics. Those advanced diagnostic approaches to provide rapid and accurate information on genetic or molecular scale are in particularly high demanded. Pathological variations are always accompanied by biochemical changes from cells, body fluids, or tissues. Vibrational spectroscopy, including Raman spectroscopy and Fourier transform infrared spectroscopy, is one of the favourite techniques being developed for personalized medicine. It owes advantages of non-destructive, rapid, label-free, high-throughput and biochemical fingerprint on molecular level. Therefore, these techniques can ideally capture the biochemical changes, especially when they are applied together. Among the samples measured by vibrational spectroscopy, body fluids are very popular due to its easy accessibility with minimal invasiveness. In particular, blood and its components are the most frequently studied samples for disease diagnostics since they can be easily obtained repeatedly. However, blood is such a complex body fluid that improper sample preparation can degrade its quality for clinical purpose. Thus, it is rather challenging to find a proper and reproducible sample preparation approach when employing vibrational spectroscopy to study blood specimen. Drop coating deposition method is one candidate to prepare blood-based samples with high quality and minimal amount. However, the redistribution of plasma proteins in the prepared droplet samples and superior measurement schematics to collect vibrational spectra for biomedical application remains as open issues. Moreover, to pave the way of vibrational spectroscopy into daily medical application, the robustness of vibrational spectroscopic analysis using minimal amounts of blood to stratify patients from different disorder cohorts still needs to be proved.

In this thesis, the aforementioned challenging issues are addressed and detailed solutions are presented, including (1) quality check and drop coating deposition method by using blood sample for spectroscopic analysis; (2) application of vibrational spectroscopy to diagnose and follow-up treatment of cardiac diseases; (3) applying Raman spectroscopy to characterize glycated haemoglobin in diabetes mellitus for diagnostics. These investigated issues involve different specific topics: (1) time delays between blood collection and centrifugation are often

unavoidable. During the different time delays, blood can undergo different changes which influence its quality and limit its clinical application. Hence, a quality check of blood specimen to investigate the spectral changes of studied samples is conducted. This study should give hints which time delays are still acceptable for reliable and reproducible subsequent spectroscopic analysis. (2) By drop coating deposition the plasma or serum sample onto Raman- or IR-free substrate, the biomolecules will be pre-concentrated at different regions due to coffee-ring effect. Understanding of plasma protein distribution in the droplet remains unclear, and study on superior measurement schematics for vibrational spectra in biomedical applications is in demanded. After figure out the issues on quality check of blood sample and the appropriate spectroscopic measurement protocol, clinical applications will be discussed in the following sections. (3) Mechanisms of various cardiac diseases are in variety, resulting in different approaches to detect the cardiac conditions and in need of versatile treatment strategies. There is room and need to investigate the differentiation of different cardiac diseases, and to study the differences between cardiac condition and healthy condition. After characterization of different cardiac disorders, two studies of different treatments corresponding to different cardiac disorder will be introduced and discussed subsequently, including immunoadsorption therapy and coronary artery bypass surgery. (4) Immunoadsorption therapy is a therapy to treat the patients who are suffering from dilated cardiomyopathy. This therapy improves left ventricular ejection fraction by substituting the original anti-cardiac antibodies with pooled immunoglobulin G. Vibrational spectroscopy is used to interpret longitudinal changes according to immunoadsorption therapy. (5) Coronary artery bypass surgery is one of the preferred procedures to restore normal blood flow to an obstructed coronary artery. This surgery can cause an inflammatory response in the patient, especially when perform with heart-lung-machine. In this context, vibrational spectra from plasma samples before and after the surgery are investigated. (6) Finally, the biomedical focus will move to the characterization of glycated haemoglobin using Raman spectroscopy. Glycated haemoglobin, a non-enzymatic glycosylation of haemoglobin product, reflects an average blood glucose level for last 120 days and becomes one of the common diagnostic methods for diabetes mellitus. Raman spectroscopy is applied to characterize glycated haemoglobin, particularly to investigate glycated haemoglobin value on single red blood cell level.

Key words: vibrational spectroscopy, blood, personalized medicine, biomedical application, cardiac disease, diabetes mellitus, chemometrics

1 Introduction

1.1 Medical need

Nowadays, we are already facing the aging society. According to the World Report on Aging and Health released by World Health Organization in 2015, the number of people aged 60 or older will rise from 12% in 2015 to 22% in 2050 globally. [1] Aging accompanies with different impairments in many body functions which are caused by molecular and cellular damage along lifelong time. Thus, the aging people hold high potential to risk disease and death, especially to experience age-related chronic diseases. In another report from World Health Organization "World health statistics 2016: monitoring health for the sustainable development goals" [2], about 68% mortality was resulted from non-communicable death, with the number of 38 million deaths per year in 2012. Over three quarters of this global premature mortality is contributed from cardiovascular disease (CVD), cancer, diabetes mellitus (DM) and chronic respiratory disease. Premature mortality refers to death at the age under 70 years old. CVD caused 17.5 million deaths in 2012 - 6 million of them were under age 70, while diabetes lead to 1.5 million deaths - 43% of them occurred under the age of 70. [3] Study has shown that between 1990 and 2013, the growth of aging and population resulted in a higher global cardiovascular mortality. [4] What even worse, as the people are growing older and older, they are easier and higher possible to suffer multi-morbidity - which means experiencing multiple (chronic) diseases simultaneously. For example, DM is a common risk factor for CVD, causing about 10% CVD. Besides the chronic unhealth condition of the aging society, the economic burden on those more age-related diseases are huge. The global cost of CVD in 2010 was 863 billion US dollars, and the cost has estimated to be 1,044 billion US dollars in 2030. [5] DM directly costs 827 billion US dollars annually, it has estimated to loss 1.7 trillion US dollars in GDP worldwide from 2010 to 2030. [3]

When the patients under the same condition are diagnosed as the same disease, they are more likely to be given the same treatment, but the clinicians have found that different patients can respond differently to the same medical intervention. The efficiency of the same treatment on the patients with the same condition can be only 30 - 60% [6]. For example, about 40% cardiac arrhythmias patients will not benefit from the cardiac arrhythmias drugs and approximately 43% in the case of diabetes patients. [7] This is easy to understand, our health is determined by many factors, like our genes, our lifestyles, and even other environmental factors. In other words, we are all unique. To better identify our healthy patterns, personalized medicine will be more superior for the symptom driven broad diagnosis. Personalized medicine is a field flourished from the human Genome project [8] , which is advancing rapidly with individual characterisation of underlying cause (a person's unique genetic, genomic, environmental, and clinical information) [9]. So far, personalized medicine has gained higher and higher global attention for its potential benefits including early disease detection, targeted disease prevention, accelerated diagnosis, and targeted therapies. Personalized medicine helps to improve clinical outcome and decrease the side-effect of inappropriate treatment. Health systems in many different countries like US, Germany, Canada, Austria, China, France and India are now working on policies and research projects to support and adopt the personalized medicine into their health care system.

Personalized medicine is able to detect or diagnose the disease at an early stage even before the onset of the symptoms. The early detection has high potential to reduce the growing burden of disease, to improve the outcomes for patients and our population, especially for the abovementioned long term disorders such as CVD and DM. The success of personalized medicine crucially depends on the identification of biomarkers and the development of accurate and reliable diagnostics. [10] There is space and demand to study advanced diagnostic methods which can help to diagnose more precisely with genetic or molecular information. Among the numerous promising diagnostic and therapeutic approaches, biophotonics is expected to play the leading role. [10] Biophotonics investigates the interaction between incident light and biological sample, and is an emerging and rapidly developing multidisciplinary research field. By employing light technique, the structures and functions on cellular or molecular level can be explored rapidly and noninvasively with utmost sensitivity and precision. These advantages make biophotonics a unique tool to understand disease on molecular level, recognise disease at early stage, target treatment of diseases and prevent disease [10]. Among the various biophotonics techniques, vibrational spectroscopy including Raman spectroscopy and Fourier transform infrared (FT-IR) spectroscopy is one of the favourite choices due to its non-destructive, rapid, label-free, and biochemical features, which will be discussed in more details later.

1.2 Motivation

Vibrational spectroscopy has high ability and possibility to monitor the biomolecule compositions and variations from samples, it holds potential to diagnose pathologies rapidly at an early stage. However, when investigating the potential of vibrational spectroscopy for diseases detection using blood samples, following issues are needed to obtain further understanding.

(1) Quality check of blood specimen

Blood, referred as 'liquid organ', is a complex biological specimen which contains many types of components with very dynamic range properties. [11] Since blood distributes through the whole body, it exhibits a wide variety of functions and reflects the real physiological condition. Blood is mainly divided into two parts - blood cells and blood plasma, for more details please refer to Section 1.3. These two parts can be separated by centrifugation according to their different physical chemistry properties. Due to its accessibility and complexity, blood is a widely used specimen for clinical study. Since the last decades, there have been a lot of studies about biomarker discovery based on plasma or serum proteomics [12-17], also based on plasma or serum metabolomics [18-20]. Blood plasma or blood serum compromise of various biomolecules such as peptides, amino acids, lipids, proteases, enzymes, cytokines, low molecular weight metabolites, electrolytes etc. When there is physiological misregulation with the presence of disease, the biomolecular variation will transit to the circulating bloodstream, then retain in blood plasma or blood serum. Thus by hunting for the biomarkers in plasma or serum, it is able to detect the disease. However, there remain challenges in biomarker discovery based on plasma or serum: (1) inherent biological variability; (2) the plasma proteomics has a large dynamic range of protein concentrations,

covering at least 10 orders from mg/ml to pg/ml; (3) plasma metabolomics is mainly interested in low-molecular weight compounds (molecular weight $< 1{,}500\ Da$) [21], without any processing in sample preparation, the metabolomics is dominated by the abundant plasma proteins including albumin, immunoglobulin, etc; (4) the variability in pre-analytic and analytic processes, including the blood collection tubes, the time delay between blood collection and centrifugation, storage temperature, storage time, the frozen-thaw circles and so on.

To minimize the aforementioned challenges, especially those non-intrinsic artefacts such as pre-analytical variables, it is necessary to follow the standard operating procedure (SOP) to obtain high quality and reproducible samples. However there are different SOPs recommended for blood specimen preparation, and the importance of pre-analytical variables still remain in questions. The use of improper blood collection tubes will affect the subsequent searching of biomarkers. The blood can be collected as anti-coagulated plasma or coagulated serum. For anti-coagulated plasma, different anti-coagulants mechanisms need to be considered to prevent blood clot. Ethylenediaminetetraacetic acid (EDTA) is an aminopolycarboxylic acid and chelates metal ions like $Ca2^{+}$, $Mg2^{+}$. EDTA blood is not a good choice for the measurement in which divalent cations are necessary. Citrate is in liquid form and will dilute the collected sample, it can bind $Ca2^{+}$ in a non-dissociation form. Citrate blood has shown artefacts for immunoassay measurements. Heparin, a sulphated glycosaminoglycan which binds to antitrombin III and accelerates the inactivation of thrombin and other clotting factors, can interference in some affinity processes. [22-25] After blood collection, in order to have high quality specimen, serum need time to clot properly while plasma can be centrifuged immediately. However, in reality it is often and easy to have a time delay between blood collection and blood centrifugation. This can be due to the geographic distance between the clinic and the blood processing facilities, the busy of laboratory equipment and centrifuge. Such pre-analytical issues will influence the quality of blood specimen, studies about the pre-analytical issues and the quality of blood specimen can be found in Ref [21-23, 25-34].

In clinic reality, many pre-analytical issues such as blood collection tubes, storage temperature are fixed, but the time delay between blood collection and centrifugation is very easy to be varied. It is common to keep the blood for up to 4 hours for further processing in clinical lab [31]. But during this prolong storage time, especially at room temperature, the intrinsic biochemical process of blood continue going, including enzymatic proteolysis and erythrocyte activity. The former endogenous proteolytic activity will cause proteins to experience degradation, while the latter alters the blood metabolome that are reflected in subsequent plasma and serum profiles. [25, 33, 35]

For clinical studies, we had collaboration with the physicians; they collected the blood from the patients and then transferred the blood to us. After we received the blood from the doctors, the blood was centrifuged according to our SOP immediately once the devices were applicable, or the blood was delayed no more than 2 hours to be centrifuged. Issues about how long can the blood delay to be centrifuged, and how stable can the blood be after certain time delay are essential to be investigated to have high quality specimen.

When using specific metrology for clinical application, the study of quality and stability of blood specimen is critical. Since the last decades, when combining the dried droplet of plasma or serum with Raman spectroscopy, there have been lots of researches about biomolecular changes from blood plasma or serum for diagnostic purposes. The technique with the name of drop coating deposition Raman (DCDR) spectroscopy was first put forward by Dongmao Zhang. [36] This technique is able to improve the detection sensitivity more than 1000 times beneficial from the pre-concentration of biomolecules. Since then, this technique has been widely investigated, especially for the biomedical application. So far, there is no study on the stability of DCDR regarding the time delay between blood collection and blood centrifugation. Thus, the investigation of Raman spectroscopy for the quality check of blood specimen about the delay between blood collection and blood centrifugation is conducted.

(2) Vibrational spectroscopic investigation of blood plasma and serum by drop coating deposition for clinical application

When a drop of body fluids, e.g. blood plasma, or blood serum, is placed on a solid substrate and allowed for drying, an interesting phenomenon called 'coffee-ring effect' will show up with ring-shape deposited at the edge of the dried droplet. Several conditions are required to form the coffee-ring effect: self-pinning of liquid-substrate contact line, higher evaporation rate at the contact line, and suppression of Marangoni flow. [37] In short words, when a drop of biological liquid is placed on a solid slide, the enhance evaporation rate at the pinned liquid–substrate contact line will induce an outward capillary flow in liquid, this outward capillary flow carries the suspended molecules from the interior to the edge. [38-40] While the droplet is evaporating, the temperature gradient along the surface of the drying droplet will lead to a surface-tension gradient which will induce thermal Marangoni flow. The Marangoni flow carries particles on the surface of the droplet inward toward the top of the droplet, and then plunges the particles downward to be absorbed on the substrates near the centre of the droplet or to be carried along the substrates to the edge causing a circular movement along the drop-air interface of the droplet. [41, 42] After drying, the droplet will have an inhomogeneous redistribution with most molecules concentrated at the edge as the co-result of coffee-ring effect and suppression of thermal Marangoni effect.

The drying process can form cracking patterns on the final dried droplet. During drying process, a particle film will be formed on the top layer of the droplet, and the substrate constraints will increase tensile stress in the drying droplet. The cracking patterns are caused by the mismatch between the horizontal shrinkage of the particle film and the substrate constraints. When the increased tensile stress exceeds the tensile strength at some locations of the film, cracks will occur to release the stress. Since most suspended particles in blood plasma and serum are soft, they can delay the occurrence of cracking by absorb more stress and reduce the evaporation rate. [37]

After deposition of plasma or serum on a wettable solid slide, most protein molecules will be driven toward the contact line and concentrated at the edge, while the high soluble inorganic electrolytes and maybe some proteins will be located towards the centre of the droplet. In the centre of the droplet, crystal patterns will be formed.

It has been a long time to investigate biomolecular changes caused by disease in dried droplet of plasma or serum. These changes are able to be utilized for diagnostic purposes, especially when combining the droplets with vibrational spectroscopic techniques like Raman spectroscopy and FT-IR spectroscopy which extract biochemical information of samples in a non-invasive and rapid way. By drop coating deposition method, the interference of solvents can be reduced or avoided to certain extent. Besides, the volume of sample preparation needs only few nanoliter, and the proteins in the sample will be pre-concentrated and segregated. These are especially advantageous for body fluids samples.

Even though there are many studies on the investigation of disease by the combination of vibrational spectroscopy and drop coating deposition method, many challenges are remained to be solved. One challenge is to reduce the droplet size, this can be achieved by robotic method via standard laboratory technique. Another challenge is to choose appropriate measurement positions better representing the whole droplet instead of measuring the big whole droplet which will be very time-consuming.

So far, many studies on the drop coating deposition combined with vibrational spectroscopy are for the disease diagnosis, or directly biomedical application. But there are request to understand the distribution of plasma proteins in the dried droplet, the superior measurement schematics for biomedical application. In this thesis, I study the locations of the most abundant albumin and immunoglobulin G (IgG) in the plasma and serum droplet, the difference between inner and outer region in the plasma or serum droplet, and the superior measurement schematics for biomedical application. To our knowledge, this is the first study to investigate the abovementioned issues.

(3) Vibrational spectroscopic differentiation of patients suffering from various cardiac diseases

Nowadays, we are already facing the aging society. The aging population will accompany a lot of health problems, especially of chronic diseases which result from molecular and cellular damage through lifelong time. In those disease conditions, CVD is the number one cause of mortality. Even worse, the death caused by CVD will rise with respect to aging, this is supported by the study of Roth and his colleagues [4]. In their study, they tried to find out the relationship between the three principal drivers (population growth, population aging, and epidemiologic changes) and global cardiovascular mortality by using the data from 1990 to 2013. Their results suggested that even though there was an overall decrease in age-specific mortality in most regions between 1990 and 2013, the population aging and population growth resulted in an increase in global CVD mortality. Aging attributed about 55% increase for this increase from 1990 while population growth contributed for 25.1% increase. Due to the high mortality of CVD, it has attracted our attentions to reduce the corresponding death. For example, United Nations has set a goal to reduce 25% premature mortality due to CVD by 2025. [43, 44]

CVD has been recognized and investigated for a long time, and the disciplinary called cardiovascular science or cardiology has been formed. Modern cardiology is considered to

begin based on the discovery of blood circulation by William Harvey in the early 17th century. Thereafter, the descriptive anatomy and pathology, auscultation, pathophysiology for CVD have been pursued for centuries. Since the advent of cardiac catheterization and surgery in 1950s, cardiology has become more complex and has been expanded into multiple higher specialized subdisciplines including coronary artery disease (CAD), arrhythmias, HF and preventive care [45]. For 21st century, incredible tools for diagnosis and treatment of heart disease have been advanced. [45] These advanced diagnosis tools mainly benefit from the understanding of blood biomarkers; multiple imaging modalities with higher sensitivity and higher spatial and temporal resolution. The treatments have been improved with further investigation of pharmacogenomics profiling, biological molecules, bionic heart, genomic discoveries and stem-cell therapy [45-49]. Thanks to the scientific advances on cardiovascular medicine including early diagnosis of cardiac risk, improved medical treatment for cardiac diseases, and also the increasing consensus of prevention, a large number of CVD has been prevented successfully thus reducing the mortality of CVD [4, 46, 50-52].

The term CVD is quite large. It is a class of diseases not only from the heart, but also contain vascular disease of the brain and the diseases from blood vessels [50]. CVD involves not only various underlying mechanisms and complex genetic factors for pathogenies, but also certain risk-factors. The variety makes some persons more prone to develop certain CVD conditions, while some will not benefit from the same treatment given to those with similar clinical presentations. It has been reported that only 30-60% efficiency of the same treatment works for the patients with the same condition. [6]

For the variety of CVD, some disorders (myocarditis, dilated cardiomyopathy (DCM), Takotsubo cardiomyopathy (TTC), and heart failure (HF)) are explained here as medical background for our patient cohorts.

Myocarditis, also known as inflammatory cardiomyopathy, is characterized as inflammatory cellular infiltrate associated with cardiac dysfunction. [53-55] Even though it is still unclear about the true incidence of myocarditis [54], acute myocarditis has been reported to have a slight prone in male than in female [56-58], which can be resulted from the protective effect of natural hormone changes on the immune responses in female [59]. Myocarditis has versatile symptoms, ranging from mild dyspnea or chest pain to cardiogenic shock and death. Also the pathogens for myocarditis are various, including viral infections in most cases, toxic or hypersensitivity drug reactions, giant-cell myocarditis, and sarcoidosis. According to the studies of virus-induced autoimmune myocarditis based on rodent models and isolated cell systems, detailed knowledge has been discovered. [54, 55] Viruses enter cardiac myocytes or macrophages through specific receptors and coreceptors, and then the innate immune system will be activated for host defence. Over weeks, adaptive immunity which is mediated by T lymphocytes and antibodies will be triggered directly against the viral pathogens. The endogenous heart epitopes will cause robust inflammation. In the early stage of viral infection, it can be accompanied by immunoglobulin M antiviral antibodies, these antibodies can change to persistent antiviral IgG antibodies in the subsequent sub-acute and chronic phases. [55] Most patients undergo viral elimination and down-regulation of the immune reaction with few permanently detrimental to the heart; while other patients can not clear the

virus pathogens thus cause persistent myocyte damage with long-term sequelaes such as DCM with chronic heart failure symdroms. Myocarditis can be diagnosed via endomyocardial biopsy invasively, and via cardiac magnetic resonance noninvasively. Besides, electrocardiogram and the increased value of cardiac troponin I can also be used as diagnostic choices. Myocarditis can adopt conventional HF therapies and sudden cardiac death prevention to improve left ventricular dysfunction. Moreover, with the advances on immune-related research, different immunomodulatory treatment can be considered as treatment approaches. These immunomodulatory approaches include immunosuppression, intravenous Ig treatment, antiviral immunomodulation with interferon, last but not least immunoadsorption (IA).

DCM, one sequelae of myocarditis as aforementioned [54, 55], is the most common cardiomyopathy. DCM is characterized by dilation and contraction dysfunction of the left or both ventricles with normal left vertricular wall thickness, but without the occurrence of abnormal loading conditions and severe coronary artery disease [60-63]. This disorder can develop at any age without preference of gender and ethnic origin [60]. But it occurs more commonly in male adult than in female adult [60]. DCM is one of the most frequent causes of HF and the most common cause for heart transplantation, [55, 60-62, 64] which has high possibility for hospital admission and will result in large cost burden. It often fails to figure out the specific etiology for DCM, since DCM is common to be diagnosed at the end-stage. The pathologies for DCM are with a variety of primary and secondary causes. These causes include infectious agents, bacterial, fungal rickettsial, mycobacterial, parasitic, toxins, excessive alcohol, autoimmune and systemic disorders etc. Among them, postviral autoimmunity is expected to play a vital role [65] with the production of anti-cardiac antibodies resulting from activation of the humoral immune system. Regarding DCM, so far a number of autoantibodies which against cardiac structures have been identified [55, 66-68]. Imaging strategies such as echocardiography, electrocardiography and coronary angiography are applied to diagnose DCM, other diagnostic methods include viral serology and endomyocardial biopsy. Similar to myocarditis, DCM can be alleviated by the conventional HF treatments in medical or surgical way, also by immunomodulatory therapies.

Unlike the most common cardiomyopathy - DCM, TTC is quite new and was initially reported by Sato in Japan in 1990. [69, 70] TTC is characterized by transient systolic and diastolic left ventricular dysfunction, involving left ventricular apex and/or mid-ventricle in the absence of blocked coronary artery disease. [62, 63, 70] TTC has an unusual shape for the left ventricle with a narrow upper portion but a lower enlarged portion, this shape resembles the Japanese ceramic trap for octopus, this is where the name from. [69, 70] This disorder, also named as stress cardiomyopathy, is most likely (85%) to be triggered by emotional or physical stress [69], maybe with a prevalence of physical triggers over the emotional triggers [71]. TTC includes predominant clinical symptoms such as chest pain, dyspnea and syncope, but also with less common pulmonary edema [69, 70] and mild enzyme elevation [63]. Most takotsubo events are reversible, and can be recovered rapidly within days or weeks. The mechanisms for this disorder remain unclear, but are suggested to be caused by multivessel epicardial coronary artery spasm, microcirculation dysfunction, obstruction of the left ventricular outflow tract, catecholamine cardiotoxicity and metabolic disturbance. [72, 73]

Besides, TTC has been reported with a prevalence in female, especially for post-menopausal women [72, 73], suggesting the facilitating role of estrogen deprivation mediated by endothelial dysfunction. So far, there are not worldwide diagnostic criteria for TTC, several diagnostic criteria have been proposed where Mayo Clinic criteria is the most commonly used one. [70] Briefly, treatments of myocardial ischemia should be managed based on the initial acute MI- like presentation. After confirmation of TTC, subsequent treatments will be determined by the complications during the acute phase. The subsequent treatments include intravenous fluids and inotropic agents for shock, and standard HF therapies with diuretics or nitroglycerin. [69, 70]

Heart failure (HF) is a syndrome rather than disease in which the heart cannot supply enough blood to the body. HF can result from structural or functional cardiac abnormalities with various symptoms (e.g. fatigue, breathlessness) and signs (e.g. pulmonary crackles, peripheral oedema). [48, 74, 75] HF is usually classified into two classes based on the contract ability of the left ventricle - HF with reduced left ventricular ejection fraction (LVEF) (≤40%) or HF with preserved ventricular ejection fraction (≥50%). Another important distinction between chronic and acute HF is that acute HF requires urgent diagnosis and management and followed by unscheduled hospital admission [75]. Several pathogenic mechanisms have been discovered for HF: hemodynamic overload for reduction in intrinsic contractility of cardiac muscle, ventricular remodeling, inadequate or excessive proliferation of the extracellular matrix, ischemia-related dysfunction, overload neurohumoral stimulation, unusual myocyte calcium cycling, accelerated apoptosis and genetic mutations. [48, 74] With the help of biomarkers, it is easier to identify the pathogenesis of HF, estimate prognosis and choose proper therapy, especially when utilizing multiple biomarkers simultaneously. These HF biomarkers include myocyte stretch markers such as brain natriuretic peptide and soluble ST2 cardiac biomarker, myocyte injury markers such as cardiac troponin I and cardiac troponin T, extracellular matrix remodeling markers such as collagen propeptides, inflammation markers such as C-reactive protein (CRP) and interleukin 6 (IL6), oxidative stress markers such as oxidized low-density lipoproteins, neurohormones marker such as angiotensin II and norepinephrine, and new markers such as galectin 3 and adiponectin. [76, 77] Treatment of acute HF has gentle changes with the focus on haemodynamics in the past decade, where chronic condition has been the prime target in new research. These therapies include but not limit to positive inotropic agents, pharmacologic treatment, stem cell therapy, cardiac remodeling and recovery, and gene therapy.

CVD has a broad range, the pathogenesis and therapy managements are various. More efforts are needed to reveal the unclear mechanisms and to propose more advanced and effective therapies. Vibrational spectroscopy, as a robust technique for clinical study, holds the potential to uncover the remaining mystery of CVD.

(4) Immunoadsorption therapy follow-up for dilated cardiomyopathy using vibrational spectroscopic methods

As abovementioned, DCM is the most common cardiomyopathy, which is defined by left chamber enlargement and left ventricular dysfunction without the presence of abnormal

loading conditions like coronary artery disease [62, 63, 78]. DCM has prevalence in male than in female, and is the number one cause for heart transplantation. [55, 64] As DCM progressed, it is often diagnosed at the end-stage without the ability to find out the specific pathology. [78] The etiology of DCM is of a variety and has not been fully understood, a lot of studies are still undergoing investigation to find out the underlying physiopathology. DCM is considered as 'mixed' cardiomyopathy, including genetic and acquired causes. [62] A familial form of up to 30% is recognized in DCM patients, suggesting a genetic basic cause for this cardiac disorder. The acquired causes for DCM phenotype are various, including the followings: infectious agents, such as viruses, bacteria, fungi, parasite; toxins, e.g. alcohol; as well as autoimmune and systemic disorders. [55, 62, 63, 78, 79] Among the various acquired causes, post-viral autoimmunity is suggested to play a critical role. [65] Furthermore, anti-cardiac antibodies are also supposed to play an important role in DCM by activating the humoral immune system. According to literatures, a number of autoantibodies against different cardiac structures have been identified [55, 66-68]; these autoantibodies include Ig against G-protein-linked receptors, troponin I, cardiac ß-1 receptors and cardiac myosin. Studies have shown that anti-cardiac antibodies belong to IgG 3 subclass and can be eliminated by IA therapy. [66-68, 80-82] However, the functional significance of these anti-cardiac autoantibodies is not clear yet and is still under debate. Symptoms related to chronic HF, i.e. dyspnea, angina, pulmonary congestion, fatigue, systolic and diastolic dysfunction and peripheral oedema may be observed in DCM patients. Additionally, DCM patients may also accompany with the complications including arrhythmias, sudden cardiac death and thromboembolic events. Before diagnosis, the history of DCM patients should be acquired, including risk factors for CAD. [9]

DCM can be characterized via different medical imaging approaches, including (two-dimensional) echocardiography, electrocardiography, and coronary angiography. Besides, viral serology and endomyocardial biopsy are also often applied to diagnose DCM. Since DCM shares the symptoms of HF, HF managements are adopted to treat DCM disorder. The HF treatments involve medical methods such as angiotensin-converting-enzyme inhibitor and ß-blocks to decrease the risk for sudden cardiac death, and surgical approaches by inserting continuous-flow pumps, assist devices or undergoing heart transplantation as the last choice. [55, 68] Apart from the HF treatments mentioned above, immunomodulatory therapies have been studied. IA therapy removes the anti-cardiac autoantibodies by removing IgG, and has shown potential to improve the heart function of DCM patients, even alleviate myocardial inflammation in some cases of DCM-induced HF. In general, IA depletes anti-cardiac antibodies from the patients' plasma, without [83] or with [66, 67, 80, 81] the substitution of IgG after the removal. In consideration of infection, IgG will be substituted after IA to restore the IgG plasma levels. IA therapy is usually under 1 course at 5 consecutive days. [81] After this 5-day treatment, fresh IgG will be substituted. [82] IA holds the potential to improve the function of LVEF and decrease cardiac biomarkers of HF and cardiac congestion such as natriuretic peptides [76, 80]. The improvements of IA on HF symptoms and LVEF can last for up to 2.5 years [55], however the mechanism of IA for DCM management is still under investigation and need to be elucidated further.

One ultimate and vital goal in clinical study is to realize diagnosis and to assess the efficacy of treatment at an early stage. Clinical vibrational spectroscopy, comprising of Raman spectroscopy and FT-IR spectroscopy, provides overall chemical information based on different samples e.g. body fluids, tissues and cells in a non-invasive and label-free approach, hence has high possibility for clinical application. [84-86] Sample preparation for vibrational spectroscopy is minimal, therefore the blood samples can be directly applied to clinical diagnosis [87]. Spectral data is often huge, thus chemometric methods comprising preprocessing and multivariate analysis are applied to interpret more valuable information [88, 89]. Vibrational spectroscopy holds high possibility to study and characterize molecular changes directly from the patients' blood samples in a simple, rapid and non-invasive manner, which makes it applicable for early diagnosis purposes [90-96]. This study is aim to investigate the potential of vibrational spectroscopy as a promising method to follow up the changes in blood plasma and serum according to IA treatment. For references, abundant plasma proteins as pure albumin and pure IgG were recorded as well.

(5) Influence of coronary artery bypass grafting on spectroscopic signature of leukocytes and plasma

Among various CVD, the most common one is coronary artery disease (CAD), also known as ischemic heart disease. It may affect at any age, but has a preference at older ages. In CAD, since there is build-up of plaque in the arteries of the heart, the coronary arteries will be narrowed; the blood flow to the heart muscle will be highly reduced. CAD may accompany with signs or symptoms of chest pain, shortness of breath, and heart attack. The view of CAD has changed from a cholesterol storage disease into an inflammatory disorder since last decades. [97, 98] Plaque or cholesterol-containing deposits and inflammation are thought to be the most common causative for CAD. When bacterial products or risk factors contact the arterial endothelium, these arterial endothelium cells will increase the expression of adhesion molecules which help to stick the blood leukocytes to the arterial intima. After resident in the inner surface of the arterial wall, the activated macrophages, T cells, and mast cells communicate with endothelial and smooth muscle cells, producing molecules which can destabilize lesions. These molecules comprise inflammatory cytokines, coagulation factors, proteases, vasoactive molecules, and radicals. They restrain stable fibrous caps formation, attack collagen in the cap, and restrain thrombus formation. Thus result in the activation and rupture of plaque, thrombosis, and ischemia. The atherosclerotic plaque can be treated via medications and surgeries. The former consists of cholesterol lowering medications, ß-blockers, nitroglycerin, while the latter includes coronary artery bypass grafting (CABG), coronary stent and angioplasty.

CABG is a surgical procedure to restore normal blood flow to an obstructed coronary artery by grafting bypass coronary arteries with autologous arteries or veins. There are two main used bypass conduits, left internal thoracic artery and the greater saphenous vein. Left internal thoracic artery is grafted to the left anterior descending branch of the left coronary artery, while saphenous-vein grafts are obtained from thigh through small incisions. [99] CABG can be performed via on-pump where cardiac arrest is needed and the cardiopulmonary bypass mimics the function of heart and lungs, or via off-pump where the heart is still beating

without the use of HLM. However, cardiopulmonary bypass is believed to cause a complex systemic inflammatory response, resulting in postoperative morbidity such as neuropsychological impairment, renal complications etc. [99, 100] Thus, off-pump was introduced to reduce postoperative complications in accordance to the use of cardiopulmonary bypass. [100-105]

In this study, patients undergoing on-pump and off-pump were included. We try to characterize changes within the plasma and white blood cells (performed by my colleague) as a result of CABG via vibrational spectroscopy.

(6) Raman spectroscopy for characterizing glycated haemoglobin in diabetes mellitus

Diabetes mellitus (DM) is a group of metabolic disorder characterized by hyperglycemia. The chronic hyperglycemia disorder is often associated with long-term complications including different organ failures such as eyes, nerves, heart, kidneys, and blood vessels. Symptoms of polyuria, weight loss, polydipsia, blurred vison and polyphagia are typical for diabetes mellitus disorder. Besides, DM is always considered as risk factor for CVD. Hypertension and lipoprotein metabolism abnormalities are often accompanied with DM. Several different pathogenesis have been identified to involve in developing this disorder. The pathogenesis are insulin deficiency because of autoimmune destruction of pancreatic ß-cells called type 1 diabetes, and insulin resistance due to abnormalities classified as type 2 diabetes. The insulin deficiency or resistance in the complex pathways of hormone action results in deficient insulin action which forms the basis of abnormalities in protein metabolism, fat, and carbohydrate in diabetes mellitus. In most of the diabetic cases, inadequate insulin secretion and insulin resistance are likely to coexist. The diabetes type of a patient can vary over time, and many diabetic patients should be assigned to multiple classes. The classification of DM is given according to their pathogenic mechanisms. Type 1 diabetic disorder results from the destruction of ß-cell which leads to absolute insulin deficiency. This form accounts about 5-10% of diabetes and is often needed to be treated with insulin. Type 2 diabetes is caused by a combination of insulin resistance and inadequate insulin secretion, attributing for 90-95% diabetic disorder. Type 2 diabetes can be asymptomatic for a long time and is non-insulin dependent. Most type 2 diabetic patients are obese. Gestational diabetes mellitus is not clearly occur prior to gestation, but will be diagnosed in the second or third trimester of pregnancy. Other specific types compromise monogenic diabetes syndromes, diseases of the exocrine pancreas, drug or chemical induced diabetes and so on. [106-108]

International Diabetes Federation has reported that there estimated to be 415 million people who tolerate diabetes mellitus while 193 million of them remain undiagnosed. [109] Currently, three recommended diagnostic tests for diabetes mellitus are using worldwide: fasting plasma glucose (FPG) value, 2h plasma glucose (2h-PG) value during a 75g oral glucose tolerance test (OGTT), and glycated hemoglobin A1c (HbA1c) test. [107, 108, 110] Someone will be diagnosed as having diabetes if fall into one of the following criteria: (1) FPG $\geq$ 126mg/dl (7.0mmol/l), or 2h-PG $\geq$ 200mg/dl (11.1mmol/l), or HbA1c $\geq$ 6.5% (48mmol/mol), or hyperglycemic symptoms and random PG $\geq$ 200mg/dl(11.1mmol/l). [108, 110] The former two tests are based on plasma glucose criteria, which quantify blood-

glucose values directly and remain as the 'gold standard' for diagnosis and monitoring diabetes mellitus [111]. The HbA1c test is based on glycated proteins, which reflects an average value of blood glucose concentration for last 120 days. [111, 112]

Most proteins react with sugars without the involvement of enzymes, termed as non-enzymatic glycation. [113] Evidences have emerged to show the potential role of non-enzymatic glycation of proteins, or Maillard reaction, in the pathogenesis of chronic diabetes complications. [114] Non-enzymatic glycation of proteins are mainly divided into three stages: early stage, intermediate stage and late stage. Early stage glycation firstly involves the formation of unstable reversible aldimine compound (the Schiff base) resulting from reaction between reducing sugar (mainly glucose, or fructose, pentose, mannose, ascorbate, galactose, xylulose) and a free amino group of molecules, secondly the unstable Schiff base will be arranged into a stable irreversible ketoamine (Amadori product). At intermediate glycation stage, Amadori product degrades into a range of carbonyl compounds through oxidation and dehydration reactions, these carbonyl compounds are more reactive than the reducing sugars and act as propagators reacting with free amino groups of proteins. At late glycation stages, advanced glycation end-products will be formed through oxidation, dehydration and cyclization reactions between the propagators gained from intermediate stage and free amino groups. Advanced glycation end-products accumulate on long-lived proteins and will cause damage to the tissues. Measurements on early glycated proteins can estimate the mean plasma glucose over a time period and control the individual's metabolism, while measurements on intermediate and late glycated products can be used to investigate the relationship between them and tissue modifications. Early-stage glycation products include HbA1c and glycated albumin (GA). [112] Glycated proteins do not require overnight fasting, thus are not affected by short-term lifestyle changes and are less variable among individuals. [111]

HbA1c is formed by the non-enzymatic reaction between glucose and N-terminal valines residues in one or both of hemoglobin ß-chains. [111-113, 115] HbA1c test has shown its clinical significance for assessing glycemic control and predictive value for diabetes complications [116], thus has been suggested to be performed routinely including initial assessment and continuing care for diabetic patients. Currently, there are several methods used to determine HbA1c, mainly employing either ion charge differences or structural characteristics. The former class compromises ion exchange chromatography by high performance liquid chromatography (HPLC) and electrophoresis. Ion exchange chromatography is based on the exchange of charged ions between mobile phase and stationary phase which is covalently attached by charged ligands. Due to less positively charged at neutral pH environment and less strongly binding to the negatively charged resin, glycated hemoglobin components will elute before the unglycated fraction. Electrophoresis separates the fast hemoglobins towards cathode by applying electric potential across support medium. However, these charge-based techniques are sensitive to environment (temperature, pH), sample-storage conditions and interference from clinical factors (uremia, ethanol ingestion). Structural characteristics based methods include affinity binding/chromatography and immunoassay. Boronate-affinity chromatography separate HbA1c from Hb solution resulting from the esterification reaction between cis-diols of glucose and boronic acid. Immunoassay determines HbA1c by employing monoclonal or polyclonal antibodies to

recognize glycated amino acids of ß-chain. [111] Immunoassay is expensive and has lower values with respect to HPLC. [112]

In order to solve the aforementioned disadvantages of the existing approaches for HbA1c determination, optical approaches are believed to be good alternatives. These optical techniques include Raman spectroscopy, infrared absorption spectroscopy, photoacoustic spectroscopy, optical coherence tomography and polarization spectroscopy. Promising results utilizing optical methods have been shown to measure blood glucose non-invasively, [111] paving the way to probe HbA1c in blood-based samples. Among the photonic methods, Raman-based spectroscopic methods seem to be the most promising one to be used in clinic. Ishikawa's group have employed surface-enfacement resonance Raman spectroscopy for sensitive and specific detection of HbA1c [117]. However, this surface-enfacement resonance Raman spectroscopy has difficult to quantify HbA1c precisely. Barman and his colleagues have shown the possibility of DCDR to investigate HbA1c within a physiological range with high accuracy and reproducibility. [118] Raman spectroscopy has also been used to monitor the glycosylation status of proteins and determinate HbA1c in clinical cohorts. [119]

To pave Raman spectroscopy for HbA1c determination into clinical routine test in reality, systematic study about the quantification of HbA1c consisting control, healthy and diabetic cohorts is needed. So far, Raman spectra reflect the average HbA1c degree over many red blood cells. However, difference in the measured red blood cells (RBCs) will affect the HbA1c values. It will have more sense if HbA1c value can be interpreted on single RBC level. In this thesis, we try to explore the potential of Raman spectroscopy to characterize HbA1c in diabetic patients, correlate Raman signal with clinical HbA1c values, and characterize HbA1c value on single RBC level.

1.3 Blood as an easy accessible body fluid sample

Blood, one of the most common body fluids, not only contains lots of proteins, lipids, sugars and DNA, but also is convenient to be collected even without any interventional procedures and can be performed easily worldwide. In addition to its fundamental involvement in human function which reflects one's physiological and pathological conditions, blood - particularly plasma and serum - represents an ideal sample for the diagnosis of disease. Blood is often referred to 'liquid organ', this is due to its complexity of many different components with very diverse properties. Blood is mainly separated into two parts according to sedimentation: blood cells - which represent about 45% volume of entire blood and are primarily produced in the bone marrow; and blood plasma - the liquid portion of blood representing approximately 55% volume of the entire blood. [11] Blood cells are slowly differentiated from homogeneous pluripotent stem cells into two different precursor cells at the fetal stage - lymphoid precursor cells and myeloid precursor cells. Subsequent in the adult stage, these two precursor cells will be further developed into adult blood cells such as different lymphocytes, thrombocytes, leukocytes and erythrocytes. [10, 11] Adult blood cells mainly contain three types: erythrocytes or red blood cells (RBCs), leukocytes or white blood cells (WBCs), and thrombocytes or platelets. They are different in size, shape, lifetime, concentration and functionality. An overview of blood sample is shown in Figure 1.

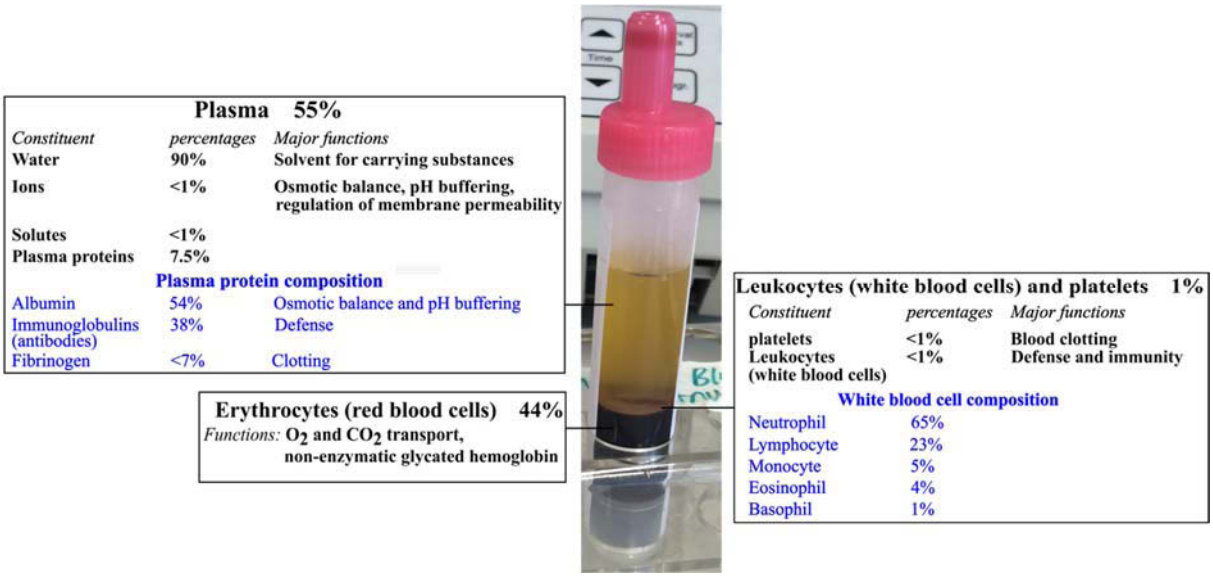

Figure 1 Overview of blood components. [10, 11]

Blood plasma contains many dissolved components which show different functions. These components include water, mineral salts, ions, low molecular weight components, high molecular weight components, gases in soluble form and metabolites. Among the various components in blood plasma, plasma proteins are the most complex one exhibiting various structural properties and functions. Plasma proteins are classified into different categories: classical plasma proteins from solid tissues and circulating in plasma are secreted by the liver and intestines, special immunoglobulins class with their extraordinary complexity, 'long-distance' receptor ligands including classical peptide and protein hormones such as insulin or erythropoietin, 'local' receptor ligands comprises cytokines and short-distance mediators, temporary passengers such as lysosomal proteins, tissue leakage products containing proteins released from cell death or cell damage. The lifetime of plasma proteins strongly depend on the molecular weight regulated by the filtration cut-off of the kidney: a small size below the filtration cut-off of the kidney brings short lifetime in plasma such as 'local' receptor ligands, whereas the large size protein presents longer in plasma such as 'long-distance' receptor ligands. Plasma proteins play a wide variety of functions: blood coagulation and fibrinolysis, the complement system, the immune system, enzymes, inhibitors, lipoproteins, hormones, cytokines and growth factors, transport and storage, and additional proteins. The main difference between blood plasma and blood serum is the absence of clotting factor in serum, it means that blood serum is blood plasma without fibrinogens. Plasma proteins cover at least 10 orders of magnitude of concentration range, comprising high-abundance serum albumin with 35-50mg/ml representing approximately 55% plasma proteins, coagulation factors with 1mg-1µg/ml, cytokines in the range of 100-1pg/ml, and low abundant interleukin-6 of only few pg/ml. The extraordinary wide concentration range brings the challenge to isolate, identify and characterise those low-abundance blood plasma proteins. Theoretically, any protein in the body can become a blood plasma protein as least temporarily. [120] Thus blood plasma or serum is a very promising solution to identify biomarkers for disease diagnosis and therapeutic monitoring.

Since blood plasma or serum is such a complex specimen containing unique biochemical information from various biomolecules, techniques to detect or discover plasma or serum biomarkers which relate to the disorder conditions are needed and in high demanded, especially those techniques which are rapid, label-free, little or no further sample preparations. Vibrational spectroscopy, including Raman spectroscopy and FT-IR spectroscopy, is such a method which conform the need of blood specimen for the clinical application.

1.4 Vibrational spectroscopy as a powerful, non-destructive analysis tool

1.4.1 Mechanisms of vibrational spectroscopy

Light is an electromagnetic wave, composing of two perpendicular vectors: an electric vector E and a magnetic vector H which two are both perpendicular to the direction of light propagation. Thus, the electric vector E, the magnetic vector H, and the direction of light propagation are perpendicular to each other. [121] When light interacts with matter, different phenomenon will occur, such as absorption, reflection, and scattering. [10] In other words, when the electric field of this electromagnetic wave interacts with matter, the energy of light can be absorbed, reflected or scattered. From modern physics, we know that light contains inherent energy, which is expressed as following:

$$E = h \times v \qquad \text{Equation 1}$$

Where h is Planck constant. v is the frequency of light, which is inversely proportional to the wavelength.

All existing matter is made up of atomic or molecular structure with different and unique energy-states. To study the different energy states, the transition processes between them are investigated. This formed the study field of spectroscopy where the radiation of various types are analysed. The energy between transition processes is expressed as:

$$\Delta E = h \times \Delta v \qquad \text{Equation 2}$$

The term of wavenumber is more frequently used in spectroscopy, and defined as the number of waves contained in one unit length, and expressed as:

$$\lambda = \frac{c}{v} \qquad \text{Equation 3}$$

Where λ is wavelength. c is the velocity of light.

The electromagnetic waves contain many different wavelengths, so the energy between different transitions can be of different range, from $10^{4} eV$ to $10^{-6} eV$. [122] When consider of biological sample, vibrational energy of molecular structure with the typical order of $10^{-1} eV$ is preferred. There are two important methods to observe vibrational spectra: Raman

spectroscopy and infrared spectroscopy. Molecular vibrations are motions that the lengths of the chemical bonds and the angels between the atoms change periodically in time.

Depending on the symmetry of the molecule, the molecular vibration can be active or forbidden in the Raman or infrared spectrum. [123] Raman active vibration occurs when the molecular polarizability is modulated by the normal vibration, and expressed as:

$$\left(\frac{\partial \alpha}{\partial q}\right)_0 \neq 0 \qquad \text{Equation 4}$$

Where α denotes the molecular polarizability. q means the normal coordinate describing the atomic motions during a normal vibration.

Infrared active vibration happens if there is a modulation of molecular dipole moment by vibration, and donated as:

$$\left(\frac{\partial \mu}{\partial q}\right)_0 \neq 0 \qquad \text{Equation 5}$$

Where μ is the molecular dipole moment.

Since the mechanisms of Raman and infrared spectroscopy are distinct, when the light quanta interact with the molecules, these two spectra can provide complementary images of molecular vibrations. In many of the analytical spectroscopic studies for biological samples, both of these two spectroscopic methods are employed.

The principal mechanisms for the vibrational states and the energy involved for infrared and Raman transitions are shown in Figure 2. In infrared absorbance (Figure 2 (a)), molecules absorbs certain amount of incident light quanta, i.e. $h\nu_0$, and are transited from the lower vibrational ground state to the upper vibrational excited states. IR absorption is frequently recorded by transmission T - the intensity ratio of the transmitted light I and incident light I_0, or as absorbance A where $A = log\left(\frac{I_0}{I}\right)$. As known from Equation 2, the absorbance band is proportional to the energy difference between the vibrational ground state and excited states. The intensity of absorbance band can be explained by the Lambert-Beer law:

$$A = \varepsilon c \lfloor \qquad \text{Equation 6}$$

Where ε is the absorption coefficient, which is dependent on $(\frac{\partial \mu}{\partial q})^2$. c donates the molecular concentration. $\lfloor$ is the pathlength of the interaction between light and sample.

The principle of Raman Effect is depicted in Figure 2 (b). When a light quanta $h\nu_0$hits a molecule, two scattering processes will be observed: elastic scattering or Rayleigh scattering where the scattered light has the same energy as the incident light, and inelastic scattering or Raman scattering where the scattered light have energies higher or smaller than the vibrational transition energy. According to Boltzmann's law, most molecules prefer to sit at their vibrational ground state at room temperature, only a few are in the vibrational excited

states. Thus during Raman process, the probability to transfer the molecule from the vibrational ground state into the higher vibrational state is much higher than to transfer the molecule from a vibrational excited stage into a lower vibrational state. The former is named Stokes Raman and the latter is called anti-Stokes Raman. As shown in Figure 2 (b), the intensity of Stokes Raman is higher than the anti-Stokes Raman. Therefore in most cases, if not required especially, the recorded Raman spectra are Stokes Raman spectra. Stokes Raman intensity is descripted classically as following:

$$I_{stokes} = constant \times N \times I_0 \times (\nu_0 - \nu_{vib})^4 \times \left[\left(\frac{\partial \alpha}{\partial q}\right)_0\right]^2 \qquad \text{Equation 7}$$

Where N is the number of molecules, I_0 is intensity of incident light. $\nu_0$means the frequency of incident light. ν_{vib}express Stokes Raman frequency.

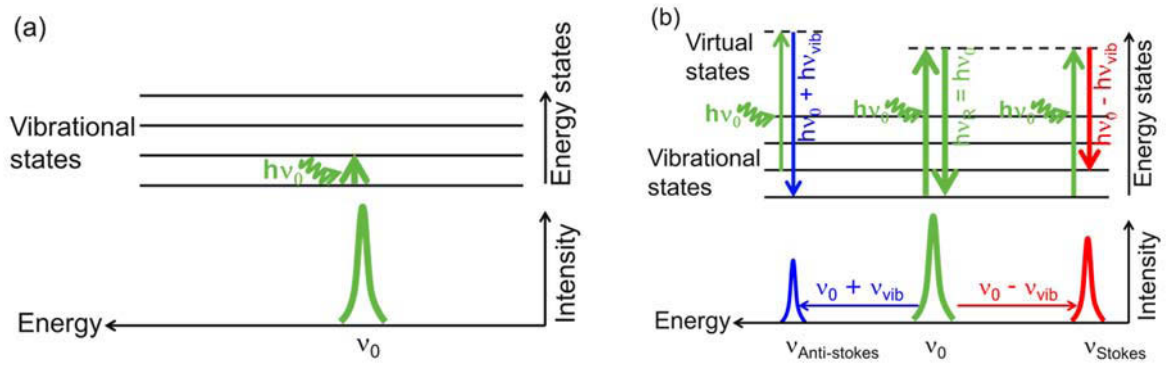

Figure 2 Principles of the infrared vibrational transition (a) and the Raman vibrational transition (b).

1.4.2 Biomedical vibrational spectroscopy

From above, it is clear that the principles for IR and Raman vibrations are different. They deliver complementary information on molecular vibrations and totality of molecule vibrational modes if being used together. Actually, these two spectroscopic modalities have a long history. The first IR experiment was performed by Herschel in 1801 and the first Raman Effect was discovered by Raman in 1928. [124, 125] These two modalities have been significantly improved for the study of biological molecules after the advent of laser Raman spectroscopy in early 1960s and FT-IR spectroscopy in late 1970s. The vibrational spectroscopic methods were moved another big step forward by the combination of the powerful computer and advanced chemometric methods. Thus since last two or three decades, FT-IR and Raman spectroscopy have become more interested and favourite methods to study the complex biological systems based on cells, tissues and body fluids, reflecting the changes according to pathological processes. Generally speaking, the variation of pathological processes is usually accompanied by changes in biochemistry of cells, tissues, or body fluids. These biochemistry changes can be ideally captured via vibrational spectroscopy, even before morphological and systemic manifestation diagnosed by conventional methods.

Keep in mind, IR and Raman spectra of biomedical materials are the expression of the total chemical and biochemistry composition. They show the active vibrational modes of all constituents in the complex biological mixture simultaneously in one single experiment.

Therefore, the complex superposition of the characteristic Raman signals or IR absorption of all constituents in biological samples will result in spectral features. These spectral fingerprints have a huge amount which is potentially useful for diagnostic purposes, thus form another 'OMICS' discipline in life science which deal with the complex biological system in entirety. Therefore, vibrational spectroscopy holds high potential to diagnose dysfunction or disease by spectral biomarkers in rapid, label-free, non-destructive, high-throughput way. There are good reviews about medical vibrational spectroscopy [85, 124, 126-130] which include various biomedical applications such as cancers, diabetes, arthritis, neurodegenerative diseases, cardiac diseases, kidney stone etc. Biomedical vibrational spectroscopy can be mainly fall into two categories: (1) spectral analysis of extracted body fluids or excised tissue, either ex vivo or in vivo; and (2) spectral imaging of extracted body fluids or excised tissue ex vivo, or spectral imaging in vivo. From the perspective of the medical doctor, biomedical vibrational spectroscopy can be summarized into following areas: (1) vibrational clinical chemistry, which analyse the spectra of analytes; (2) vibrational pathology, which show cytopathology and histopathology in spectral way; (3) vibrational radiology, which use vibrational radiation source for biomedical imaging; (4) vibrational spectroscopy beyond direct disease control, like monitoring the interactions with drugs.

Even though cells and tissues are the main samples for biomarker discovery at the beginning of biomedical vibrational spectroscopy [84], nowadays the study focus has been expanded to body fluids benificial from its easily accessibility and minimal invasiveness. These advantages are especially superior for large studies. Body fluids associate strongly with dysfunction of cells and tissues, these dysfunction manifests on the biochemical difference from protein, lipid, carbohydrate, and nucleic acid. Regarding body fluids, due to the ease of availability and repeatability, blood and its components are the most frequent and convenient used sample. Blood presents in all body organs and contains a huge range of proteomes from surrounding cells and tissues.

Biomedical vibrational spectroscopy, especially with the use of the most common body fluid such as blood and its components, will revolutionise the current clinical environment into a more rapid, label-free, non-invasive, non-destructive, cost-effective and automatic way for diagnostic purposes, which can highly reduce the rising global disease burden.

1.5 Aims

My Ph.D thesis aims to cover all aspects from technical development by using small amount of blood sample for vibrational spectroscopic analysis to the demonstrations for the potential of vibrational spectroscopy to investigate age-related diseases. The thesis can be mainly divided into three topics: (1) technical development by using blood sample for spectroscopic analysis; (2) application of vibrational spectroscopy to diagnose and follow-up treatment of cardiac diseases; (3) applying Raman spectroscopy to characterize glycated haemoglobin in diabetes mellitus for diagnostics.

Therefore, different specific sub-projects are involved: (1) Quality control of blood specimen; (2) Vibrational spectroscopic investigation of blood plasma and serum by drop coating

deposition for clinical application; (3) Vibrational spectroscopic differentiation of patients suffering from various cardiac diseases; (4) Immunoadsorption therapy follow-up for dilated cardiomyopathy using vibrational spectroscopic methods; (5) Influence of coronary artery bypass grafting on spectroscopic signature of leukocytes and plasma; (6) Raman spectroscopy for characterizing glycated haemoglobin in diabetes mellitus.

For each sub-projects, individual aims are pursued:

(1) To investigate the spectral changes and to check the quality of blood specimen due to prolonged waiting time delays.

(2) To understand the redistribution of plasma proteins in the dried droplet, and to determine best measurement principle to capture all chemical variations and components from dried plasma droplet.

(3) To investigate the differentiation of different cardiac diseases, and to study the differences between cardiac condition and healthy condition.

(4) To interpret longitudinal changes in dilated cardiomyopathy according to immunosdsorption therapy.

(5) To characterize spectral changes within WBCs (performed by my colleague) and plasma due to CABG surgery.

(6) To characterize glycated haemoglobin via Raman spectroscopy, particularly to investigate glycated haemoglobin value on single red blood cell level. (experiments was performed by master student)

To answer the questions and challenges above, the topic of my PhD thesis is to investigate and characterize the potential of vibrational spectroscopy for the stratifying patients of different diseases using minimal amounts of blood samples.

2 Materials and Methods

2.1 Blood samples collection

Blood samples were collected for patients and healthy donors, respectively, after giving informed consent (Ethic number: 4736-04/16; 4004-02/14; 3558-09/12; 3558-08/12). For blood samples from patients, venous blood were collected onto EDTA monovette for plasma or serum monovette for serum (Sarstedt, Germany) by our collaborating doctors and then transferred to our lab for further sample preparations. Venous blood from healthy donors were collected onto respective monovette for EDTA plasma or serum (Sarstedt, Germany) in our lab by trained colleagues, or by collecting capillary blood from the fingers onto minivette for EDTA plasma (Sarstedt, Germany) via Lancets by myself. The capillary blood from healthy donors was collected for glycated hemoglobin study, while venous blood from both healthy donors and patients was recruited for other projects.

2.2 Blood samples preparation

2.2.1 Centrifugation

Blood sample was separated into different components e.g. plasma or serum, RBCs and WBCs via centrifuge. Centrifuge is a widely used device to separate particles from studied solution. Inside the centrifuge, a rotating unit called rotor has fixed holes which are fixed to certain angel. Sample tubes will be placed into the holes and the sample will be separated when the motor is spun. Centrifuge is used in balance, meaning that the rotor holes at opposite directions need to be used simultaneously. Centrifuge is based on sedimentation principle. At certain centrifugal force, the sedimentation velocity is proportional to the particles' size and the difference between the densities of particles and liquid. Due to centrifugal acceleration, the denser particles inside the sample tube will settle down to the bottom of the tube whereas the low-dense particles rise up to the top. [131]

The centrifuges used in this thesis are Universal 320R from Hettich and miniSpin from Eppendorf. Collected blood was prepared into different components according to our respective SOPs, more details about sample preparations will be given below.

2.2.2 WBCs isolation

Mix $4ml$ $10x$ BD lysis with 36ml Ampuwa water; pipette $4ml$ blood into a falcon, add $40ml$ $1x$ BD lysis buffer into the blood falcon and incubate about $10min$ at room temperature (RT); centrifuge the incubated sample ($5min$, $300g$, $150mm$ rotor, RT); disregard the supernatant carefully; add $1ml$ phosphate buffered saline (PBS) into the remaining sample, mix gently; add $39ml$ PBS into the sample and mix gently; centrifuge again ($10min$, $300g$, $150mm$ rotor, RT); remove supernatant; add $1ml$ PBS.

2.2.3 RBCs isolation

Centrifuge the collected EDTA blood ($2000rcf$, $10min$, $20°C$); remove plasma and leukocyte buffy coat; add one fourth volume of PBS into monovette, mix gently and transfer the solution into a new falcon, add one fourth volume of PBS into monovette again, mix gently and transfer the solution into the falcon, centrifuge ($2000rcf, 5min, 20°C$); discard the supernatant, add double volume of PBS into the falcon, centrifuge ($2000rcf, 5min, 20°C$); redo the last step once.

2.2.4 Plasma / serum isolation

Centrifuge EDTA monovette and serum monovette according to respective parameters (plasma: $2000rcf, 10min, 20°C$; serum: $2500rcf, 10\ min, 20°C$). After centrifugation, aliquots of plasma and serum were stored at $-80°C$ for further use.

2.2.5 Glycated haemoglobin incubation

Add PBS and $10\mu M$ ampicillin solution to glucose solution with different concentrations ($0mM, 5mM, 30mM, 50mM, 60mM, 70mM, 90mM$), adjust pH of the mixed solution around 7. Then add the isolated RBCs of 50% haematocrit to the mixed solution with equal volume, and incubate in an incubator with $160rpm$ at $37°C$ for$24h$.

2.2.6 Blood smear

Pipette $7\mu l$ EDTA blood onto one side of a clean CaF_2 slide. Fix the CaF_2 slide, and hold a clean glass slide at the opposite side between $30 - 60°$. Gently forward the glass slide to the blood drop with fixed angle. Once the glass slide reaches the blood drop, stop few seconds for it to spread. Pull the above glass slide at the same angle towards the opposite direction of the blood drop gently till it reaches the end of the CaF_2 slide. After finishing blood smear, keep the slide under sterile hood about $30min$ for drying.

2.2.7 Sample preparation for vibrational spectroscopy

Before spectral measurements, thaw aliquots of plasma or serum to room temperature with ice and deposit $1\mu l$ sample on CaF_2 slide and keep under sterile bench about $30min$ for drying. For IR measurement, dilute plasma and serum samples with Milli-Q water in a ratio of 1:10. deposit $1\mu l$ diluted sample onto a CaF_2 slide and dry. Prepare RBC sample via blood smear as shown above.

2.3 Vibrational spectra collection

For spectroscopic measurements, the experimental set-up can be mainly separated into three components: radiation light source, analyser, and detection system. [122] The studied sample will be placed in the analyser. According to the specific application, combination of different light source, different analyser and different detection system will be utilized.

2.3.1 Raman spectroscopy

2.3.1.1 Confocal microscopy

Confocal imaging was firstly introduced in 1957 by Marvin Minsky. [132] The principle set-up of a confocal microscope is shown in Figure 3. The point light source (usually laser) is focused into the sample plane via an objective; after light-matter interaction, the back-scattered signal is collected by the same objective which guides and focuses the collected signal through a pinhole in front of the detector (usually charge-coupled device (CCD) detector). Confocal microscopy focuses the light at two positions - the light source as a point and the pinhole in front of detector, the name 'confocal' stands for this configuration. Confocal microscopy ensures the detection of signal only from the image focal plane, thus highly reduces the unexpected background from the out-of-focus light. In other words, confocal microscopy improves image contrast and spatial resolution greatly. By choosing pinhole with smaller diameters, the lateral resolution of confocal microscopy can be enhanced, but the detection efficiency will be decreased. Thus pinhole size and detection efficiency should be used in compromise.

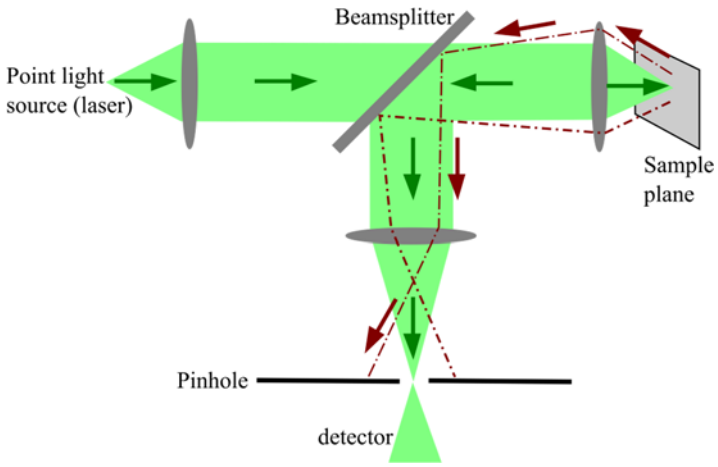

Figure 3 Principle setup of confocal microscope. [133]

When combining confocal microscope with Raman spectrometer, the so-called confocal Raman microscope is adverted. Two Raman systems are used in this thesis - WITec alpha300 and Renishaw inVia Qontor.

2.3.1.2 WITec alpha 300 Raman microscope

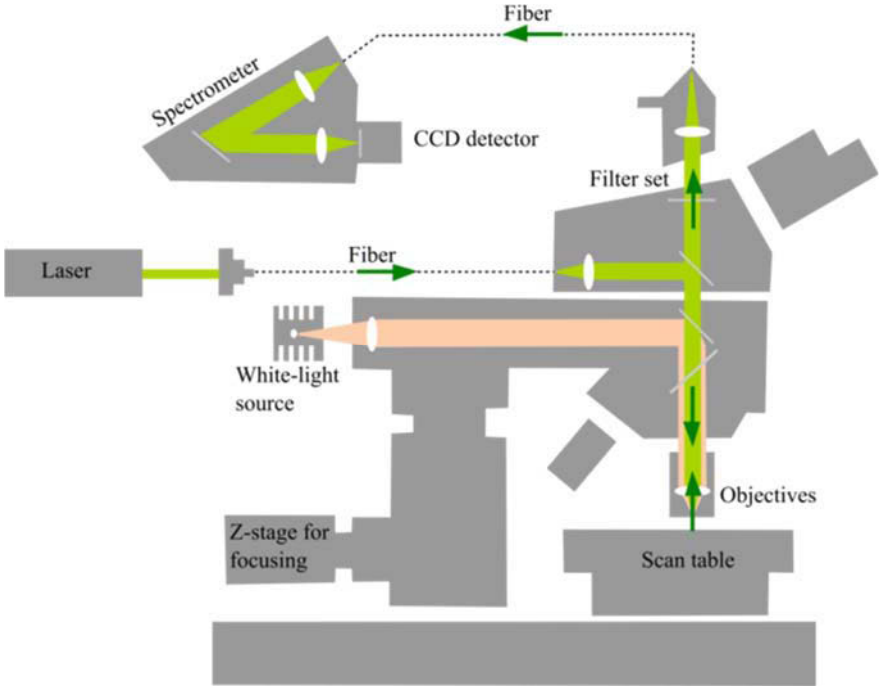

Figure 4 Setup of WITec alpha300 Raman microscope. [133]

Setup of WITec alpha300 Raman microscope is shown in Figure 4. This Raman microscope consists of two laser sources ($532nm$ Toptica Photonics AG, $785nm$ Toptica Photonics AG), fibers (single-mode and multi-mode), upright microscope, spectrometer (UHTS 300, WITec, Germany) and CCD detector (Andor iDus, Oxford Instruments, United Kingdom). Laser is guided to the objective of the upright microscope through single-mode fiber. The back-scattered light from the sample plane is focused back to the same objective, and then the Rayleigh light will be filtered out by the filterset. Later on, the filtered Raman light will be focused on the multi-mode fiber and sent to the grating-based spectrometer, finally detected by CCD detector.

2.3.1.3 Renishaw inVia Qontor Raman microscope

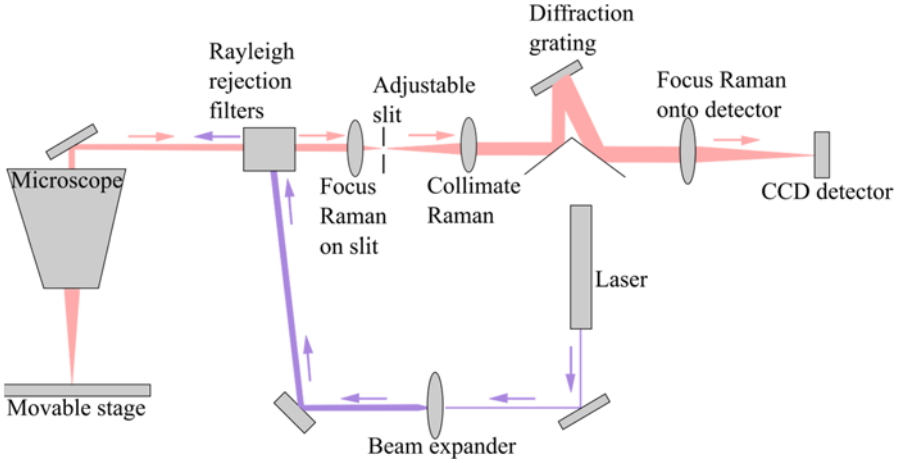

Figure 5 Setup of Renishaw inVia Qontor Raman microscope. [134]

Figure 5 shows the set-up of Renishaw inVia Qontor Raman microscope. This system consists of two laser sources ($532nm$ RL532C Renishaw, $785nm$ RL785 Renishaw), filterset, grating

diffraction-based spectrometer, CCD detector and Leica upright microscope. Laser excitation will be expanded and guided to the sample on the focus of the microscope, then the back-scattered light will be sent to the Rayleigh rejection filters to filter out Rayleigh light and the remaining Raman light will be focused on the slit and collimated to the diffraction grating of the spectrometer, finally the dispersed Raman signal is focused onto the CCD detector.

2.3.1.4 Raman data collection

In this thesis, laser with excitation wavelength around $785nm$ in WITec alpha 300 Raman microscope was used to measure blood plasma and serum for most of the studied projects, except for the glycated haemoglobin project which was measured on RBCs by using Renishaw inVia Qontor Raman microscope with $532nm$ excitation laser.

For the first 5 studies, Raman spectra were collected in back scattering geometry by WITec system using $785nm$ radiation with about $175mW$ laser power on the focal plane, the $2s$ scatter spectrum were collected by $20x$ objective with 0.8 numerical aperture. Blood samples were recorded in triplicates (3 batches) from three different aliquots on three different days. For albumin and IgG, average Raman spectra were calculated from 6 and 5 random points on the dried droplet respectively. The Raman spectra were collected from 20 different positions, 10 random from the central zone and 10 random from the outer ring.

For glycation haemoglobin study, heme structure changes due to glycation, Renishaw inVia Qontor with 532nm laser was used since heme is resonant at this wavelength. Raman spectra were recorded via a diffraction grating of 1800 lines/mm with $1cm^{-1}$ spectral resolution over the spectral range of $200-2200\text{cm}^{-1}$. Objective (Leica N plan EPI 50×0.75 N.A. BD) was used to guide the laser at the sample plane focus, and to gather the scattered Raman signal to the CCD detector. An average laser power of 4.5mw was on the focus of the sample plane. 200 RBCs were chosen to measure with 5s integration time.

2.3.2 FT-IR spectroscopy

2.3.2.1 Michelson interferometer

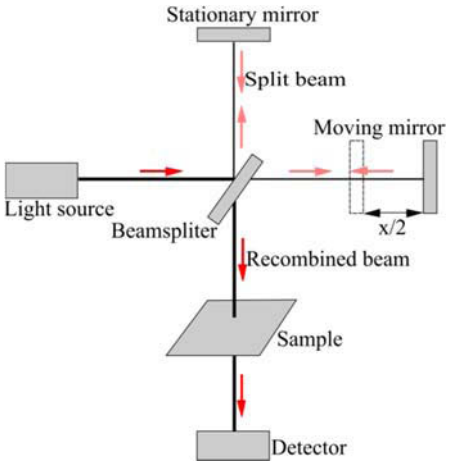

Figure 6 Principle schematics for Michelson interferometer. [135, 136]

Since most FT-IR spectrometer is based on Michelson interferometer, principle of this interferometer will be described (see Figure 6). Light emitted from light source is split into two beams after striking the beamsplitter (commonly 50% - 50% beamsplitter). These two beams strike a fixed mirror and a moving mirror, respectively, then reflected and recombined at the same beamsplitter again. At each position of the moving mirror, a signal will be detected by the detector. By changing the position of the moving mirror, an interference pattern will be generated during the movement. If the moving mirror is moved $\frac{x}{2}$, an optical pathlength difference of x is induced (double by the reflection). If the light source emits light with a spectrum $A(v)$, the light intensity obtained by the detector is

$$\boldsymbol{I}(x) = \int_0^\infty A(v) cos^2\left(\frac{x\pi v}{c}\right) dv = \left(\frac{1}{2}\right) \int_0^\infty A(v) \left[1 + \cos(\frac{2x\pi v}{c})\right] dv \qquad \text{Equation 8}$$

Where v is the frequency of the light, c is the velocity of light.

Expression $J(x) = \left(\frac{1}{2}\right) \int_0^\infty A(v) \cos(\frac{2x\pi v}{c})\, dv$ is called interferogram. Absorbance at each position infers each wavelength (or wavenumber). Interferogram is the signal recorded at all positions of the moving mirror during one periodical movement. Thus an interferogram contains spectrum from all measured wavelengths (or wavenumber).

Spectrum $A(v)$ can be calculated from $J(x)$ with Fourier transform algorithm as shown in Equation 9, and this gives the name FT-IR for this kind of 'Fourier transform Infrared spectrometer'. [135]

$$A(v) = \int_0^\infty J(x) \cos\left(\frac{2x\pi v}{c}\right) dx \qquad \text{Equation 9}$$

FT-IR spectrometer does not use a slit to limit the light to be detected, it can record all light reaching the detector, thus produces higher signal-to-noise information. FT-IR improves the sensitivity of small absorptions and details in the spectrum of a sample such as the case of protein. Commercially, a laser will be installed into an FT-IR spectrometer served as the light source for the interferometer. The laser-source interferometer can measure precise positions of the moving mirror, and the laser is also a reference for precision and accuracy of the infrared spectrometer. For reference purpose, this laser can determine the IR wavelength more precisely, additionally align and calibrate the spectrometer when various IR source are used. Thus FT-IR spectrometer is very stable for a long period, e.g. years. [136] In this thesis, FT-IR measurements were performed with Cary 670 FT-IR spectrometer coupled with Cary 620 microscope.

2.3.2.2 Cary 670 FT-IR spectrometer coupled with Cary 620 microscope

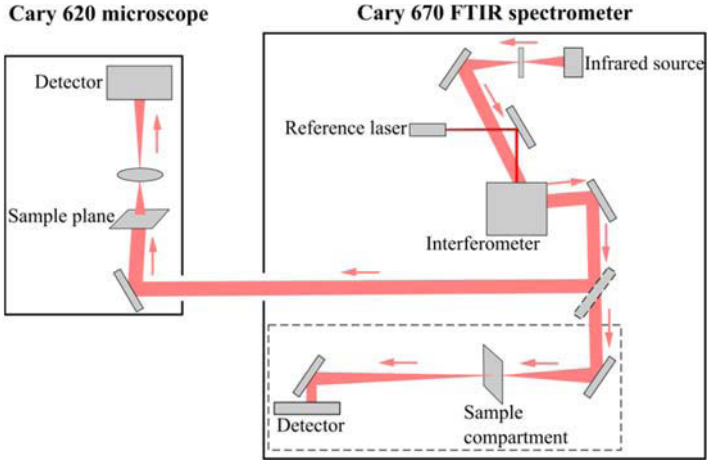

Figure 7 Setup of Cary 620 microscope and Cary 670 FT-IR spectrometer. [137]

Cary 670 FT-IR spectrometer (Agilent, USA) consists of mid-infrared light source, reference laser, interferometer, inside sample compartment and detector. Cary 620 microscope (Agilent, USA) includes two detectors - liquid nitrogen cooled focal plane array (FPA) imaging detector of 64*64 pixels and mercury cadmium telluride (MCT) spectra detector. The broadband mid-infrared light from Cary 670 FT-IR spectrometer is guided to the interferometer. The recombined beam in the interferometer will be obtained from the two interfering beams which are separated from the original beam. Then the recombined beam will be guided to the sample placed on the Cary 620 microscope. The absorbed light from the studied sample can be collected in transmission or reflection mode which is collected on the opposite or the same side as the sample plane, respectively.

2.3.2.3 FT-IR data collection

For FT-IR measurements, blood plasma or serum droplet was focused on the sample stage of Cary 620 microscope and the absorbed signals were recorded by either of the two detectors in Cary 620 microscope.

FT-IR spectra were recorded via Cary 670 FT-IR system over $900 - 3900cm^{-1}$ with spectral resolution of $4cm^{-1}$ over 16 scans in transmission mode for both background and all studied samples. For DCM project, the diluted blood samples were recorded with FPA detector of 64*64 pixels for 5 different scans. Each scan includes 4096 spectra while 1000 randomly chosen spectra from each scan were used for data analysis. For reference albumin and IgG, MCT detector with an imaging aperture size of $50\mu m * 50\mu m$ was applied due to some technical problems of FPA detector. For other studies, the diluted blood samples were collected via MCT detector with $50\mu m * 50\mu m$ aperture from 10 random positions at the center and 10 at the ring. Background was collected on sample-free substrate nearby the sample area per session.

2.4 Immunoturbidimetry assay

Immunoturbidimetry assay was performed by Cora Richart in clinical chemistry lab to quantity total IgG. Introduction about general Immunoturbidimetry method is given briefly below, subsequently followed by the specific Immunoturbidimetry assay used to quantify total IgG.

Due to the scattering effect of biomolecules, the intensity loss of transmitted light can be measured by turbidimetry. By interpreting the amount of absorbed light during the measurement, the number of investigated biomolecules can be obtained. By binding the specific antibody to the interested studied antigen, the concentration of the investigated biomolecules can be obtained, this is called immunoturbidimetry.

Total IgG based on plasma and serum samples was quantified with immunoturbidimetry according to an immunoturbidimetric assay via Architect system (Abbott, Germany) with 9D99 Immunoglobolin G Reagent Kit (Abbott, Germany) at the institute of Clinical Chemistry and Laboratory Diagnostics from the Jena University Hospital. The recommended commercial immunoturbidimetry assay by Abbott laboratories was applied and descripted shortly as following: plasma/serum was incubated with buffer R1 from 9D99 Immunoglobulin G Reagent Kit, then the incubated solution was measured as blank sample before adding buffer R2 from the same kit. After the measurement, concentration of total IgG was determined as a function of turbidity as result of the formation of immune complexes.

2.5 Data analysis

The collected raw vibrational spectra consist of not only the interested fingerprint, but also fluctuation by other confounding factors. Chemometric methods are commonly applied to remove these unwanted effects and to derive biochemical information of interest from the complex spectra, which helps to translate vibrational spectroscopic techniques into realistic clinical applications.

Chemometrics in spectral analysis mainly includes two stages: (1) preprocessing to improve data quality, (2) statistical modeling to withdraw biological conclusions based on spectral variations. Statistical modeling can be separated into dimension reduction to retrieve the most significant information and classification to translate spectral information to high-level biological knowledge.

All data analysis included in this thesis was carried out with in-house written scripts based on GNU R environment [138].

2.5.1 Preprocessing: Raman spectra

The unwanted signals in Raman spectra include cosmic spikes resulting from high energy particles hitting the CCD detector, Gaussian distributed white noise and Poisson distributed shot noise, fluorescence and thermal fluctuation from CCD. [88, 139] In order to minimize these unwanted variabilities and to retrieve more relevant information from the sample,

preprocessing steps are needed. Preprocessing for Raman spectra usually includes cosmic spikes removal, quality check, wavenumber and intensity calibration of Raman spectrometer, smoothing, fluorescence background correction, normalization and other manipulations. [88, 139-145]

A lot of pre-processing methods and algorithms are available and used for Raman data: de-nosing via principal component analysis (PCA) [146], Savitzky-Golay smoothing [147], wavelet denoising [148], or minimum noise fraction [149]; baseline correction based on user-defined polynomial points, extended multiplicative scattering correction [150], and asymmetric least squares smoothing [151]; normalization to correct sample and experimental variables by using vector normalization [141, 143], min-max normalization [141, 143], or amide I/II peak normalization [152].

In this thesis, the raw Raman data was firstly performed despike by comparing the two consecutively measured spectrum. The resulted spectra were wavenumber calibrated based on 4-acetamidophenol. Then the baseline was corrected via asymmetric least squares smoothing [151] or sensitive nonlinear iterative peak clipping algorithm [153]. All spectra were truncated to reserve only fingerprint regions ($600 - 1800cm^{-1}$and $2800 - 3020cm^{-1}$, or $600 - 1800cm^{-1}$) and then vector normalized.

In chemometrics, it is known that the prediction of unknown dataset is often worse than the prediction of training data. [154] When using a statistical model to predict new dataset, it is needed to improve the prediction of the model. Model transfer is such a technique which can achieve satisfactory prediction on the unknown dataset. A model transfer was conducted by extended multiplicative scatter correction according to Ref.[155], which is aimed to remove inter-batch variations.

2.5.2 Preprocessing: IR spectra

Preprocessing for IR spectra is slightly different as for Raman spectra. It involves outlier removal, smoothing, baseline correction, normalization and other manipulations. [139, 142, 143, 152, 156] In particular, the background baseline, which is mainly caused by Mie scattering, can be corrected via the baseline correction methods aforementioned, as well as differentiation coupled with Savitzky-Golay smoothing, resonant Mie scattering correction, etc. In this thesis, the background baseline was removed with sensitive nonlinear iterative peak clipping algorithm; wavenumber region was truncated to $900 - 1800cm^{-1}$ and $2700 - 3700cm^{-1}$ within which vector normalization was performed.

2.5.3 Dimension reduction

Dimension reduction can be realized by feature extraction and feature selection. Feature extraction works by projecting the original data onto a new basis system that better reveals the properties of the dataset. The coordinates on this new basis are then used as the features in the subsequent analysis. Often the new basis possesses a lower dimension than original dataset, hence a dimension reduced data is resulted from the feature extraction. Dimension reduction can recognize relevant pattern from the huge dataset. Popular methods for feature extraction

include PCA, and partial least squares. [141] Feature selection picks variables in the original data space that are the most significant for the classification or regression model. Common feature selection approaches include COVAR [157], forward feature selection [158], and choosing specific wavenumbers to determine spectral biomarkers [141].

PCA was performed on our data to obtain information of the most interest. PCA aims to represent the variances present in the data using a smaller number of factors (called principal component (PC)). Mathematically, PCA is an orthogonal transformation. The PCs are orthogonal to each other and each represents a different variance source in the data. The original data is linear combination of the PCs. [146, 159, 160]

2.5.4 Classification or regression model

Classification and regression are popularly used for diagnostics analysis, to derive disease levels or concentration of certain substances, respectively. In both cases, a statistical model is built based on a training dataset to relate the spectral information to the required high-level knowledge. Thereafter, a testing dataset independent to the training dataset will be used to validate the classifier. Common supervised machine-learning approaches to build a statistical model are linear discriminant analysis (LDA), support vector machine (SVM), artificial neural network, random forest, and partial least squares regression (PLSR). [141, 142] Sample size was proven to highly influence the performance of a statistical model. If appreciable, a sample size of 75-100 should be chosen to train classifier in order to get good precision and validation. [161] Besides, a robust model can be built through two stage training - firstly use cross-validation (CV) approach to find optimal parameters where the highest accuracy is achieved, secondly use the optimal parameters to build a proper classifier from the training dataset. [162]

Classification algorithm including SVM and LDA were employed for our data. The classification models were built via two-layer cross-validation, with the aforementioned PCA involved in the validation loop. The inner layer was based on training data where a 10-fold cross-validation was conducted and the parameters were optimized according to the accuracy of the model. The built model was used to predict the testing data that was from a different batch as the training data. To be specific, the outer layer was performed through a leave-one-batch-out cross-validation, where each batch was used once as testing data and the rest batches were used as training data. The model was benchmarked by accuracy of the prediction. In this study, the PCA-SVM model was built to classify the different IA treatment stages from the DCM patient, while PCA-LDA model was built to differentiate the Raman spectra collected from different time delays.

To predict HbA1c values from Raman spectra based on RBCs, PLSR regression model was built via 2-layer cross-validation as described above: 1st leave-one-sample-out-cross-validation, 2nd 10-fold cross-validation. The optimal components used in PLSR were chosen automatically when the lowest CV error was firstly achieved – according to the root mean squared error of prediction (RMSEP). The predictive ability of the model was validated by calculating R^2 of the model.

2.5.5 Workflow of data analysis

To better visualize data analysis procedures, the workflows corresponding to Raman data and FT-IR data are given below.

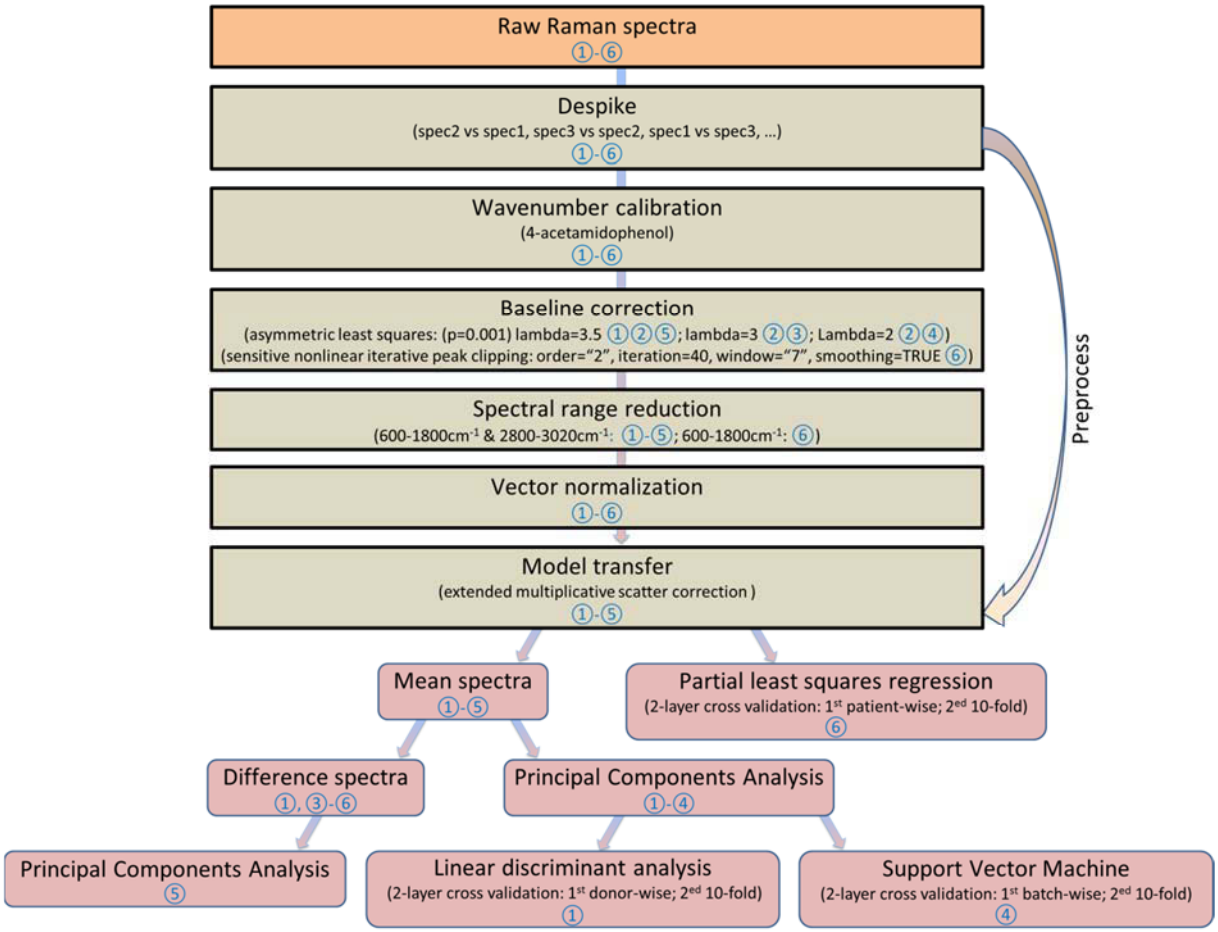

Figure 8 Workflow of Raman spectra analysis. Project number ①②③④⑤⑥, corresponding to the order of motivations and aims given in Section 1.2 and Section 1.5 respectively.

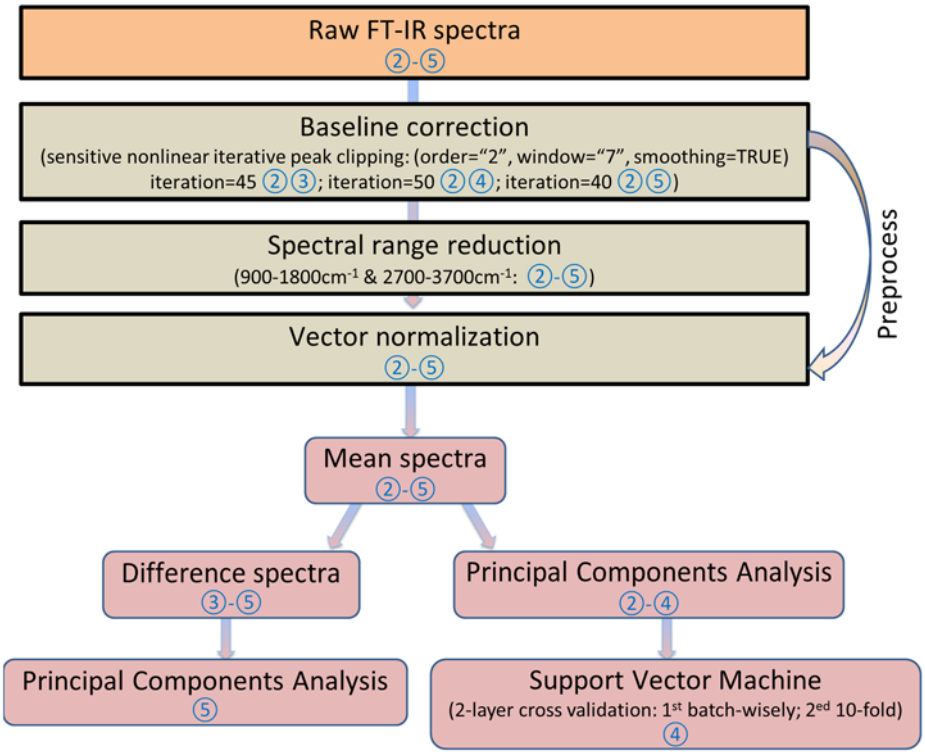

Figure 9 Workflow of FT-IR spectra analysis. Project number ①②③④⑤⑥, corresponding to the order of motivations and aims given in Section 1.2 and Section 1.5 respectively.

3 Results and Discussion

3.1 Technical development for using blood as sample for spectroscopic analysis

This section demonstrates quality check of blood specimen by using drop coating deposition Raman (DCDR) spectroscopy, and vibrational spectroscopic investigation of plasma by drop coating deposition for clinical application.

3.1.1 Quality check of blood specimen

Sample cohort. Serum blood from five healthy donors are collected, and stored at room temperature before serum centrifugation. The four different storage time (called time delays below) are given in Table 1. From clinical chemistry, variations are observed during these time delays, and these changes are mainly contribution from different metabolites.

Table 1 Information for healthy cohorts

Donor (n)	5			
Time delay (n)	4			
	$30min$	$60min$	$120min$	$240min$

Mean spectra. The spectra were captured via drop coating deposition Raman (DCDR) spectroscopy. The mean Raman spectra of different time delays from five individual donors are shown in Figure 10, the well overlay mean spectra of the four different time delays indicate that the sample are stable during the prolong processing time, only gentle difference occur. To better visualise the variation, difference spectra between different time delays were calculated and show in Figure 11.

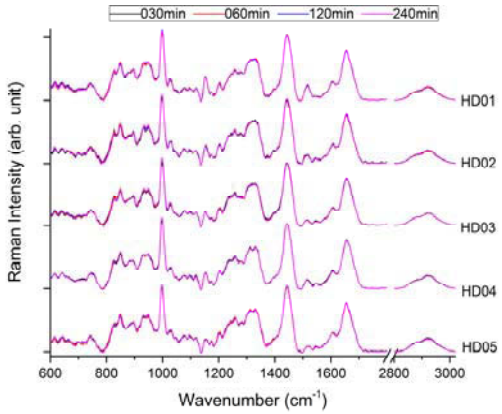

Figure 10 Mean spectra of different time delays from five individual donors.

Difference spectra. Variations of the time delays from serum samples are shown in the difference spectra (Figure 11). The changes are mainly attributed from the spectral marker around $800cm^{-1}$, especially when comparing the difference between $30min$ and $60min$, between $30min$ and $120min$, and between $30min$ and $240min$ time delays as indicated in Figure 11 (a, b, c). After $120min$ delay, no change is observed in spectra (Figure 11 f). Blood

will undergo changes if being stored for long time, these changes do not have an identical patterns for all individuals (see Figure 11 a, b, c, d, e), giving a hint for the role of intra-sample variation in the changes. To verify these changes are due to time delay in sample preparation, PCA analysis was performed.

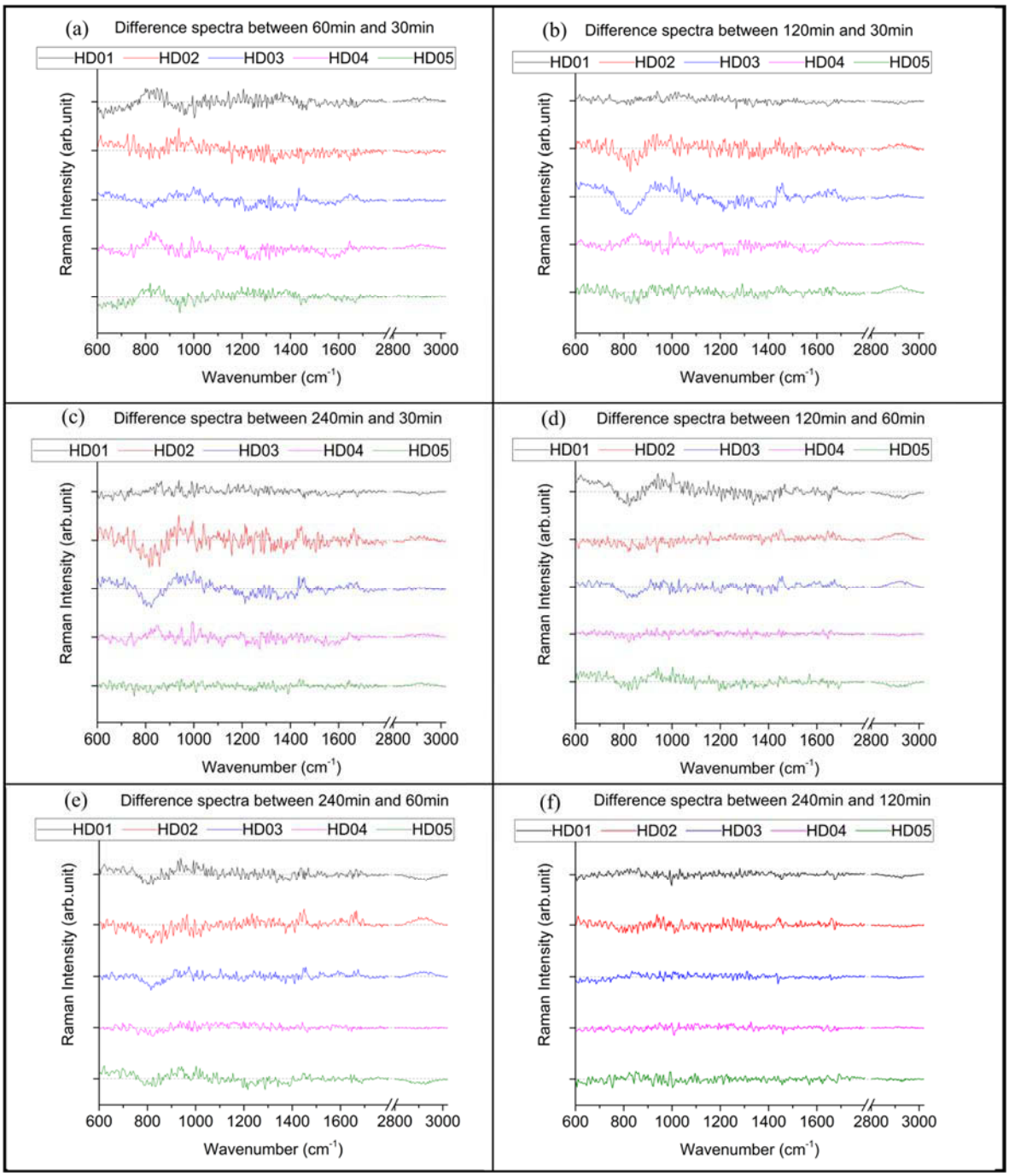

Figure 11 Difference spectra of different time delays from five individual donors.

PCA analysis. PCA analysis based on different time delays was calculated for individual donor and five donors together. PCA scatter plot were presented in Figure 12. The sera from the four time delays cannot be differentiated, neither for the individual donor nor for all five donors together. PCA analysis shows no difference due to time delay in sample preparations. But different PCA patterns were visible for different donors. Hence to obtain further

information, coefficients of measurement factors were calculated and presented later. The un-differentiable can be due to the following reasons: (1) the biochemical difference between these four time delays are too small; (2) individual heterogeneity plays a role; (3) the analysis algorithm is not robust enough, more robust algorithm is needed to be performed on the data. The first two are intrinsic property, and cannot be solved with data analysis methods.

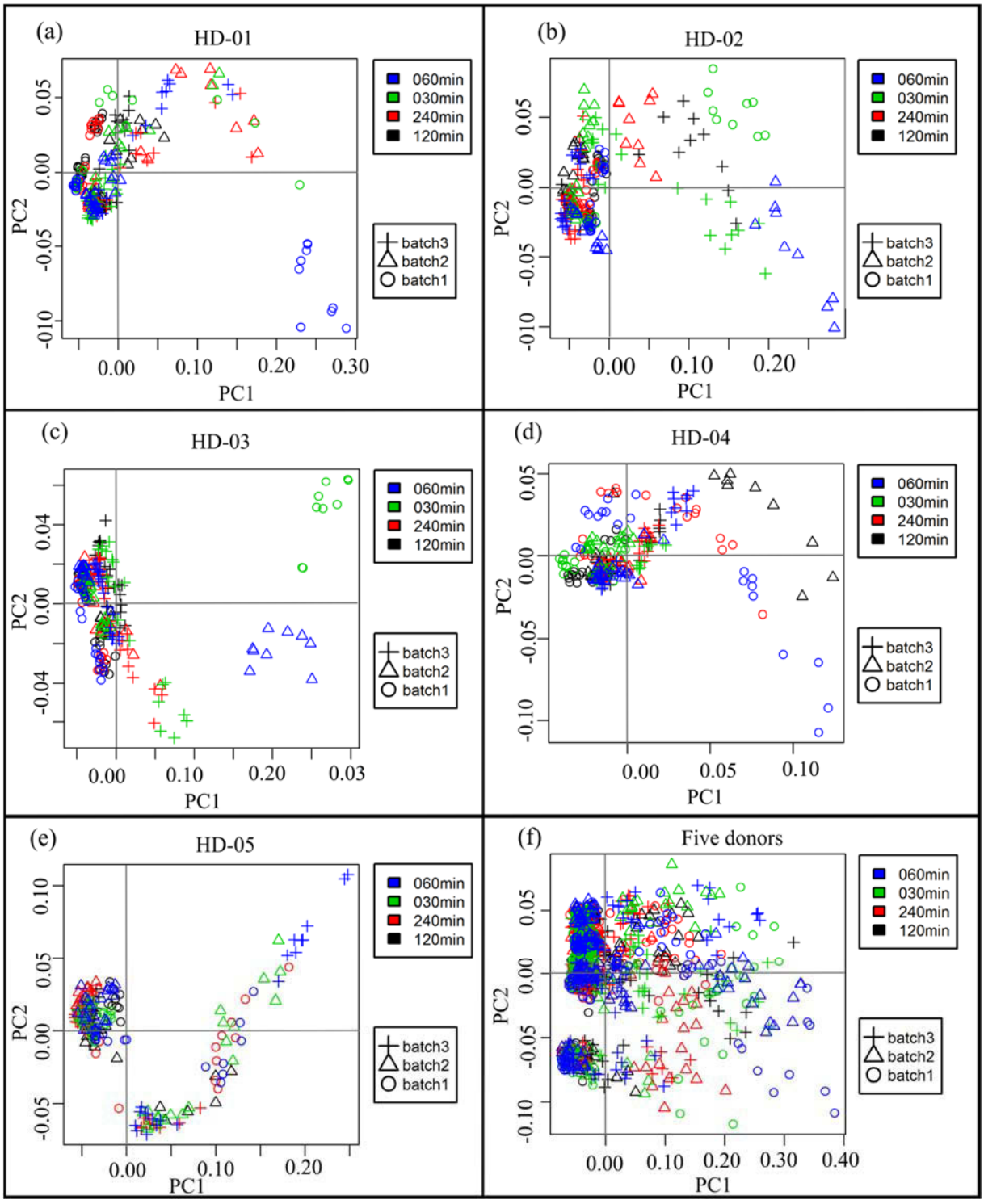

Figure 12 PCA scatter plot between different time delays from five individual donors and five donors together.

PCA-LDA model. To test the arguments presented, PCA based LDA model with leave-one (donor)-out cross-validation was performed on the spectra from all five donors. The PCA-LDA model was used to cluster the collected spectra into different groups corresponding to different time delays. The results for the PCA-LDA model are shown in Table 2, indicating that the spectra cannot be grouped into respective time delays.

Table 2 Confusion matrix of PCA-LDA model with leave-one (donor)-out-cross-validation

Test	Predict			
	$30min$	$60min$	$120min$	$240min$
$30min$	**2**	9	40	9
$60min$	0	**20**	27	13
$120min$	0	13	**40**	7
$240min$	3	10	35	**12**

Coefficients of experimental factors. In order to understand the variance further, the coefficients of experimental variations were calculated using ASCA method (ANOVA-simultaneous component analysis). To explain in brief, the data matrix from recorded spectra was decomposed as contributions of different experimental factors as shown in Equation 10 for all donors together:

$$Data = mean\ spectra + Batches + Time + donors + interaction\ (Time\ \&\ batches) + interaction\ (donors\ \&\ batches) + interaction\ (donors\ \&\ batches) + other\ factors$$

Equation 10

Table 3 Contributions of individual experimental factors for five donors together

Factors	Batches	Time	Donors	Batches & Time	Batches % Donors	Donors % Time	Other factors
%Var	2.26%	2.34%	14.07%	1.80%	5.05%	3.59%	70.90%

or expressed as Equation 11 for individual donor:

$$Data = mean\ spectra + Batches + Time + interaction\ (Time\ \&\ batches) + other\ factors$$

Equation 11

Table 4 Contributions of individual experimental factors for individual donor

Donor	Factors	Batches	Time	Batches & Time	Other factors
HD_01	%Var	7.92%	6.77%	16.03%	69.29%
HD_02		9.29%	6.89%	22.64%	61.18%
HD_03		9.25%	6.94%	18.60%	65.22%
HD_04		12.80%	7.09%	23.83%	56.28%
HD_05		4.09%	6.90%	31.05%	57.96%

The calculations show that the most significant factor affecting the variation is other factors. When considering the data from the five donors together, the donors' variation is the second major factor for the variation, this confirms the result from Ref [30]. Above all, coefficients of factors show that individual heterogeneity has second highest contribution after other factors.

Summary and discussion. From the results above, some minor differences can be captured via DCDR if prolong the time delay between blood collection and blood centrifugation, but donor heterogeneity is high. The PCA and PCA-LDA analysis show that the serum is quite stable and only few non-significant changes will occur when keeping up to 4 hours before centrifugation [26, 27, 34]. The variance calculation indicates that the time delay affects the changes of the sera in Raman spectra at a least extent, confirmed by small contribution values of time in Table 3 and Table 4. According to the literatures, the changes inside the blood under certain time delay of preparation are mainly from the small molecules in metabolites reflecting erythrocyte activity [21, 30, 31, 33] and from low-molecular-weight proteins [23, 25, 28]. To observe these small metabolites or proteins, the macromolecules need to be depleted; otherwise the Raman spectra will be dominated by the major high-molecular-weight proteins such as albumin, IgG, ect. This can be a reason that the DCDR spectra are not able to differentiate the serum prepared with different time delays. In our study, no protein was removed in sample preparation, because it is very often that the interested biomarker is unknown in clinical application, we would like to keep the integrity of the measured specimen. Above all, DCDR spectra seem to have stable biochemical information from the blood specimen up to 4 hours delay before centrifugation. Thus it is reasonable and reliable to use DCDR to search biomarkers from blood specimen. To investigate the biochemistry in the blood specimen for time delay between blood collection and separation, other methods need to be conducted: depletion of the abundant plasma protein, use the sample in liquid form with advanced Raman spectroscopy such as stimulated Raman spectroscopy and surface-enhanced Raman spectroscopy, apply attenuated total reflection FT-IR method for capturing changes in the small proteins. Moreover, a large donor cohort also needs to be considered in further study.

When we use good quality blood specimen for clinical application, the sample can be prepared via drop coating deposition method, but further understanding about drop coating deposition method via vibrational spectroscopy is needed to be investigated.

3.1.2 Vibrational spectroscopic investigation of plasma and serum by drop coating deposition for clinical application

Sample cohort. Blood samples were collected from healthy donors (n=17) and patients (n=18). These included the patients who had different cardiac diseases, e.g. dilated cardiomyopathy (DCM), heart failure (HF), and coronary artery bypass grafting (CABG) surgery. Both plasma and serum sample were investigated. For plasma we had 7 healthy donors and 18 patients, for serum we had 10 healthy donors and 2 patients.

Morphology from white light image. The typical morphology of microscopic white light image for dried plasma or serum droplet is shown as Figure 13. The dried droplet is separated into two different parts, the central zone with crystal pattern and the ring zone at the edge, indicated by inner and outer individually in this thesis. These two regions accumulate different molecules, thus to take the inhomogeneous coffee-ring effect into account and better represent the whole dried droplet, a measurement geometry for the samples with 10 random points in the inner and 10 random points in the outer was used. For plasma and serum sample from healthy donors measured via FT-IR spectroscopy, 5 locations are randomly chosen in both the inner and outer region.

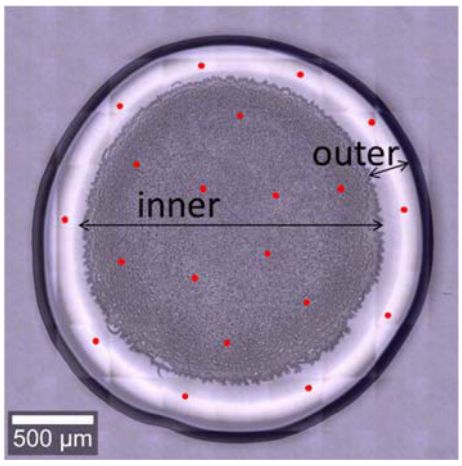

Figure 13 White light image of dried plasma droplet from healthy donor, the droplet is separated into two parts: the central zone (inner) and the ring zone at the edge (outer), the inner is crystalized. The 20 red dots represent 20 different measurement points.

Raw spectra collected from inner and outer. As shown in Figure 13, different biomolecules form different morphology of the dried droplet, which represent different biochemical fingerprint [37, 163-165]. To better understand the separated morphology difference, raw spectra comparison between inner and outer region are done and shown in Figure 14. From Figure 14, it is clear that the Raman signal for plasma and serum droplet in the outer is higher than in the inner. However, the spectra collected from inner have similar

Raman pattern as from outer. This is the same for the FT-IR spectra. It can be explained by the aggregation of biomolecules (mainly proteins with the amide bands shown in Figure 14) in the outer due to the coffee-ring effect which drive the particles to the ring. However, there are proteins remained in the inner of the droplet but with few quantities (see the raw spectra collected from inner in Figure 14) [37]; this can result from the suppression of coffee-ring phenomenon by Marangoni effect which carries the particles toward the inner [37, 42].

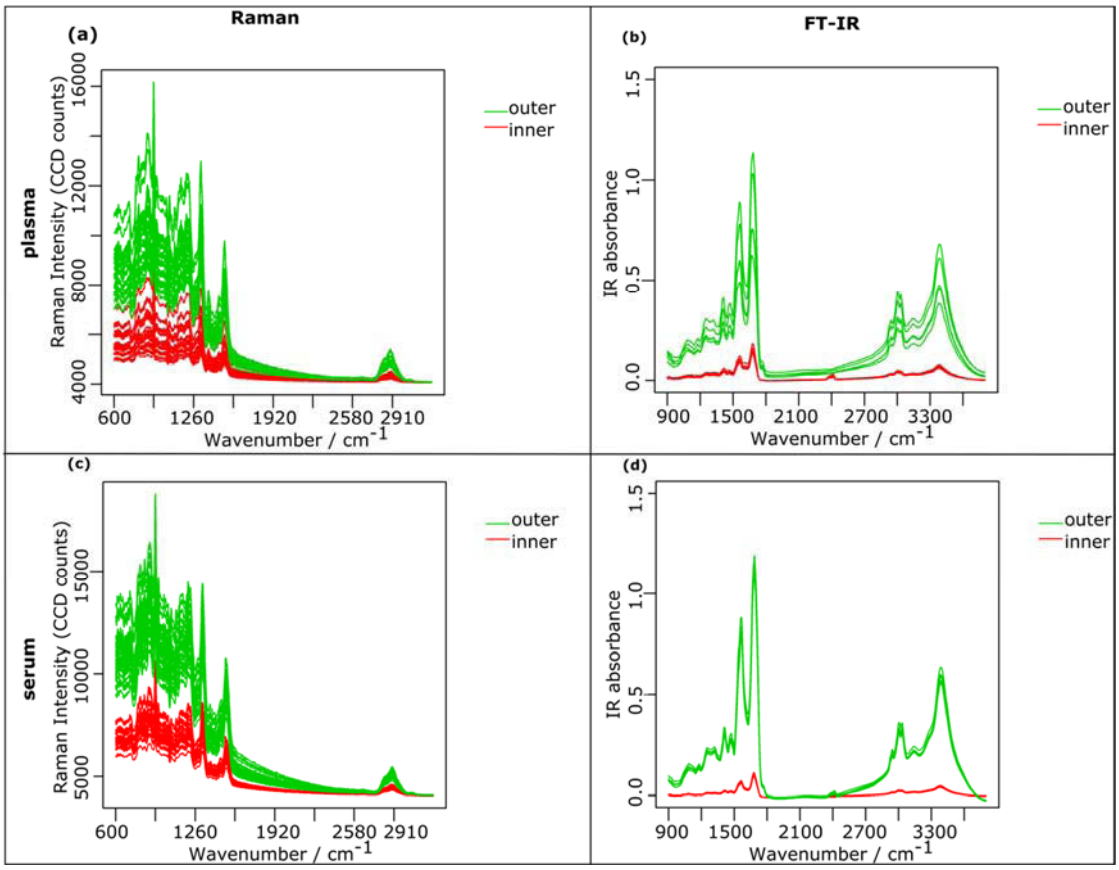

Figure 14 Raw spectra comparison between outer (green color) and inner (red color) from Raman data and FT-IR data of healthy donor (n=1).

It is well-known that in blood plasma and blood serum, the most abundant blood protein albumin accounts for nearly 55% of the overall blood proteins. The second most predominating proteins are Ig (or antibodies), which constitutes about 38% of blood proteins. Within all Ig, IgG has majority contribution, attributing about 75% of Ig. It is still not clear about the origins for crystal-like patterns in the central part of plasma droplet. Chen and Mohamed suggested that the crystal-like patterns were albumin by using fluorescent microscopy. [166] And other researchers have suggested that the central part of the dried plasma droplet can be crystals combinations of proteins and salts. [167, 168] We can confirm presence of proteins and visualize crystal structures in inner. However, Yakhno proposed that the crystal patterns were salts on the gelled protein matrix. [169] The contradiction is whether the crystal pattern in inner is only salt but above the gelled protein matrix, or the crystal pattern is the combination of salt and proteins. They agree with the presence of proteins in inner, but disagree on the origin for crystal patterns in inner. In this thesis, I try to clarify the locations of abundant plasma proteins including albumin and IgG in the droplet rather than to

find out the origin of central crystal-like patterns via Raman spectroscopy and FT-IR spectroscopy.

Preprocessed spectra. In order to find out the contributions of albumin and IgG in the dried droplet, Raman and FT-IR spectra from pure albumin and IgG were recorded as references. Figure 15 shows the corresponding Raman and FT-IR pattern of albumin and IgG. The inner and outer of the plasma and serum droplet share the same Raman fingerprints, which are mainly contributions from albumin. Besides, IgG also influences the Raman profile for plasma and serum droplet around $756cm^{-1}$, $1240cm^{-1}$, $1340cm^{-1}$, and $1552cm^{-1}$. The presence of albumin in the droplet can also be verified with the FT-IR spectra shown in Figure 15 (b). The vibrational spectra shown in Figure 15 confirm the presence of albumin and IgG not only in the ring but also in the central part of dried droplet. But the distribution of albumin, IgG and other proteins are inhomogeneous across the whole droplet as result of coffee-ring effect. The pre-processed spectra collected from inner and outer are overlaid in Figure 15, some differences between them can be observed. PCA analysis based on spectra collected from inner and outer was performed to dig out more information about the differences, and the results are presented in the following.

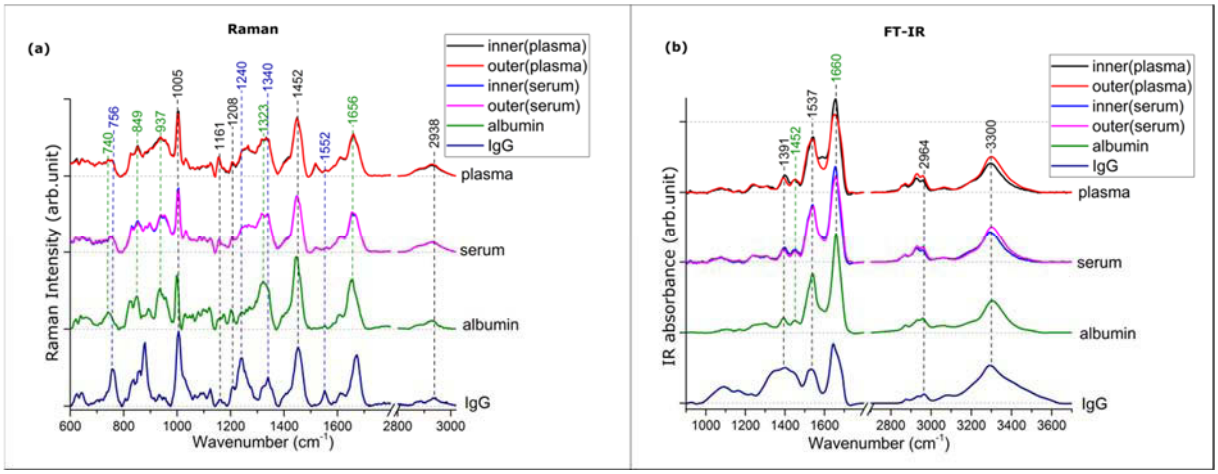

Figure 15 Spectra comparison of blood droplet (inner and outer) from healthy donor, albumin and IgG.

PCA analysis for spectra collected from healthy donors. When prepared body fluid sample through drop coating deposition method, the biochemical difference or similarity between inner and outer region of the dried droplet need to be tested before any real application. That means, it is very critical to choose an optimal collection protocol which can represent the whole dried droplet by taking the coffee-ring effect into account. In order to check the differentiation or similarity of the biochemical information between inner and outer regions, PCA analysis based on inner and outer regions from healthy donors (n=17) is performed and PCA scatter plots (donor, n=1) are presented in Figure 16, which shows that the Raman and FT-IR spectra obtained from the inner and outer regions can be distinctly separated into two clusters, indicating the different biochemical compositions between these two regions. For all healthy donors, PCA scatter plots are the same as Figure 16, results are not shown here.

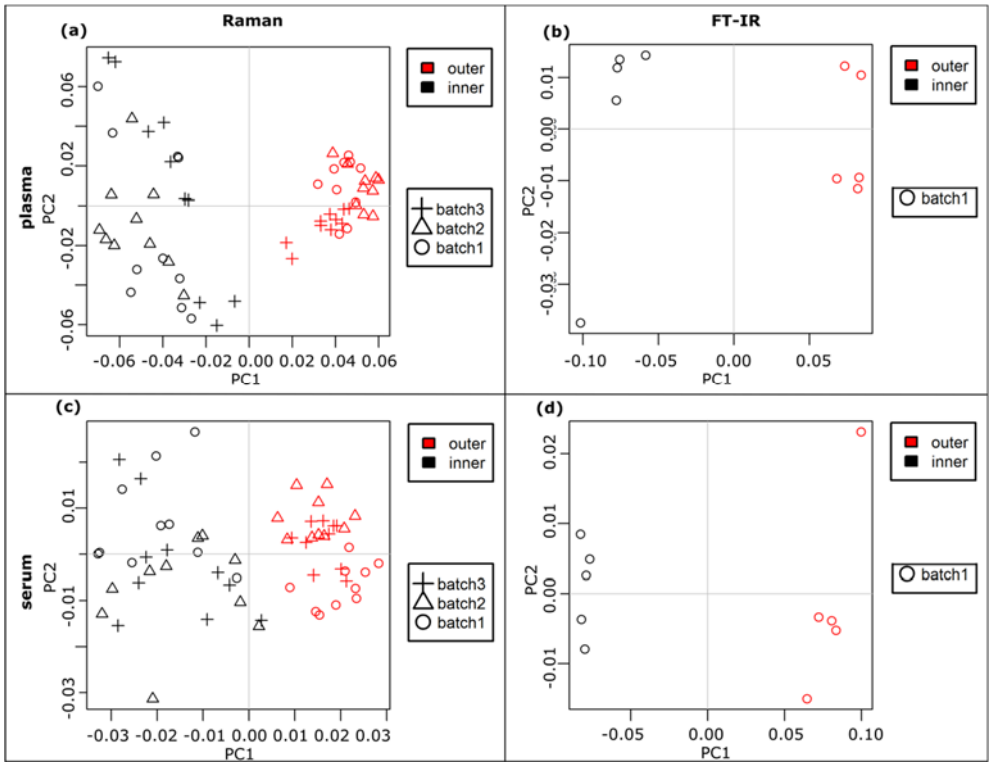

Figure 16 PCA analysis of vibrational spectra of inner and outer region from healthy donor (n=1).

To better understand the biochemical difference between inner and outer, the corresponding PC loadings of PCA are shown in Figure 17. From Figure 17, it is obvious that the biochemical difference between the inner and outer are mainly contributions from proteins, indicated by the typical protein Raman bands around Try ($857cm^{-1}$, $1208cm^{-1}$), Pro ($857cm^{-1}$), tyrosine ($857cm^{-1}$), Phenylalanine ($1004cm^{-1}$), amide I ($1659cm^{-1}$) and C-H stretching ($2933cm^{-1}$); and FT-IR fingerprints around amide II ($1512cm^{-1}$), amide I ($1655cm^{-1}$, $1695cm^{-1}$), C-H stretching ($2962cm^{-1}$). The Raman pattern to differentiate the inner and outer is very similar for the plasma samples from all healthy individuals. This means that the different distribution of biomolecules in inner and outer is a common feature among all individuals. However, when considering serum sample with Raman spectroscopy, the spectral difference differentiating the inner and outer regions is inconsistent as the difference observed in Figure 17 (c). This is due to the different PC values regarding to inner and outer. For HD_01 and HD_04, outer is clustered into negative PC1 values while inner is clustered into positive PC1 values. Opposite clustering happens to other serum samples. The PC1 loading is similar for HD_01 and HD_04, but opposite to other serum samples (see Figure 18). For the FT-IR spectral loadings, both plasma and serum samples have similar biochemical difference between the inner and outer regions; these differences are mostly contributions from proteins.

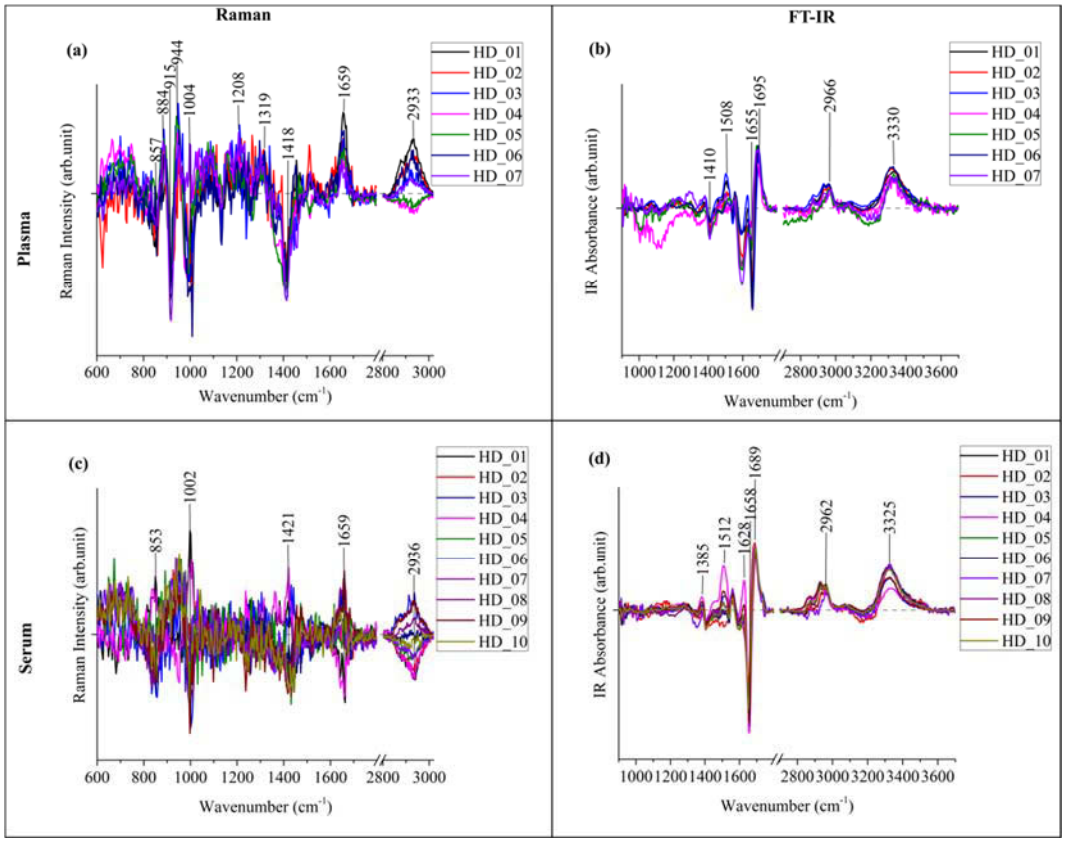

Figure 17 PC loadings of vibrational spectra of inner and outer region from healthy donor (plasma: n=7; serum: n=10).

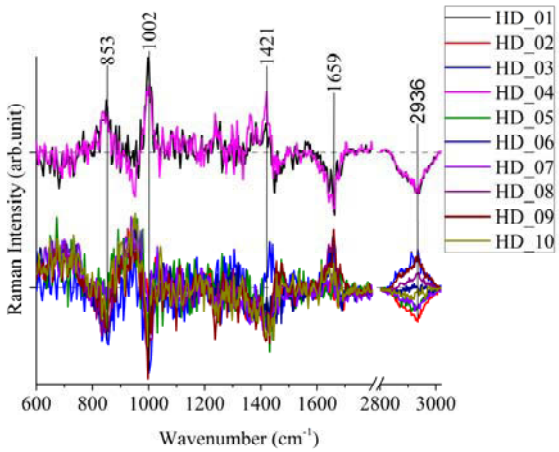

Figure 18 PC loadings of Raman spectra of inner and outer region from healthy donor (serum: n=10).

The PCA analysis and respective loadings in Figure 16, Figure 17, and Figure 18 indicate that distribution of biomolecules varies between inner and outer regions of the dried sample droplet. Despite it is still unclear about the pattern formation of the droplet, this drop coating deposition method has been used for medical diagnosis since 1950s. The traditional droplet evaporation research derives information from the dried droplet directly; the information obtained is morphology of crystal aggregates, crystal shape and size, and morphology of crack patterns. [170] With the increase in advanced analytical methods including Raman spectroscopy and FT-IR spectroscopy, more information beyond the aforementioned traditional droplet analysis can be interpreted from the same droplet. When combining

vibrational spectroscopy with droplet coating method for clinical application, one important issue is to find out the proper measurement positions representing the whole sample area. However, it needs to be less time consuming and can produce data with high signal-to-noise ratio. To answer this question, PCA analysis of vibrational spectra combining with drop coating deposition technique on different biomedical applications will be discussed. As examples, the following Raman and FT-IR spectroscopic data will be discussed: a DCM patient undergoing IA treatment, a HF patient undergoing treatment, cardiac patients receiving CABG surgery.

PCA analysis of DCM patient. The DCM patient remained highly depressed (18%) LVEF after 9 months pharmacological HF treatment, and was recommended for IA therapy. IA therapy was given at five different time points (donated as stage - S), the potential of vibrational spectra to characterize these five different stages to follow up therapy outcome was studied. Here the PCA analysis for different regions of dried droplet is performed and the PCA scatter plots for inner region, outer ring and whole droplet of plasma and serum obtained via Raman spectroscopy are shown in Figure 19. The Raman spectra from different collection locations of the droplet form similar cluster patterns as observed in the PCA scatter plot, and the lowest intra-group scattering is obtained when the Raman spectra from the whole droplet are used, thus have a better discrimination of different IA treatment time points. For FT-IR spectra, data were collected from five randomly chosen mapping images, the information regarding inner and outer was not captured, thus FT-IR spectra are not discussed for this patient here.

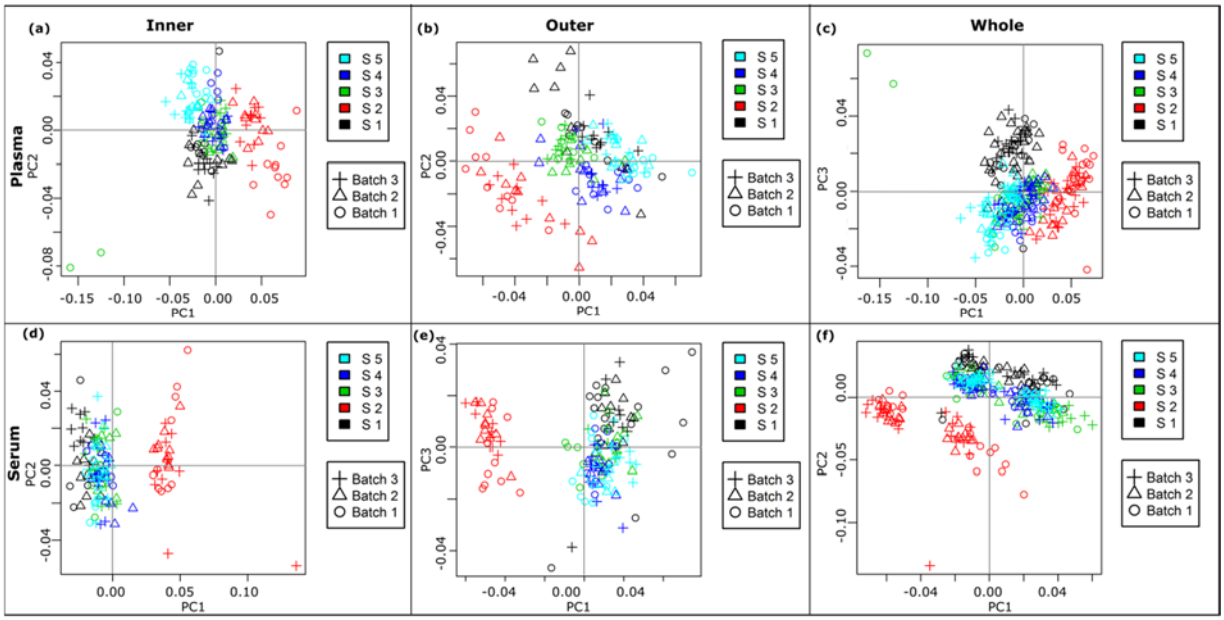

Figure 19 PCA analysis of Raman spectra of inner and outer region from plasma and serum samples from DCM patient underwent IA therapy. (n=1)

PCA analysis of HF patient. HF is a rather complex syndrome in which the heart cannot supply enough blood to the body, resulting from various structural or functional cardiac abnormalities. Raman and FT-IR spectra from inner region, outer ring, and whole droplet based on plasma sample are used for PCA analysis, the results are shown in Figure 20. For

Raman data (Figure 20 (a, b, c)), the molecules located in inner, outer or the whole droplet can deliver the information responding to different treatment stages. But for FT-IR case (Figure 20 (d, e, f)), it is clear that only the spectra from inner region can separate the three different treatment stages, neither the spectra collected from outer region nor from the whole droplet can differentiate the three stages. For this case, the signal from inner region captures disease specific information, hence the measurement points from inner region are recommended. However, for serum sample, Raman data collected from these three geometry cannot be separated into different treatment clusters, while the FT-IR data show similar patterns as in Figure 20(d, e, f), results are not shown in the thesis.

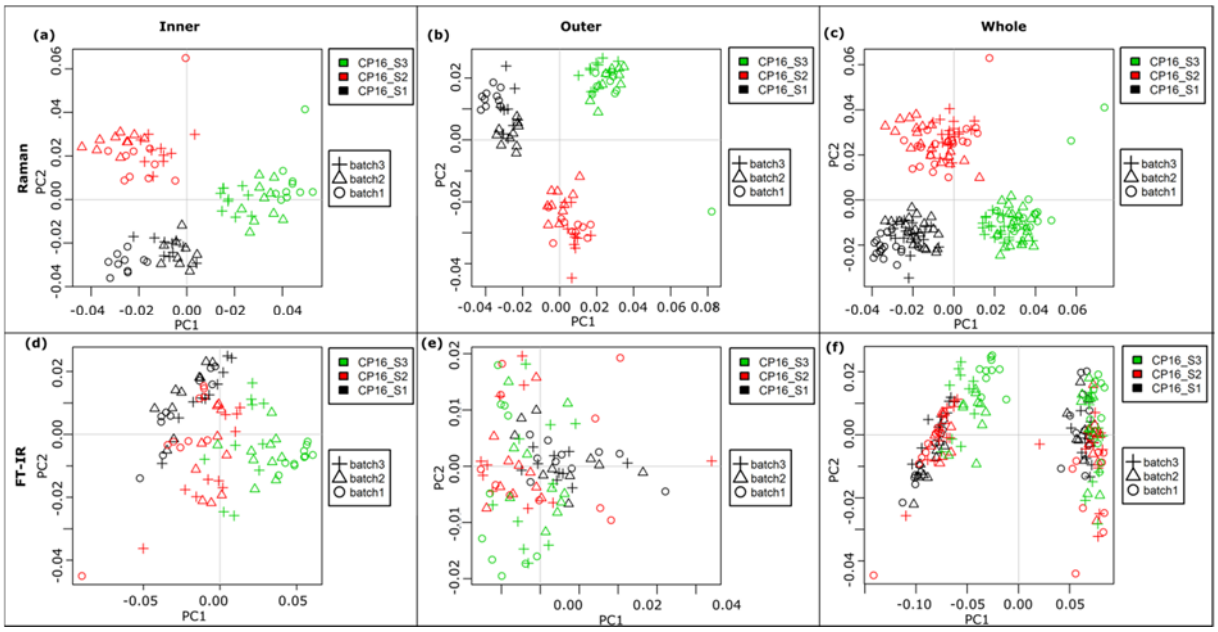

Figure 20 PCA analysis of vibrational spectra of inner and outer region from plasma sample from HF patient. (n=1)

PCA analysis of CABG patients. When the coronary artery was obstructed due to arteriosclerosis or fat deposition on the wall of artery, the patients suffers from severe coronary heart disease. These patients usually undergo cardiac surgery, especially CABG to improve blood flow to the heart. To evaluate changes in the blood, plasma samples were collected before surgery (BS) and after surgery (AS). PCA analysis for Raman spectra and FT-IR spectra collected from inner region, outer ring, and whole droplet of plasma are represented for two different CABG patients as shown in Figure 21 and Figure 22.

From Figure 21, it is observed that the Raman and FT-IR spectra from inner region, or from outer region, or from the whole droplet can separate the plasma samples regarding to BS and AS. For this patient, the spectra collected from just inner or outer ring are sufficient. This measurement geometry holds true for ten of the fifteen CABG patients, data are not showed. However, for the second patient, this is not true.

When the same PCA analysis was performed to the plasma sample from the second CABG patient, the spectra from either inner region or outer ring perform differently to the whole droplet. The spectra only from the inner region or outer ring can be differentiated into two clusters, while the spectra from the whole droplet are not clustered into corresponding

separate groups. For this case, the spectra from either inner region or outer ring are suggested, but not the spectra from whole droplet. This geometry is applicable for other four CABG patients, which data are not shown.

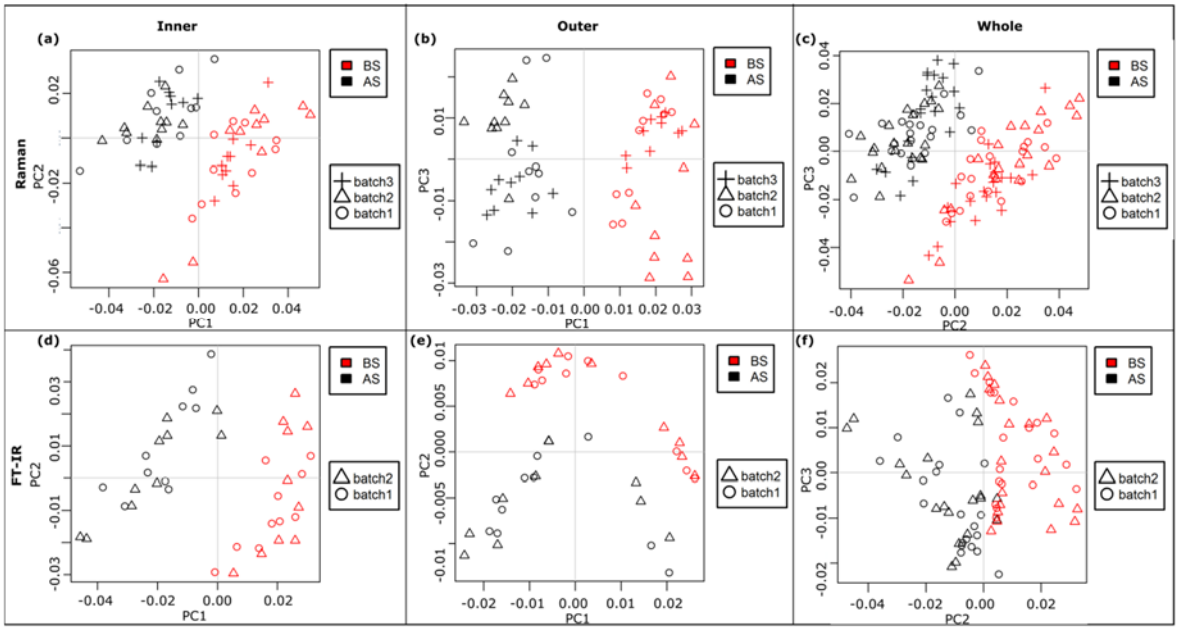

Figure 21 PCA analysis of vibrational spectra of inner and outer region from plasma sample from CABG patient I. (n=1)

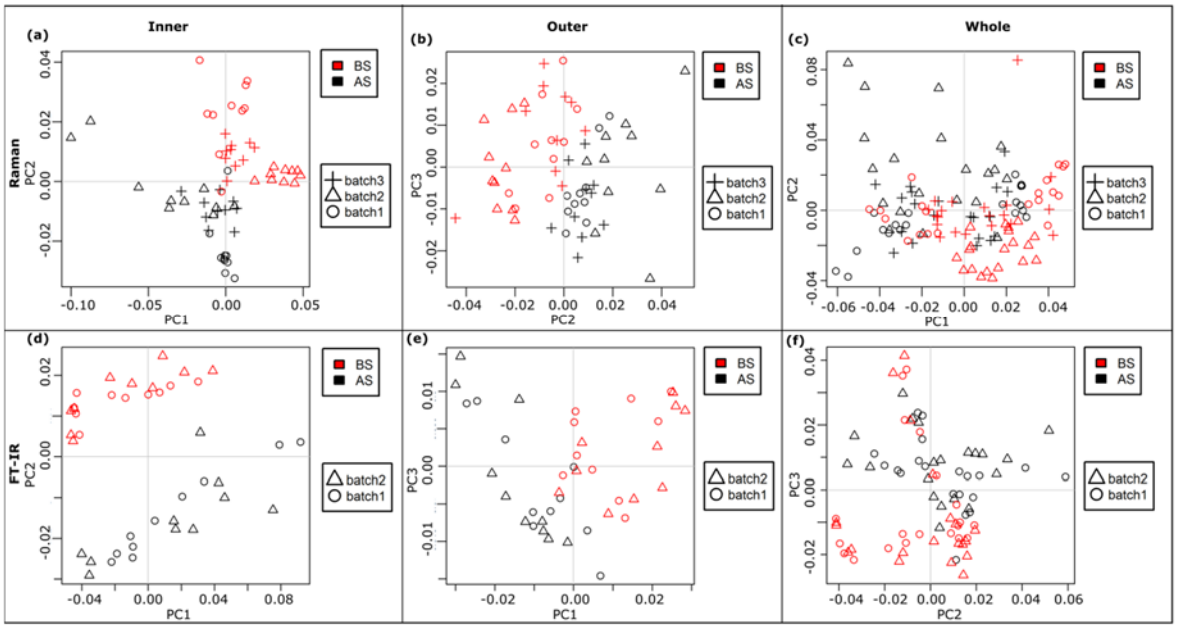

Figure 22 PCA analysis of vibrational spectra of inner and outer region from plasma sample from CABG patient II. (n=1)

Summary and discussion. When a dried droplet is formed on a solid substrate, the distribution of different biomolecules will be separated due to the coffee-ring effect and the reverse Marangoni power. The microscopic morphologic image from the droplet show different patterns formed by different biomolecules at different regions of the dried droplet. The different distribution due to various biomolecules will relate to specific biochemical

fingerprint. This is confirmed by the spectra comparison, PCA analysis and PC loadings from inner region and outer ring which is show in Figure 14, Figure 16 and Figure 17 individually. The spectra intensity is much higher for the biomolecules from the outer ring than from inner zone. Even though the proteins are pre-concentrated in the outer ring via drop coating method, the best measurement geometry varies depending on different cases when applied for real biomedical applications. The consideration of whole droplet with equal collecting points from inner and outer is better for DCM case. But for the HF patient, FT-IR spectra collected only from inner is able to be differentiated into corresponding treatment stages. While for CABG application, the schematics of equal measurement positions from whole droplet and from either only inner zone or outer ring is suggested for different patients.

When seeking biomarkers in blood sample, many studies have been performed. Since the abundant albumin and IgG dominate the vibrational spectroscopic signals, depletion of those abundant proteins can be applied if the interested biomarkers are masked by the signal of those abundant proteins. However, the depletion can remove some information for the unknown biomarkers of interest, thus the intact sample will be a more appropriate choice in this case. Based on the results and discussion above, when combing the vibrational spectroscopy to search biomarkers on plasma or serum samples, the measurement geometry of equal collection positions from inner zone and outer ring will be suggested. By this schematic, the consideration of different biomolecules in the whole sample will be included, and the contribution of different biomolecules can be studied when taking into account of the different morphology and distribution of biomolecules at different regions of the dried droplet.

3.2 Application of vibrational spectroscopy to cardiac diseases: diagnostics and treatment control

Based on the previous sections about technical development for using blood as sample for spectroscopic analysis, this section will move to the biomedical applications on cardiac diseases.

3.2.1 Vibrational spectroscopic differentiation of patients suffering from various cardiac diseases

Sample cohort. 18 patients undergoing different cardiac disorders were recruited in the study (Ethic number: 4736-04/16). One patient was diagnosed with DCM, one was characterized as TTC, one was HF, and other patients had different cardiac conditions which are not yet unblinded. One $9ml$ EDTA blood and one $9ml$ serum blood were collected from each patient. As reference control, healthy volunteers were also recruited with 7 plasma and 10 serum samples individually.

Vibrational spectra for cardiac patients. Since the 18 cardiac patients had different cardiac disorders, the physiopathology and clinical presentations were characterized to be different. The differences can influence the Raman and FT-IR spectra. Thus the mean spectra of Raman spectroscopy and FT-IR spectroscopy was calculated and shown in Figure 23. From Figure 23, it is observed that 17 cardiac patients have similar Raman profiles for both plasma and serum sample, except for the cardiac patient with ID CP04 which has very distinct Raman spectra from others. However, when considering FT-IR spectra, the distinctiveness of CP04 is vanished; all the 18 cardiac patients share similar FT-IR fingerprints. More information can be interpreted if the clinical information of these patients were known, whereas the clinical information is still waiting to be provided by the collaborating physician doctor.

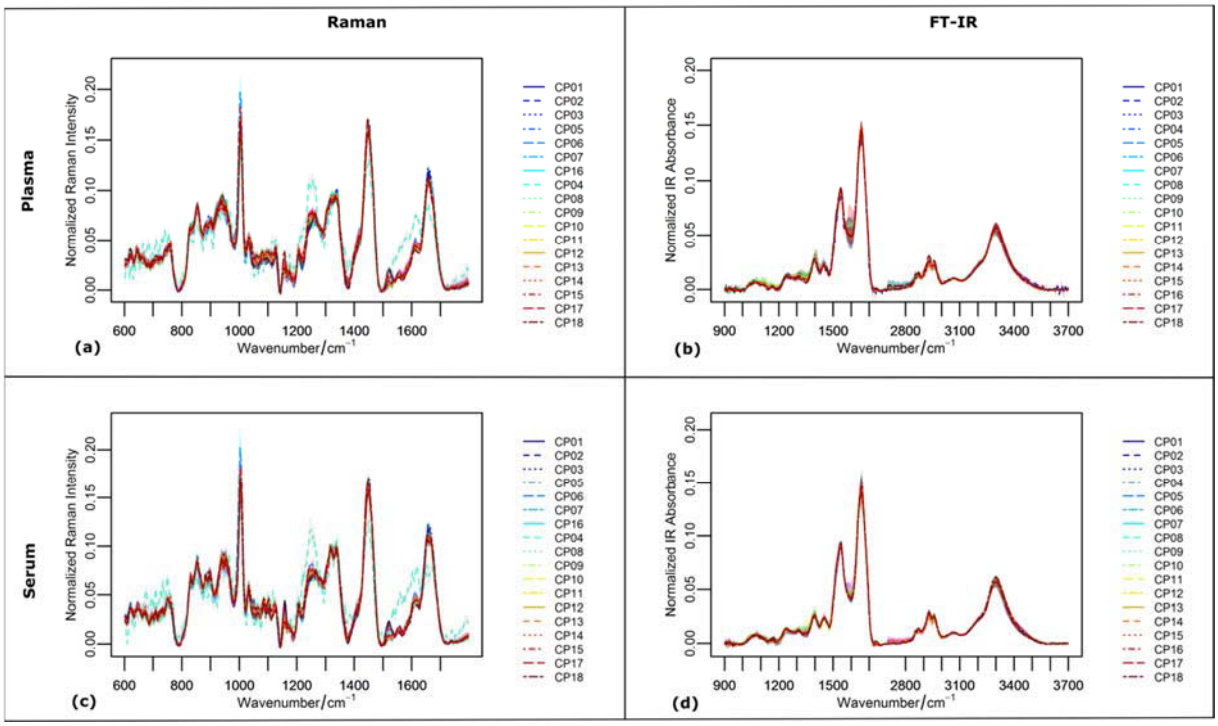

Figure 23 Vibrational spectra of plasma and serum sample from cardiac patients. Left panel: Raman; right panel: FT-IR. Top panel: plasma; low panel: serum.

PCA analysis for cardiac patients. To better visualize the similarity and difference between the 18 cardiac patients, PCA analysis was performed, and the corresponding PCA scatter plot and PCA loadings are shown in Figure 24 and Figure 25 respectively. The distinctiveness of CP04 from Raman spectra was confirmed via the clusters on the left panel in Figure 24. The distinctiveness is mainly from the contributions of proteins as observed from the corresponding loadings shown in the left panel of Figure 25, where PC1 separates patient CP04 from others. CP01, CP02, CP03, CP05, CP16 and CP17 are grouped together with negative scores of PC1 and positive scores of PC2 in Figure 24 (a) and (c).; whereas CP06, CP15 and CP07 are clustered into one group due to negative scores of PC1 and PC2. For FT-IR spectra, different clusters were formed based on the FT-IR contributions as observed from PCA loadings shown on the right panel in Figure 25. For plasma sample, CP02 and CP13 are quite distinct from others; while other patients are clustered closely which indicates the similarity among them. But for serum sample, CP11 clusters separately, CP06, CP07, CP13, CP15 and CP18 cluster close to each other according to negative scores of PC2 shown in Figure 24 (d).

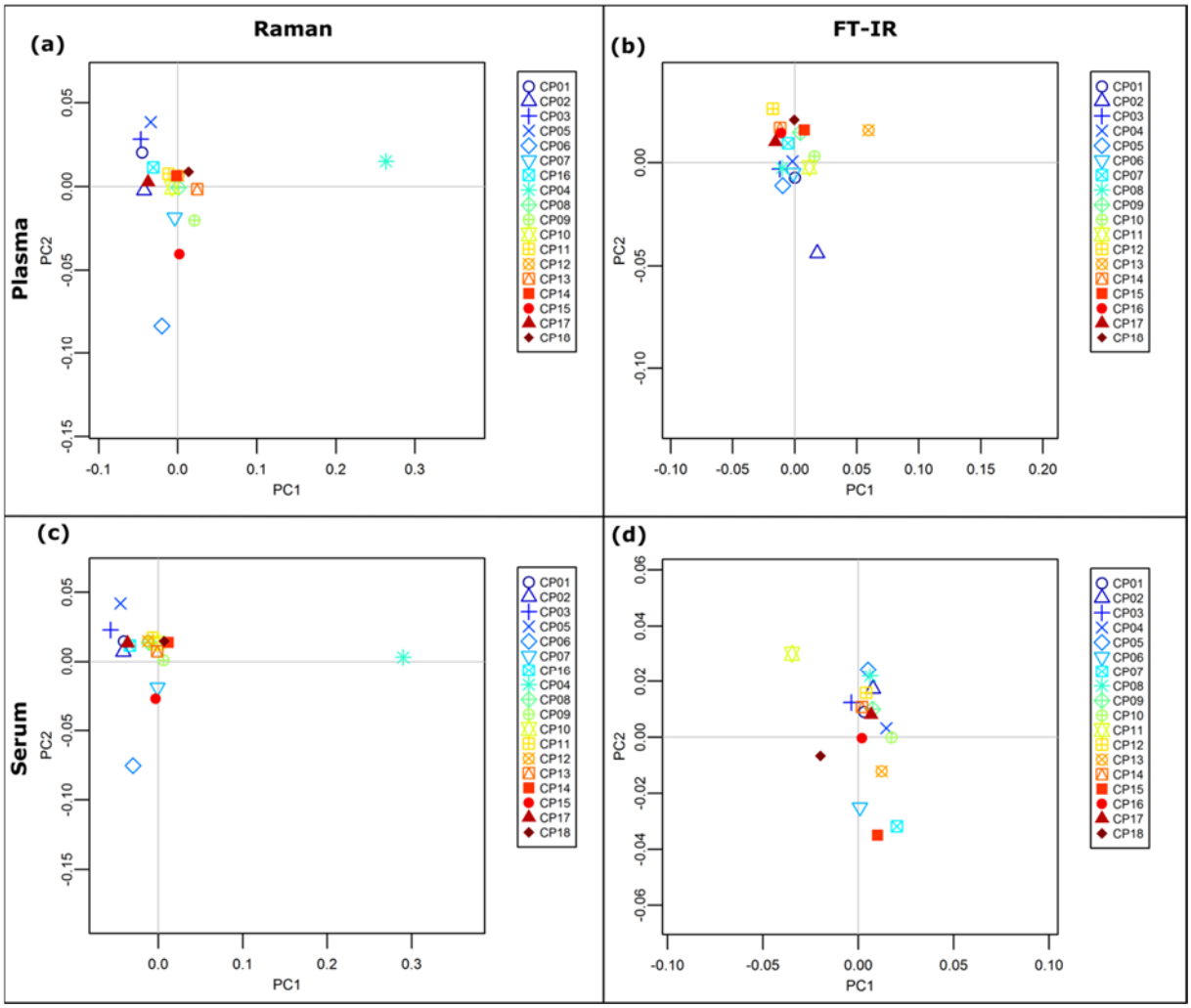

Figure 24 PCA scatter plots of plasma and serum sample from cardiac patients. Left panel: Raman; right panel: FT-IR. Top panel: plasma; low panel: serum.

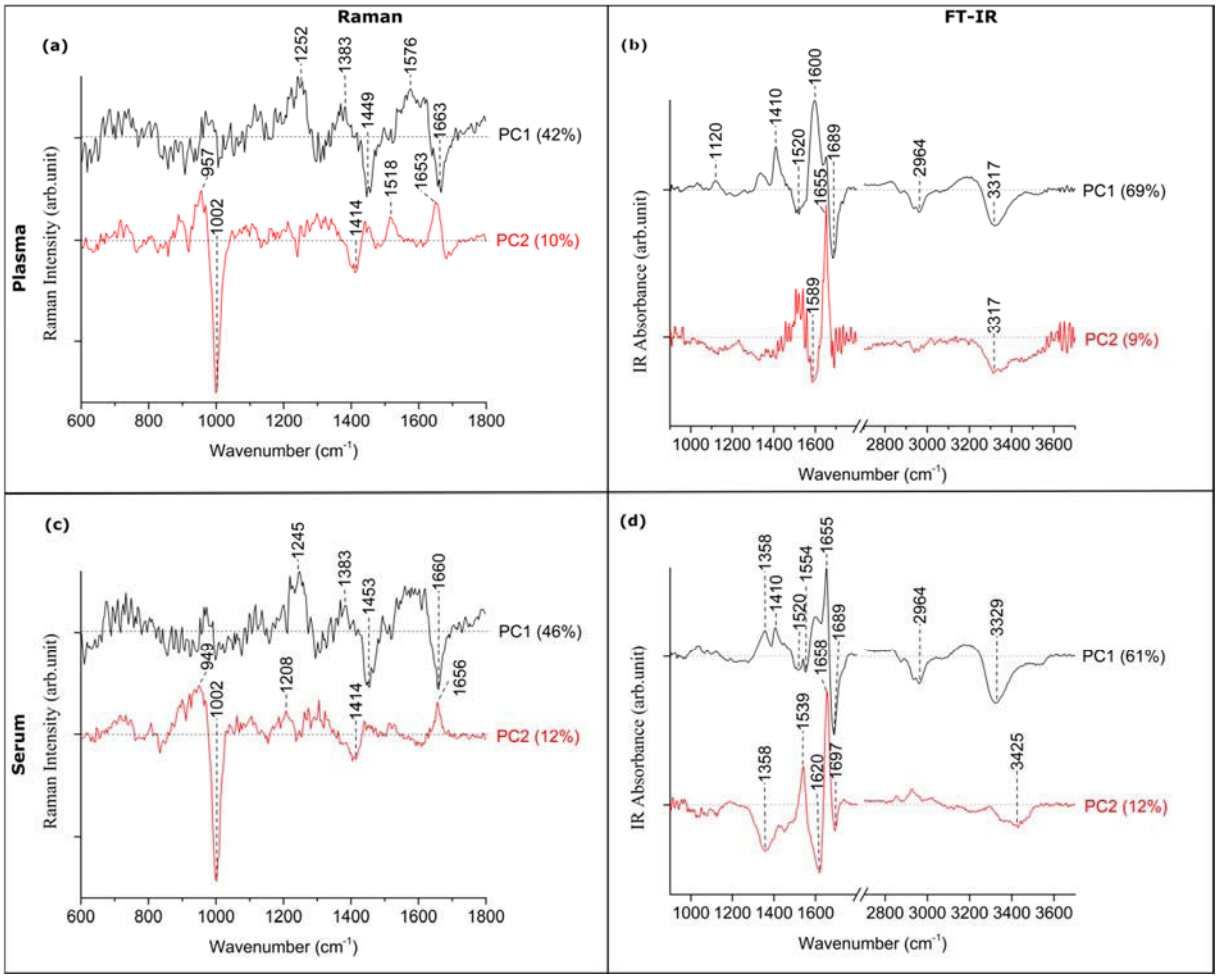

Figure 25 PCA loadings of plasma and serum sample from cardiac patients. Left panel: Raman; right panel: FT-IR. Top panel: plasma; low panel: serum.

Vibrational spectra from healthy donors and cardiac patients. The 18 cardiac patients had different cardiac disorders, the vibrational spectra from these cardiac disorders and healthy donors were compared and shown in Figure 26. From Figure 26 (a) and (c), the difference between the healthy donors and cardiac patients based on Raman spectra are clearly observed while these differences are not so pronounced for FT-IR spectra in Figure 26 (b) and (d).

To better visualize and interpret the differences, difference spectra between healthy donors and cardiac patients were calculated and shown in Figure 27. The contributions to differentiate healthy donors and cardiac patients are mainly from proteins with the Raman spectra from amide III, amide I, and FT-IR spectra from amide II and amide I. Moreover, carotenoids play a role in the difference between the healthy and cardiac disorders indicated by Raman spectra around $1158cm^{-1}$ and $1520cm^{-1}$. [171, 172] The contribution of carotenoids can be due to its antioxidant properties such as scavenging free radicals like reactive oxygen species, lipid peroxyl radicals and nitric oxide. Carotenoids can protect the circulating low density lipoproteins from oxidation and decrease the number of cholesterol being carried into blood stream. In some studies, lycopene (member of carotenoids family) has shown to lower the risk of CVD through reducing serum cholesterol level. [173-175]

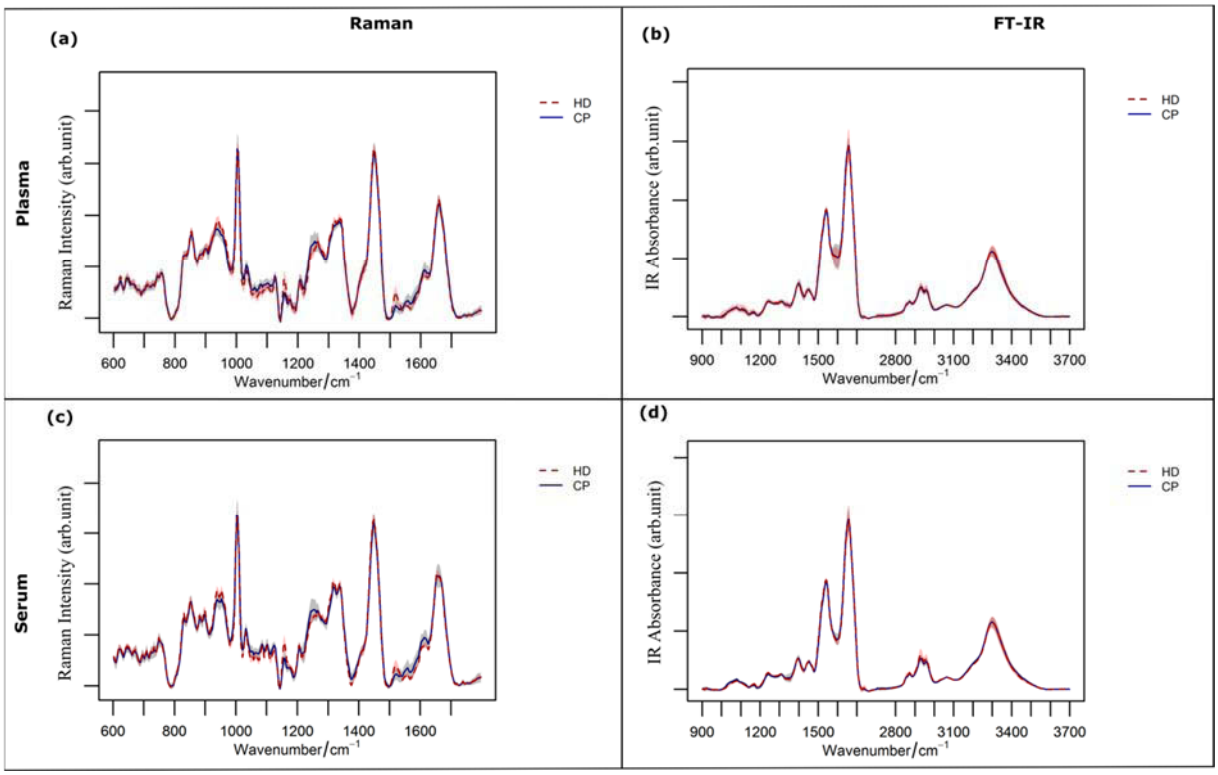

Figure 26 Vibrational spectra of plasma and serum sample from healthy donor (HD) and cardiac patients (CP). Left panel: Raman; right panel: FT-IR. Top panel: plasma; low panel: serum.

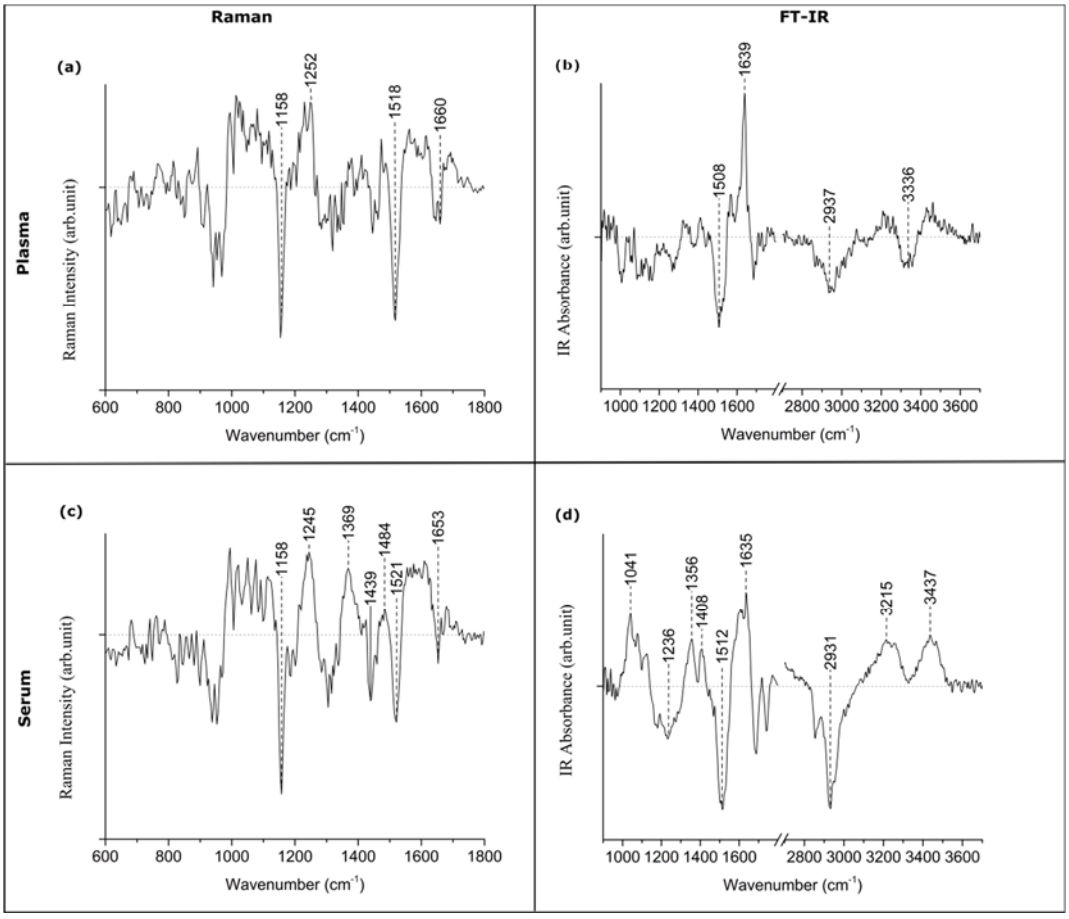

Figure 27 Difference spectra of plasma and serum sample from healthy donor (HD) and cardiac patients (CP). Left panel: Raman; right panel: FT-IR. Top panel: plasma; low panel: serum.

PCA analysis of vibrational spectra from healthy donors and cardiac patients. Unsupervised PCA analyses were performed based on the dataset from healthy donors and cardiac patients. The PCA scatter performances were different based on the corresponding Raman (Figure 28 (a) and (c)) or FT-IR spectra (Figure 28 (b) and (d)) according to the contributions from respective PCA loadings on Figure 29. For Raman dataset, CP04 is very distinct from either the healthy donors or other cardiac patients, as indicating by the yellow-filled circle in Figure 28 (a) and green-filled circle in Figure 28 (c). The healthy donors were differentiated from cardiac patients mainly due to the carotenoids, confirmed by the negative contributions around $1158cm^{-1}$ and $1520cm^{-1}$ shown in Figure 29 (a) and (c) [171, 172]. PC2 clusters health into negative scores (see Figure 28 (a) and (c)), these negative scores correlate with the negative bands of carotenoids in Figure 29 (a) and (c), giving a hint of higher presence of carotenoids in health than in cardiac patients [174, 175].

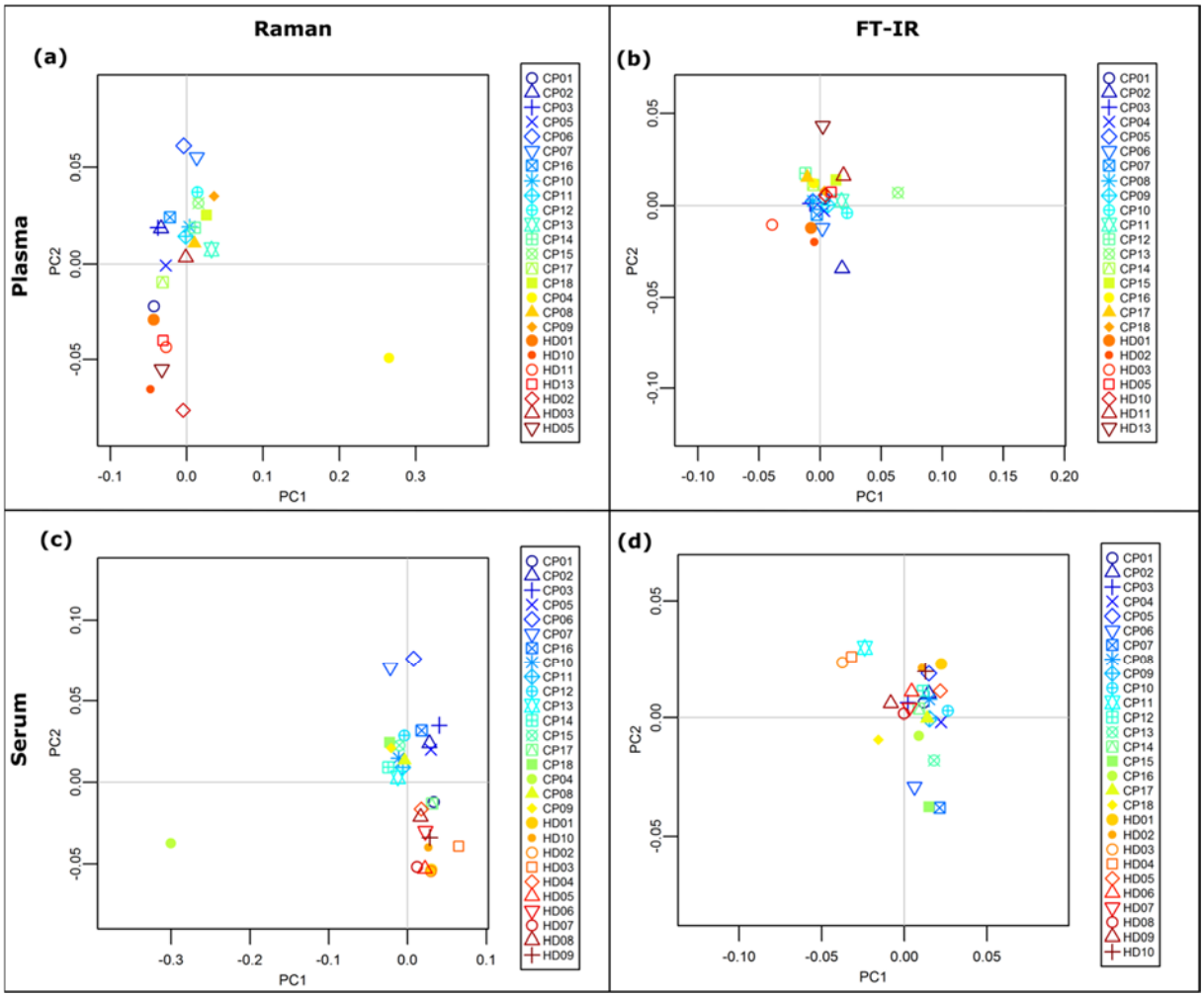

Figure 28 PCA scatter plots of plasma and serum sample from healthy donors (HD, plasma: n=7; serum: n=10) and cardiac patients (CP, n= 18). Left panel: Raman; right panel: FT-IR. Top panel: plasma; low panel: serum.

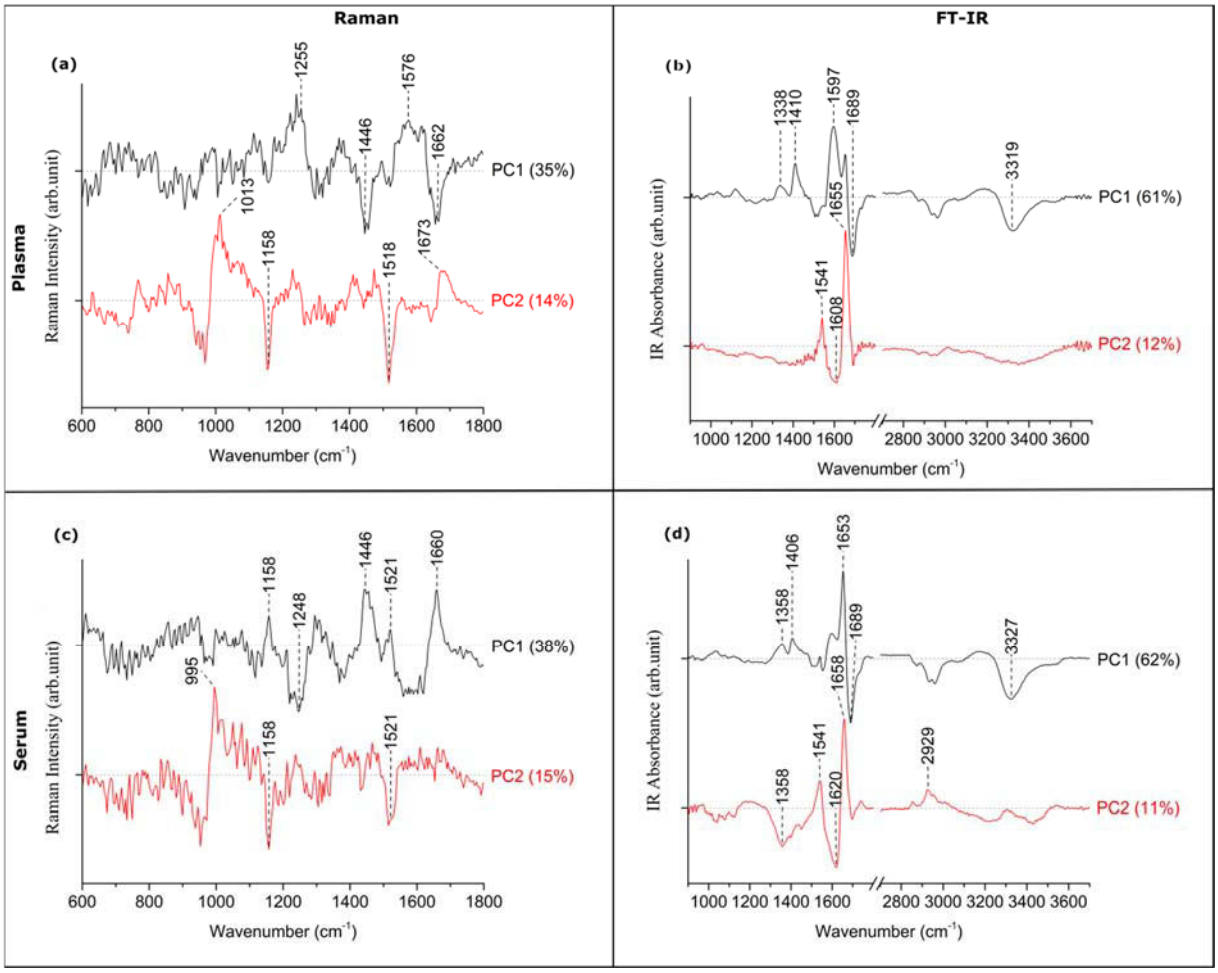

Figure 29 PCA loadings of plasma and serum sample from healthy donor (HD) and cardiac patients (CP). Left panel: Raman; right panel: FT-IR. Top panel: plasma; low panel: serum.

Summary and discussion. CVD is various and the research to investigate CVD has begun long time ago and are still undergoing as hot topics. By the combination of advanced analytical methods such as Raman spectroscopy and FT-IR spectroscopy in combination with chemometric approaches, the 18 patients with different cardiac disorders are clustered into different groups, the PCA loading indicates different biomolecular contributions. More details from the studied spectral data can be interpreted if the clinical information can be provided by the collaborating physician doctor. When considering the healthy and CVD cohorts, carotenoids play a key role between these two cohorts. The less presence of carotenoids in CVD cohort can be an indication to characterize cardiac disorder.

This study demonstrates the potential of vibrational spectroscopy to characterize different cardiac conditions. Two studies of different treatments response to different cardiac disorder will be introduced and discussed in the following sections, these include the follow-up of immunoadsorption therapy in dilated cardiomyopathy using vibrational spectroscopic methods in section 3.2.2 and vibrational spectroscopic investigation of patients undergoing coronary artery bypass grafting in section 3.2.3.

3.2.2 Immunoadsorption therapy follow-up for dilated cardiomyopathy using vibrational spectroscopic methods

Patient characteristics. After informed consent (Ethic number 4736-04/16), a 52-year old female patient was selected for this study. DCM was characterized by severely depressed LVEF (15%) via echocardiography and left ventricular angiography. CAD was excluded through coronary angiography method. The patient was treated with completion of pharmacological HF treatment for 9 months, but LVEF still remained as 18% severely depressed. Therefore, IA treatment was suggested for this patient which is a certified therapy in Germany financed by the health care insurance system after individual application.

Blood samples including EDTA blood and serum blood were collected from the patient. This study was performed according to the Helsinki Declaration which was revised in 2013. Blood samples were collected at five different time points according to the IA treatment, which represent five different treatment stages (see Figure 30).

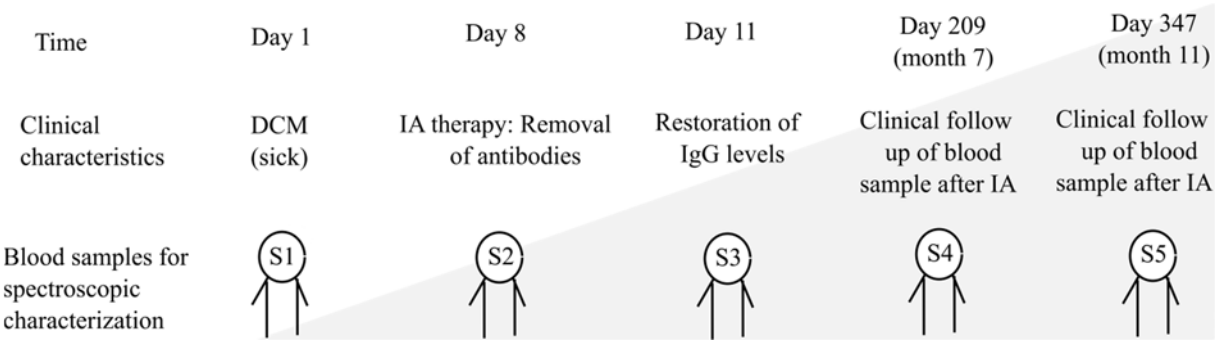

Figure 30 Schematics showing treatment stages (S1-S5) and blood sampling time points

For the reference samples, albumin powder (bovine serum, Merck) was dissolved into sterile ultra-pure water (Ampuwa, KabiPac) to yield a physiological concentration of $40mg/ml$, while stock IgG solution of $5mg/ml$ (rabbit, Abcam) was used directly. The reference samples were also prepared as described in Section 2.2.7, but without dilution for FT-IR experiments.

Immunoadsortpion (IA). This DCM patient was undertaken in one IA course. After 5 consecutive IA treatment session days at day 5, $0.5g/kg$ polyclonal IgG (Venimmun N, ZLB Benning, Switzerland) was substituted according to the protocols published [80]. Following is a brief description of IA therapy: blood is separated into plasma and cellular constitutes by filtering; then the filtered plasma goes through protein-A IA absorber columns, which contain immunoadsorber for IgG (Immunosorba, Fresenius Medical Care AG, Germany). After the depletion of IgG, the filtered plasma is reinfused back to the DCM patient. IA system being used in this study is a double-column system, where one absorber column is perfused with plasma while the other is being regenerated at the same time. During IA process, anticoagulation is performed with intravenous infusion of anti-coagulate additives as heparin, and/or with citrate if needed additionally. The follow-up of the treatment was assessed by clinical examination based on blood sample and echocardiography.

Spectra of plasma, serum, albumin and IgG. Figure 31 shows vibrational spectra of IgG, albumin, serum and plasma prior to IA treatment. Typical vibrational fingerprints of proteins are shown, which compose as the major components of dried plasma and serum. A detailed band assignment is shown in Table 5. Albumin is the most abundant blood plasma protein accounting for most 55% of all blood plasma proteins, and the spectra of albumin and blood samples are expected to share similar Raman and FT-IR patterns as shown in Figure 31. The second most predominating proteins are Ig; which constitute about 38% of blood plasma proteins while IgG is the major contributions for all Ig with a percentage of 75. IgG is rich of ß-sheet structure reflecting Raman bands around $1240cm^{-1}$ in amide III and around $1672cm^{-1}$ in amide I. [92, 121] However, the IR spectra have a broader bandwidth of ca. $59cm^{-1}$ around $1642cm^{-1}$ (Figure 32), which can be a hint to a preparation-induced denaturation of IgG (unordered segment) [176].

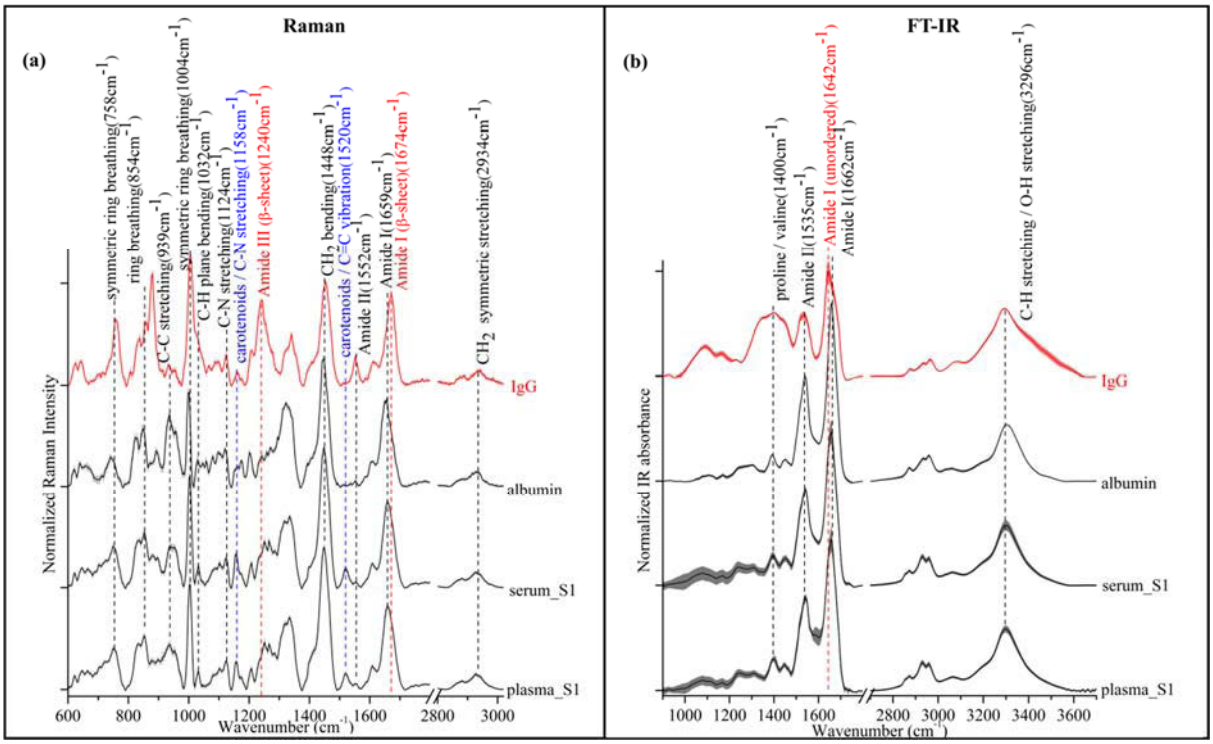

Figure 31 Vibrational spectra of blood samples: left panel: Raman; right panel: FT-IR. From top to bottom: IgG (from rabbit, 5mg/ml), albumin (bovine serum, 40mg/ml), serum and plasma from DCM patient before IA treatment (stage S1). Spectra are shifted along the y-axis for clarity.

Table 5 Assignment of Raman [90-92] and IR bands [93-96, 177] based on literatures

Raman shift (cm^{-1})	IR shift (cm^{-1})	Protein	Nucleic acid	Lipids	Carbohydrate
758		Tryptophan (symmetric ring breathing)			
854		Try, Pro, tyrosine (ring breathing)			
939		C-C stretching backbone (α-helix)			
1004		Phenylalanine (symmetric ring breathing)			
1032		Phe (C-H in plane bending)			
	1038	ν C-0	DNA, RNA		Deoxyribose /ribose
	1078	C-O stretching	$P0^{-}_2$ symmetric stretching /DNA, RNA		Glycogen (C-O stretching) /deoxyribose /ribose
	1118		C-O stretching of RNA	Lipids	
1124		C-N stretching		C-C stretching	
1158		Carotenoids (C=C) /C-C /C-N stretching			
	1170			Ester C-O asymmetric stretching	
1209		Phe, Tyr (C-C_6H_5 stretching)			
1240	1220-1330	Amide III			
1252		Amide III		=CH deformation	
1268		Amide III			
1318		C-H deformation, collagen	G	CH_3CH_2 twist	
1334		CH_3CH_2 wagging	CH_3CH_2 wagging		
	1392	CH_3 deformation		Lipids	
	1398	C=O stretching of COO-			
	1400	Proline /valine			
	1416			CH_3 asymmetric stretching	
1434				CH_2	
1448		CH_2 bending		CH_2 bending	
	1452	CH_2 scissoring			
	1514	Amide II (ß-sheet structures) /δ N-H /ν C-N			
1520		Carotenoids (C=C vibration)			
	1535	CH2 bending /Amide II		CH_2 bending	
1552	1554	Amide II			

	1589	Amide II			
	1642	Amide I (unordered)			
	1655	Amide I (antiparallel ß-sheet /aggregated strand)			
1659	1662	Amide I			
1674		Amide I (ß-sheet)			
	1695	Amide I (antiparallel ß-sheet /aggregated strand)			
	2872	CH_3 symmetric stretching			
	2920	CH_2 symmetric stretching			
	2929			Lipids	
2934		CH_2 symmetric stretching			
	2958	CH_3 asymmetric stretching			
	3282	H-O-H stretching			
	3296	C-H stretching /O-H stretching			

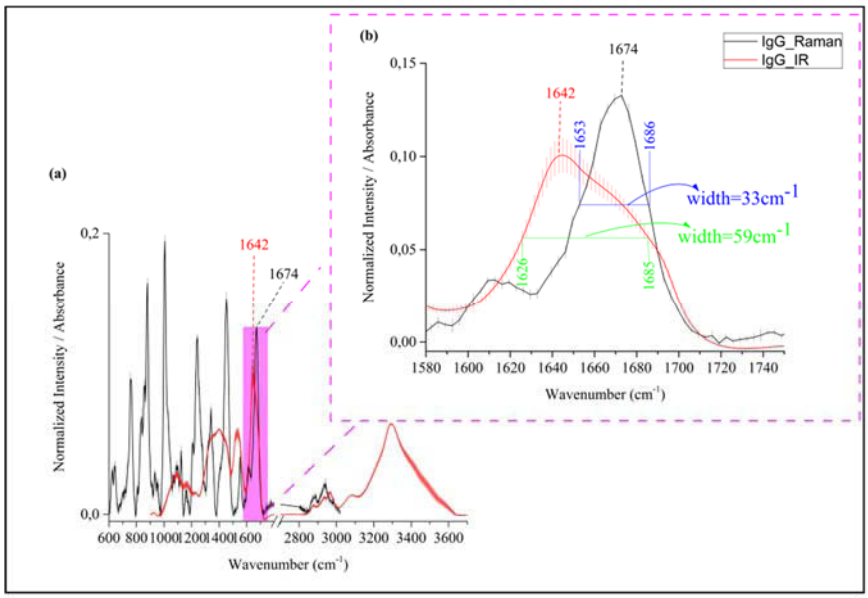

Figure 32 Bandwidth comparison of amide I in IgG from vibrational spectra: Raman $33cm^{-1}$; IR $59cm^{-1}$.

Mean spectra of different IA treatment stages. Figure 33 show the vibrational spectra of plasma and serum samples from the five different stages for Raman and FT-IR respectively, the corresponding spectra share very similar spectral patterns overall, and only minor changes are detected.

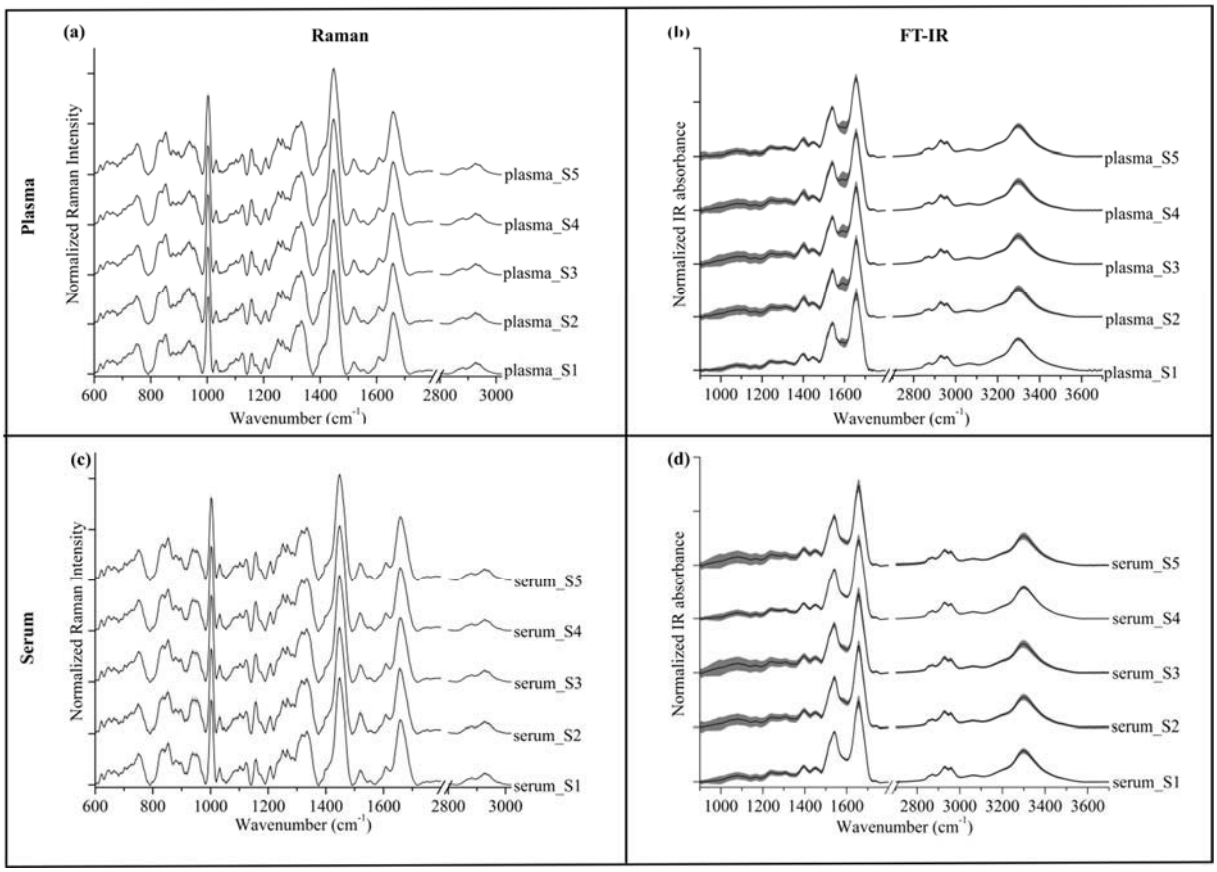

Figure 33 Mean spectra with standard deviation (shadows) of different stages during IA treatment: Left panel: Raman; right panel: FT-IR; top panel: plasma; low panel: serum.

Difference spectra between different IA stages. To better interpret variations in the chemical composition of plasma and serum samples and visualize changes in chemical composition from the detected vibrational spectra between different IA treatment stages, two sets of difference spectra are calculated. One set is based on the difference between all stages and stage 2 shown in Figure 34, because largest variations are expected to occur at S2. A similar pattern can be seen for all computed difference spectra. For Raman spectra, dominant variations occur around $1158cm^{-1}$ (positive), $1240cm^{-1}$ (negative), $1520cm^{-1}$ (positive) and $1674cm^{-1}$ (negative). For FT-IR spectra, significant changes show in $1597cm^{-1}$ (positive), $1642cm^{-1}$ (negative) and $1662cm^{-1}$ (positive).The negative bands imply higher spectral intensities in other stages than at S2, while positive bands mark spectral features that are more prominent in S2. The positive bands around $1158cm^{-1}$ and $1520cm^{-1}$ from Raman spectra indicate that carotenoids increase immediately after IA therapy (difference spectra S2-S1), thereafter decrease (difference spectra S2-S3, S2-S4, S2-S5). Negative bands around $1240cm^{-1}$and $1674cm^{-1}$ from Raman spectra and 1642cm^{-1} from FT-IR spectra can be due to variations of IgG during IA treatment. The concentration of anti-cardiac antibodies (and related Igs) is expected to be lowest at stage 2 due to active removal during therapy, and increase after stage 3 as a result of IgG restoration.

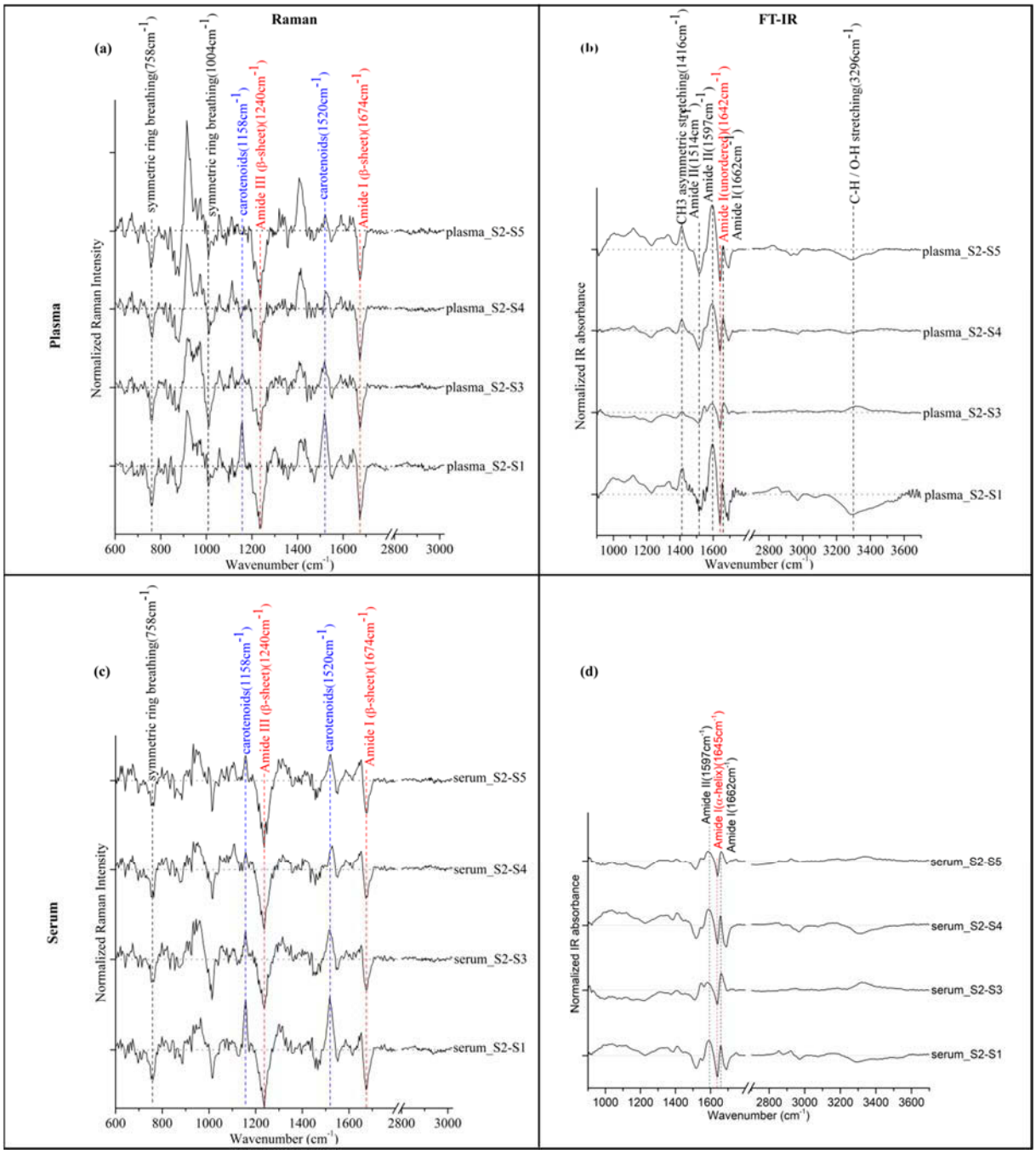

Figure 34 Difference spectra between S2 and other stages during IA treatment: left panel: Raman; right panel: FT-IR; top panel: plasma; low panel: serum.

The other different set of difference spectra are based on consecutive treatment stages (Figure 35). Figure 35 clearly shows that major changes appear in the difference spectra at which S2 is involving. In other words, the strong negative bands around $1240cm^{-1}$ and $1674cm^{-1}$ from Raman difference spectra give a hint of higher protein content at S1 than at S2, whereas the same bands are found as positive contributions in the Raman difference spectra between S3 and S2. These phenomena can be explained by the removal of IgG at S2 but the restoration of antibodies at S3 as result of the substitution of fresh, pooled IgG. Other major positive bands observed in Raman difference spectra between S1 and S2 around $1158cm^{-1}$ and $1520cm^{-1}$ are characteristics for C-C and C=C vibration from the contributions of carotenoids. Although carotenoids are well-known antioxidants, its level are found to relate to

fruit and vegetable uptake, [178] thus no further discussion about the variation of carotenoids will be given here due to the limited sample size of only one patient in this study. For difference spectra between S4 and S3, and between S5 and S4, the visible gentle variations can be a hint of the stable situation and well recovery of the patient almost one year after IA therapy. For FT-IR difference spectra shown in Figure 35, significant peaks around $1597cm^{-1}$, $1642cm^{-1}$, and $1662cm^{-1}$ are observed, which are mainly from proteins. The changes of these fingerprints can also be explained by the depletion and restoration of antibodies corresponding to IA treatment as discussed above.

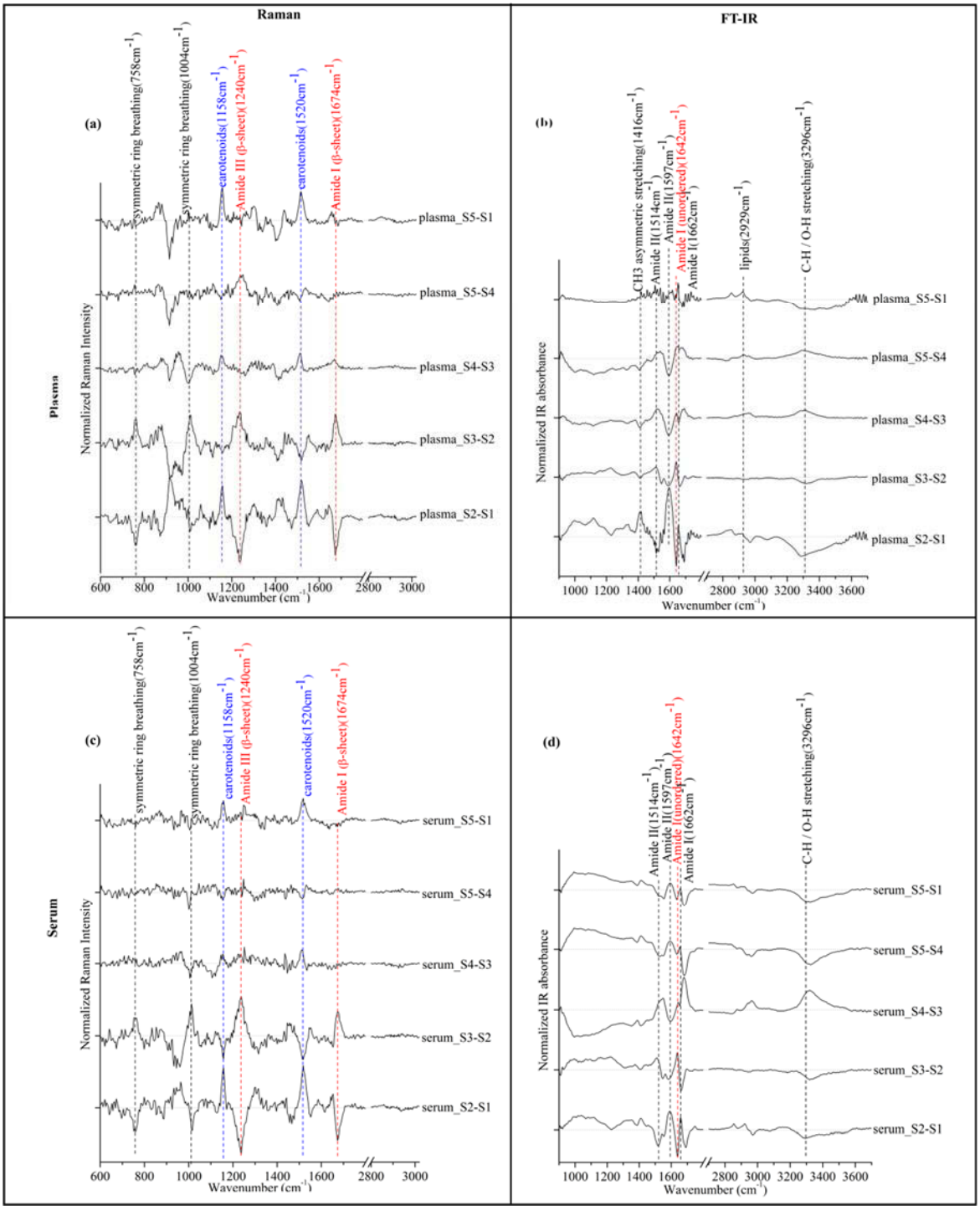

Figure 35 Computed difference spectra between different treatment stages during IA therapy: left panel: Raman; right panel: FT-IR; top panel: plasma; bottom panel: serum.

Correlation of IgG content from immunoturbidimetry and vibrational spectra. As shown in Figure 34 and Figure 35, the most distinct stage during IA treatment is S2 where the concentration of IgG is lowest at this stage due to the removal of anti-cardiac antibodies. The variation of IgG in the blood samples from the five different IA treatment stages was quantified via immunoturbidimetry. The immunoturbidimetry results and the correlated IgG content from vibrational spectra were shown in Figure 36. Raman bands around $1674cm^{-1}$ and IR bands around $1642cm^{-1}$ were chosen to interpreted the intensity of IgG. Similar trend can be observed from Raman data (Figure 36 b, e) and FT-IR data (Figure 36 c, f) as for immunoturbidimetry (Figure 36 a, d). Since anti-cardiac antibodies belong to IgG 3 subclass, by measuring total IgG, the relative IgG content can be accessed indirectly via Raman and FT-IR spectroscopy without the need of immunoturbidimetry.

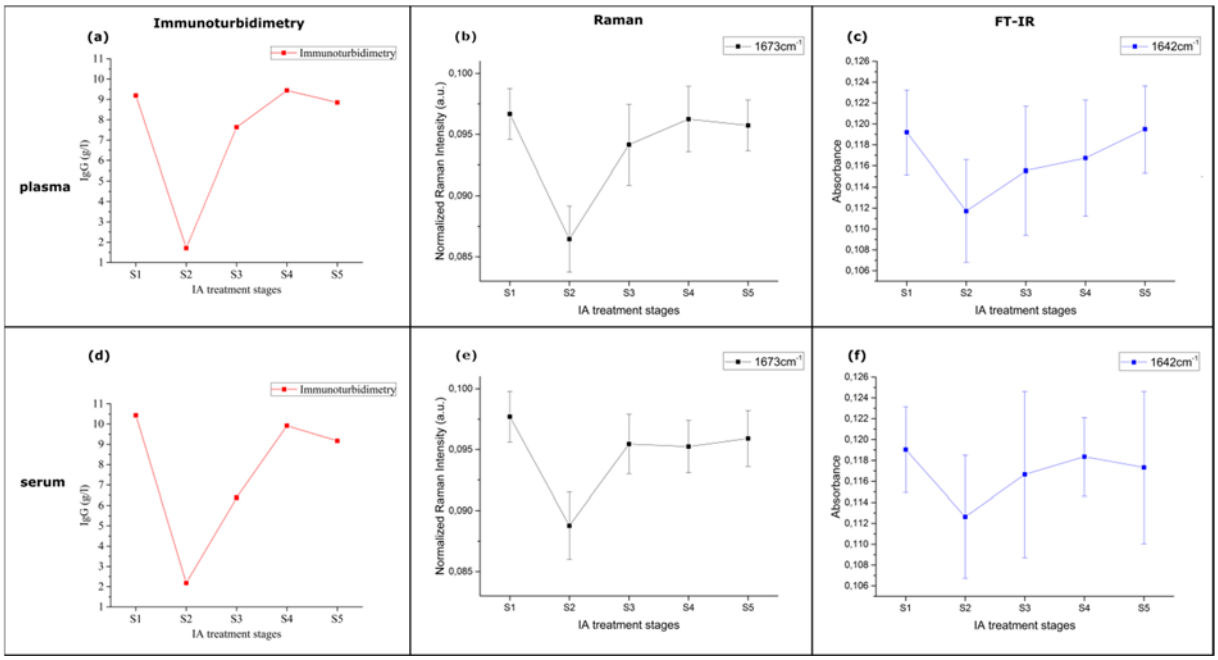

Figure 36 Changes of IgG content during IA therapy as quantified by immunoturbidimetry (a, d) as well as extracted from the vibrational spectra using $1674cm^{-1}$ (Raman: b, e) and $1642cm^{-1}$(FT-IR: c, f). Top panel: plasma, bottom panel: serum.

PCA analysis. Unsupervised PCA analysis was performed to visualized spectral differences and similarities responding to different IA stages and the corresponding PCA scatter plots are shown in Figure 37. Well separated groups representing different IA stages are observed: S2 is obviously grouped far from other stages as result of the removal of anti-cardiac antibodies; S1 is the second most distinct stage; whereas S3, S4 and S5 are likely to be clustered closely with the IgG restoration for these three stages.

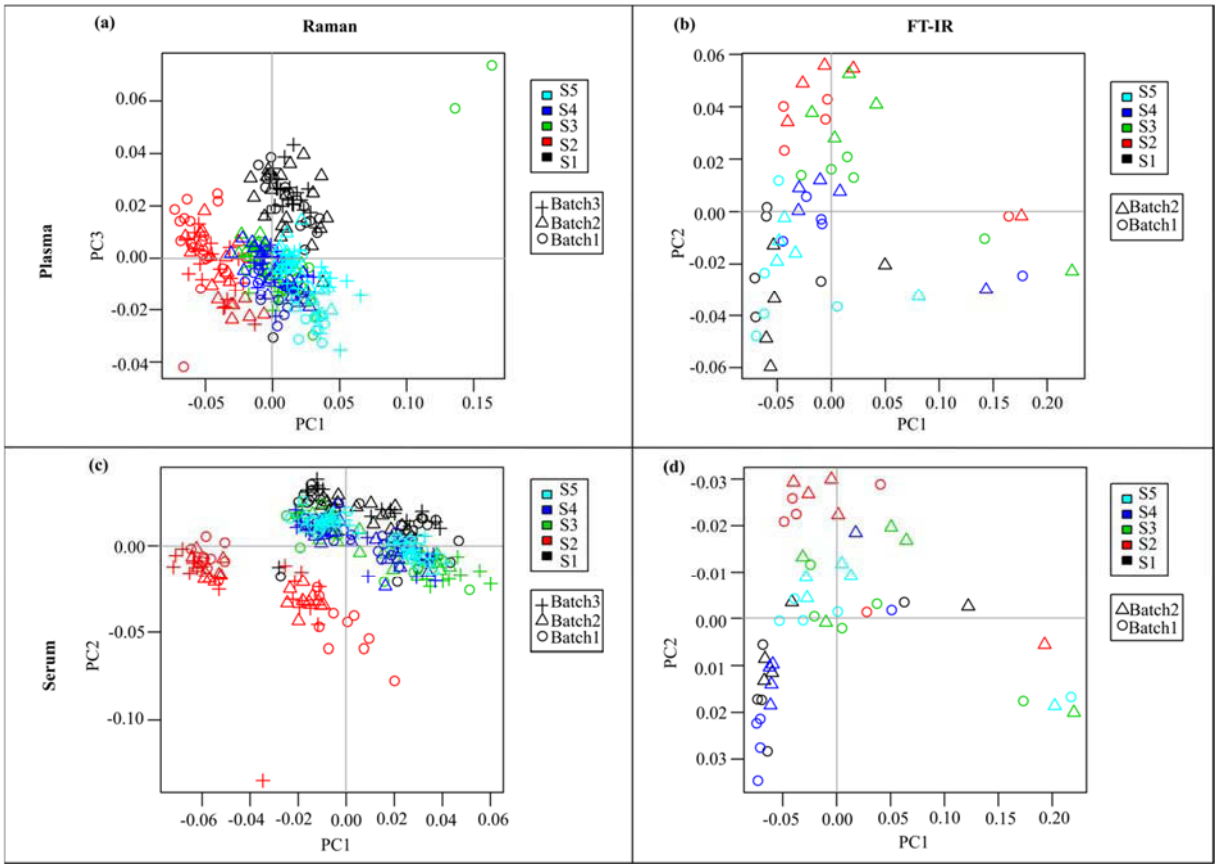

Figure 37 PCA scatter plots for vibrational spectral data: left panel: Raman; right panel: FT-IR; top panel: plasma; bottom panel: serum. All Raman spectra for 5 stages are used, where mean spectra of each scan from two different batches for 5 stages are applied in FT-IR case.

The corresponding loadings for PCA analysis are shown in Figure 38. Separation of different stages from Raman spectral variance is 22.6% for the first principal component on plasma sample and about 19.9% for serum. PC1 from Raman data mainly contains contributions from proteins including $1240cm^{-1}$ and $1674cm^{-1}$ from IgG as discussed above. The corresponding positive peaks in PC1 are hint for higher IgG contents. Carotenoids also play a role with the bands around $1158cm^{-1}$ and $1520cm^{-1}$ in the loadings. For FT-IR data, unordered segment of IgG around $1642cm^{-1}$ is observed for both plasma and serum which differentiate different stages. The main contributions to differentiate the five different stages come from amide II and amide I.

PCA-SVM statistical model. PCA-SVM statistical model was built to differentiate the different five stages. The results for this model are shown in Table 6. For Raman dataset, mean classification accuracy of 96.00% and 89.00% were achieved for plasma and serum samples respectively. Whereas in the case of FT-IR, prediction accuracy of 80.70% and 83.98% were approached for plasma and serum respectively.

Table 6 shows that S3, S4 and S5 are very similar, where most misclassification is observed. If consider these three stages into one stages as after IA, higher accuracies of 99.01% and 97.66% could be achieved for plasma and serum respectively (Table 7).

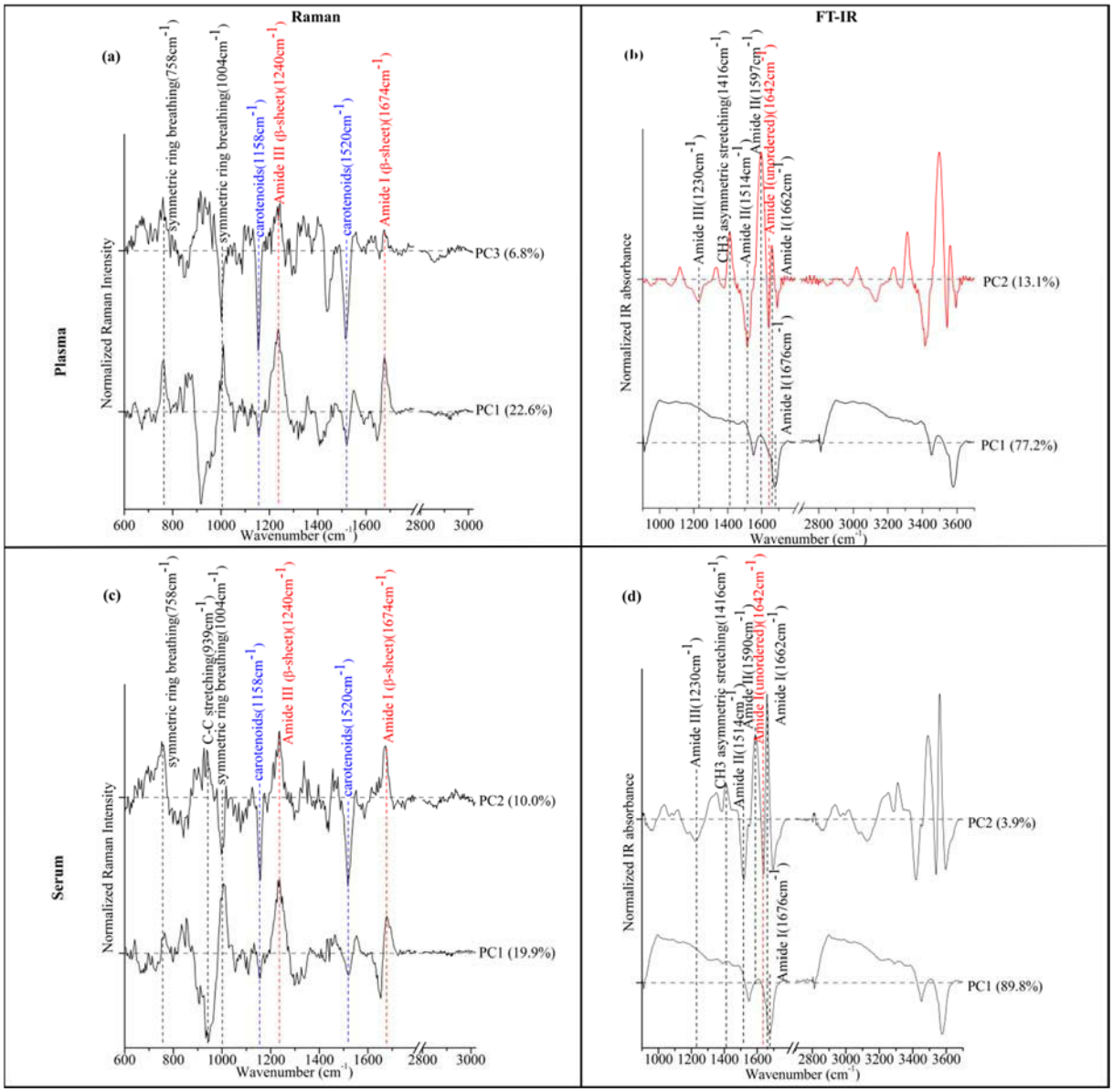

Figure 38 PCA loadings for vibrational spectral data: left panel: Raman; right panel: FT-IR; top panel: plasma; bottom panel: serum.

Table 6 Identification of SVM classification model on single spectra level

Prediction / True		Raman						FT-IR					
		Before IA	After IA	Follow-up of IA			Sensitivity	Before IA	After IA	Follow-up of IA			Sensitivity
		S1	S2	S3	S4	S5		S1	S2	S3	S4	S5	
Plasma	S1	**20**	0	0	0	0	**100.00%**	**4992**	0	7	0	1	**99.84%**
	S2	0	**19**	0	0	1	**95.00%**	0	**4927**	42	20	11	**98.54%**
	S3	0	0	**20**	0	0	**100.00**	0	81	**2180**	1920	819	**43.60%**
	S4	0	0	0	**20**	0	**100.00%**	2	30	849	**3488**	631	**69.76%**
	S5	1	0	2	0	**17**	**85.00%**	43	10	64	296	**4587**	**91.74%**
	Specificity	**98.75%**	**100.00%**	**97.50%**	**100.00%**	**98.75%**		**99.78%**	**99.40%**	**95.19%**	**88.82%**	**92.69%**	
	Accuracy	**96.00%**						**80.70%**					
Serum	S1	**18**	0	0	0	2	**90.00%**	**4930**	18	5	45	2	**98.60%**
	S2	0	**17**	2	1	0	**85.00%**	0	**4994**	3	0	3	**99.88%**
	S3	1	0	**19**	0	0	**95.00%**	17	152	**4487**	117	227	**89.74%**
	S4	0	0	1	**19**	0	**95.00%**	199	6	900	**2366**	1529	**47.32%**
	S5	1	0	0	3	**16**	**80.00%**	58	77	412	236	**4217**	**84.34%**
	Specificity	**97.50%**	**100.00%**	**96.25%**	**95.00%**	**97.50%**		**98.63%**	**98.74%**	**93.40%**	**98.01%**	**91.20%**	
	Accuracy	**89.00%**						**83.98%**					

Table 7 Identification of SVM classification model on single spectra level with combined treatment groups

	Prediction / True	Raman				FT-IR			
		Before IA	**After IA**	**Follow-up of IA**	**Sensitivity**	**Before IA**	**After IA**	**Follow-up of IA**	**Sensitivity**
		S1	S2	S3-S5		S1	S2	S3-S5	
Plasma	S1	**20**	0	0	**100.00%**	**4992**	0	8	**99.84%**
	S2	0	**19**	1	**95.00%**	0	**4927**	73	**98.54%**
	S3-S5	1	0	**59**	**98.33%**	45	121	**14834**	**98.89%**
	Specificity	**98.75%**	**100.00%**	**97.50%**		**99.78%**	**99.40%**	**99.19%**	
	Accuracy	**98.00%**				**99.01%**			
Serum	S1	**18**	0	2	**90.00%**	**4930**	18	52	**98.60%**
	S2	0	**17**	3	**85.00%**	0	**4994**	6	**99.88%**
	S3-S5	2	0	**58**	**96.67%**	274	235	**14491**	**96.61%**
	Specificity	**97.50%**	**100.00%**	**87.50%**		**98.63%**	**98.74%**	**99.42%**	
	Accuracy	**93.00%**				**97.66%**			

Summary and discussion. The results above show that by combining vibrational spectroscopy with chemometric methods, the treatment stages during IA therapy of DCM disorder can be differentiated based on blood plasma and serum samples. The Raman and FT-IR spectra of both plasma and serum are dominated by the contributions from proteins. Characteristic changes can be revealed via different spectra between different IA stages. In particular, S2 is distinct from other stages where all or most anti-cardiac antibodies are depleted. Excellent agreement for the relative changes of IgG content is found when extracting the spectral data and immunoturbidimetry measurement. One very important advantage of vibrational spectroscopy compared to conventional IgG quantification can be that vibrational spectroscopy allows deriving whole chemical information from the studied samples. This case study shows the promising possibility to follow variations in blood samples during IA treatment. Further studies can be elucidated to investigate the potential of non-invasive, label-free manner for the differentiation of responders and non-responders of IA therapy.

3.2.3 Vibrational spectroscopic investigation of patients undergoing coronary artery bypass grafting

Patient cohort. Blood samples were collected before surgery (BS) and after surgery (AS) from 15 patients undergoing CABG (Ethic number: 4004-02/14). Four patients underwent surgery without the use of heart-lung machine (HLM), and the remaining 11 patients had surgery applying HLM. The clinical characterizations of all patients are shown in Table 8. 53% of female were recruited. The average age for these 15 patients was 70.5(± 7.25). Blood hemogram including RBC, WBC (neutrophils, lymphocytes, monocytes and eosinophils), neutrophil to lymphocyte ratio (NLR), monocyte to lymphocyte ratio (MLR), and platelet to lymphocyte ratio (PLR) were recorded. Besides, plasma biomarkers such as interleukin 6 (IL 6), procalcitonin (PCT), C-reactive protein (CRP) and cortisol were also included. Moreover, SOFA scores were documented.

Table 8 Clinical characterization of CABG patients

Demographic and Clinical information		
Patient (n)	15	
Gender		
Female	53%	
Male	47%	
Age	70.5(±7.25)	
BMI	≥23	
Blood Hemogram	**Before surgery (BS)**	**After surgery (AS)**
RBC (Tpt/l)	4.13 (±0.47)	3.43 (±2.07)
WBC (Gpt/l)	6.51 (±2.79)	11.85 (±5.29)
Neutrophils (%)	61.53 (±10.66)	77.87 (±7.02)
Lymphocytes (%)	25.73 (±7.39)	15.20 (±5.03)
Monocytes (%)	8.73 (±2.66)	5.00 (±2.27)
Eosinophils (%)	3.53 (±3.74)	2.07 (±2.69)
NLR	2.71 (±1.34)	5.83 (±2.50)
MLR	0.35 (±0.12)	0.36 (±0.19)
PLR	135.85 (±44.75)	111.52 (±45.27)
Biomarkers		
IL6 (pg/ml)	11.65 (±10.76)	312.71 (±217.95)
PCT (ng/ml)	0.08 (±0.01)	0.13 (±0.14)
CRP (mg/l)	8.77 (±19.34)	3.37 (±2.07)
Cortisol (nmol/l)	342.86 (±102.99)	386.73 (±188.35)
SOFA	6(±2.54)	2.33 (±1.99)
Operative (Elective surgery)		
On Pump	11	
Off Pump	4	

Vibrational spectra of leukocytes and plasma based on all patients. Leukocytes and plasma from the blood samples were measured with WITec alpha320 Raman system. Plasma was measured via FT-IR spectroscopy as well. Raman spectra of leukocytes, Raman spectra of plasma, FT-IR spectra of plasma from CABG patients BS and AS, and the corresponding difference spectra between AS and BS are shown in Figure 39. The mean vibrational spectra of individual samples of BS and AS are very similar (see top panels in Figure 39), thus corresponding difference spectra between AS and BS were calculated and shown in the bottom panels in Figure 39. From the difference spectra, differences between AS and BS are observed. These variations are mainly contributions from proteins confirmed by amide bands. Raman peaks around $1005cm^{-1}$, $1266cm^{-1}$, $1447cm^{-1}$, $1572cm^{-1}$, $1673cm^{-1}$, and IR

fingerprints on $1242cm^{-1}$, $1342cm^{-1}$, $1412cm^{-1}$, $1516cm^{-1}$, $1602cm^{-1}$ and $1687cm^{-1}$ are clearly observed.

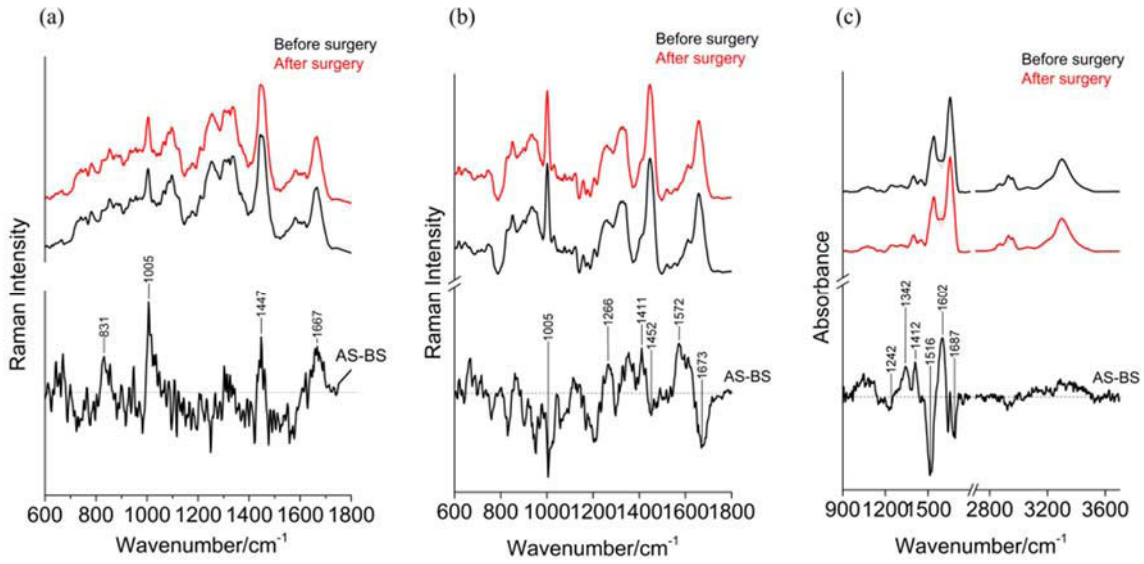

Figure 39 Vibrational spectra of leukocytes and plasma, a) Raman spectra of the leukocytes, b) Raman spectra of plasma, c) FT-IR spectra of plasma. Mean spectra are plotted with standard deviation. Difference spectra between AS and BS are presented at bottom panels.

Vibrational spectra of leukocytes and plasma based-on gender. The chosen of on-pump or off-pump CABG in our study depends on the patient's condition. We did not observe any changes for on-pump and off-pump surgery. This can be due to low patient numbers in our study. The following analysis for this study will be based on gender. Mean spectra of AS and BS, and the resulting difference spectra corresponding to different genders are shown in Figure 40. On average, the variations between AS and BS are stronger in female than in male patients based on leukocytes, confirmed by higher Raman peaks in the difference spectra shown in Figure 40 (a) than in Figure 40 (d). For plasma samples, both genders have similar plasma composition for Raman and FT-IR spectroscopy, which are mainly contributions from proteins, with specific vibrational peaks shown in Figure 40 (b, c, e, f).

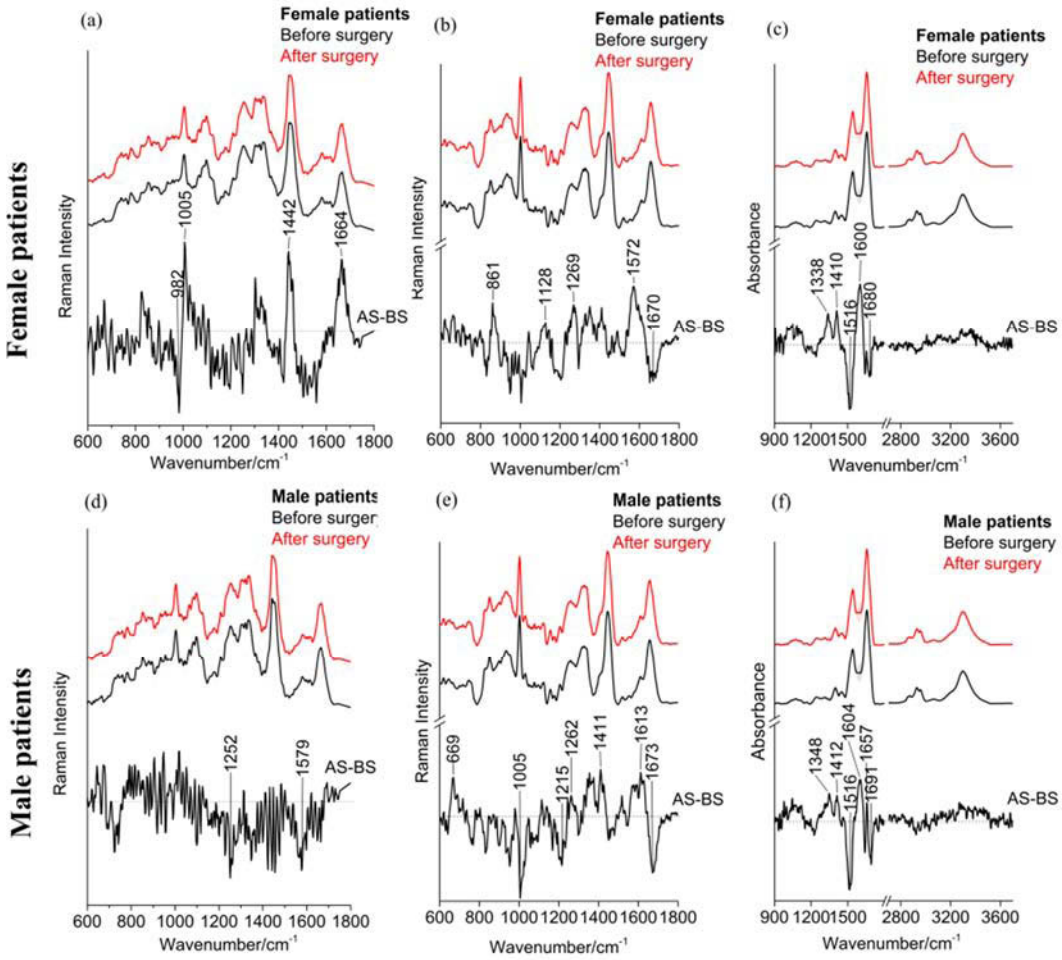

Figure 40 Vibrational spectra of leukocytes and plasma based on gender-wise: a) Raman spectra of the leukocytes from female patients, b) Raman spectra of the plasma from female patients, c) FT-IR spectra of the plasma from female patients, d) Raman spectra of the leukocytes from male patients, b) Raman spectra of the plasma from male patients, c) FT-IR spectra of the plasma from male patients. Mean spectra are plotted with standard deviation. Difference spectra between AS and BS are presented at bottom panels.

PCA analysis based on difference spectra. PCA analysis based on difference spectra between AS and BS for these 15 CABG patients was performed to better visualize the differences or similarities among them, and to dig out more information about these patients. PCA scatter plots from Figure 41 show that there are some distinct outliers among these cohorts. Outliers P07 and P10 in Figure 41(a) are both female with body mass index (BMI) of $31.2cm/kg$ and $34.9cm/kg$ individually, while outliers P02 and P06 in Figure 41(d) are both female with BMI of $22.7cm/kg$ and $27.5cm/kg$ respectively. Some patients underwent different conditions or complications during or after the cardiac surgery: for example P12 had a longer intensive care unit stay and hospital stay compared to other patients, and is outlier in Figure 41 (b, c, f), P14 had infection and is distinct from others in Figure 41 (d).

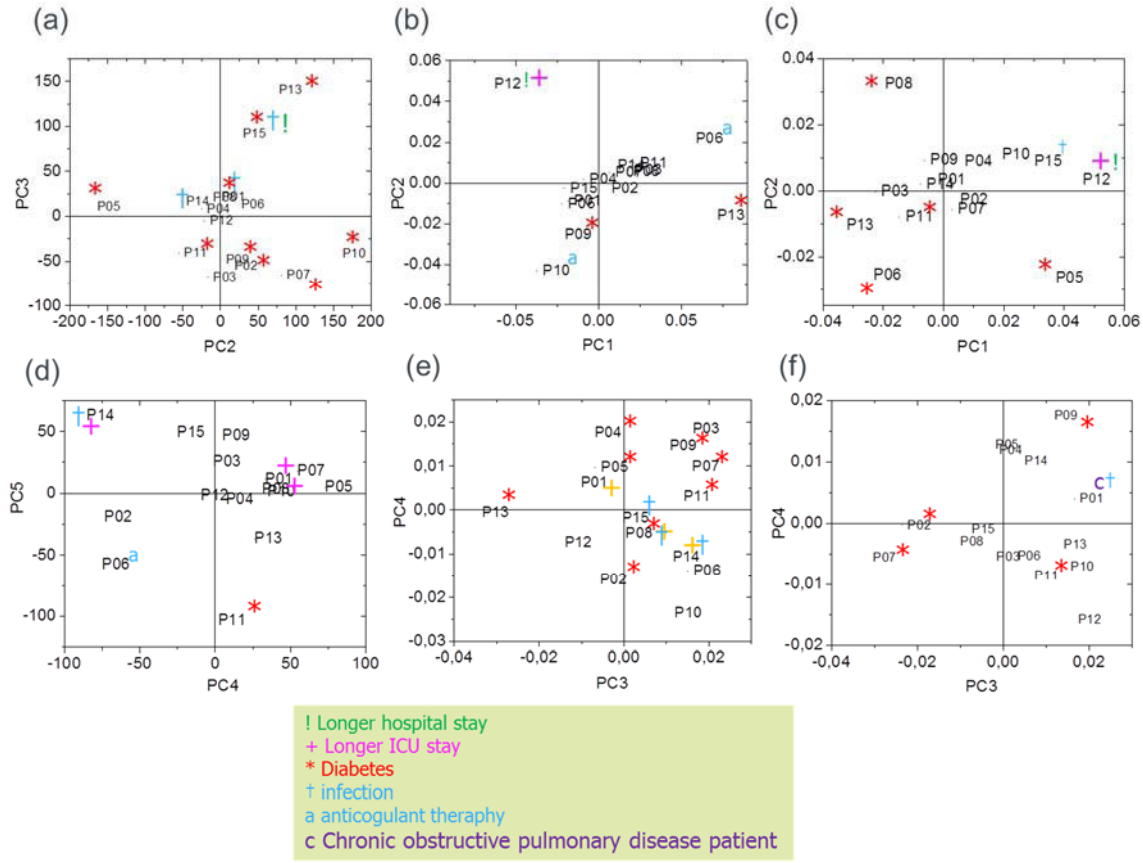

Figure 41 PCA scatter plots for vibrational spectral data: a, d) Raman spectra of leukocytes, b, e) Raman spectra of plasma, c, f) FT-IR spectra of plasma.

The behaviors of PCA scatter plots were not identical, efforts to explain these scatter plots are tried with corresponding PCA loadings. PCA loadings in Figure 42 show that contributions to PCA analysis based on the difference spectra are mainly from proteins, in particular with Raman peaks around amide I ($1660cm^{-1}$, $1676cm^{-1}$), amide II ($1556cm^{-1}$, $1578cm^{-1}$), amide III ($1230cm^{-1}$, $1241cm^{-1}$, $1250cm^{-1}$), CH_2 scissoring ($1452cm^{-1}$), CH_2 bending ($1446cm^{-1}$), and phenylalanine ($1002cm^{-1}$); in addition with IR peaks on amide I ($1604cm^{-1}$, $1657cm^{-1}$, $1676cm^{-1}$, $1689cm^{-1}$), and amide II ($1518cm^{-1}$, $1591cm^{-1}$). However, the proteins contributions are different in differentiating the CABG patients before and after cardiac surgery, confirmed by different vibrational peaks above. This can be assigned to the different biomolecule components in WBCs and plasma when comparing Figure 42 (a) and Figure 42 (b), and distinct Raman scattering and IR absorbance for the same plasma when considering Figure 42 (b) and Figure 42 (c).

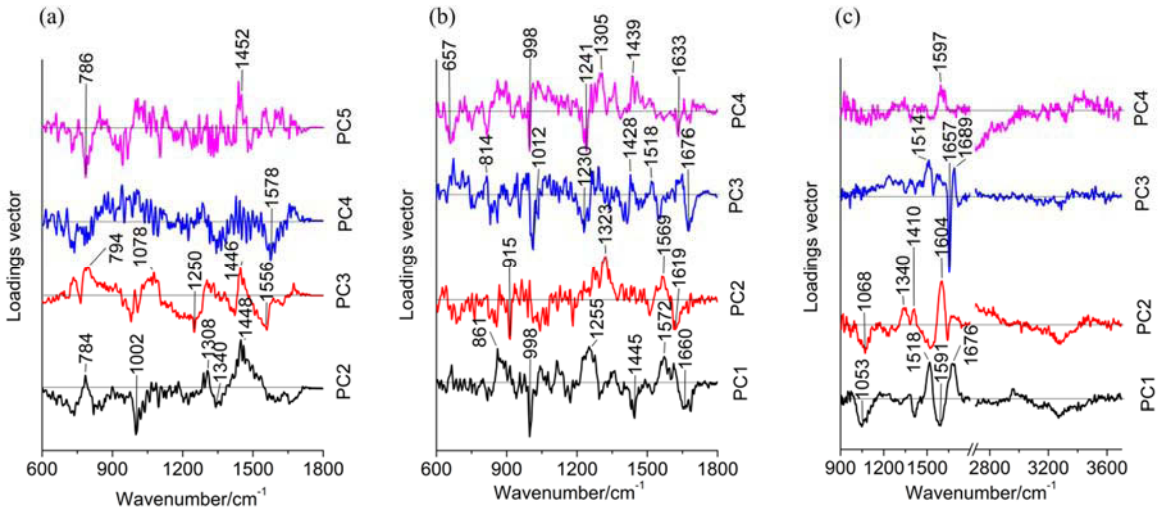

Figure 42 PCA loadings for vibrational spectral data: a) Raman spectra of leukocytes, b) Raman spectra of plasma, c) FT-IR spectra of plasma.

Clinical biomarkers based on WBCs and plasma. The influence of cardiac surgery based-on leukocytes and plasma were recorded and the gender-wise performances were plotted in Figure 43. The impact of the surgery on WBC counts, NLR, MLR and PLR are similar for both genders, indicating similar changes of leukocytes in female and male patients. After the cardiac surgery, more WBCs inside the patient can be activated. The increase of WBC is consistent with the results from other studies [100, 179-181], and can be explained by the demargination of neutrophils resulting from glucocorticoids, delayed migration of neutrophils into tissue, neutrophils apoptosis rate, and response to interleukins. [181, 182] Regarding different WBCs responding to the surgery, neutrophils will increase after the surgery and peak after 24 postoperative hours, monocytes will be unchanged and increase after 24 postoperative hours, whereas lymphocytes and platelets will decrease. [100, 104, 181] The trends support our results shown in Figure 43 (a, b, c, d) as our sample were collected during the surgery or few hours after the surgery.

When considering plasma biomarkers, IL-6 increased significantly during and after the surgery as shown in Figure 43 (e). The increase of IL-6 can be due to the inflammatory response, exposure of myocardium to cardioplegic arrest, the exclusion of lungs from circulation, activation of T cells as source for IL-6 production, stimulation and growth of hematopoietic precursor cells and fibroblasts. [100, 183] The gentle increase of cortisol in Figure 43 (f) can be due to the quick collection time after the surgery in our case whereas the increase peak will show up in the first postoperative day or from 4-12 hours after surgery. [184, 185] PCT is a useful marker for infection or severe sepsis or organ failure, and quite stable in patients without the occurrence of aforementioned complications. [186, 187] In our patient cohort, only three patients underwent infection or sepsis, thus it is not surprising that the mean PCT values did not change. CRP was reported to increase in the early days after surgery [100] and more probably triggered by surgical trauma instead of HLM [186], since our sample were collected in a short time during or after the surgery, the CRP may not response yet.

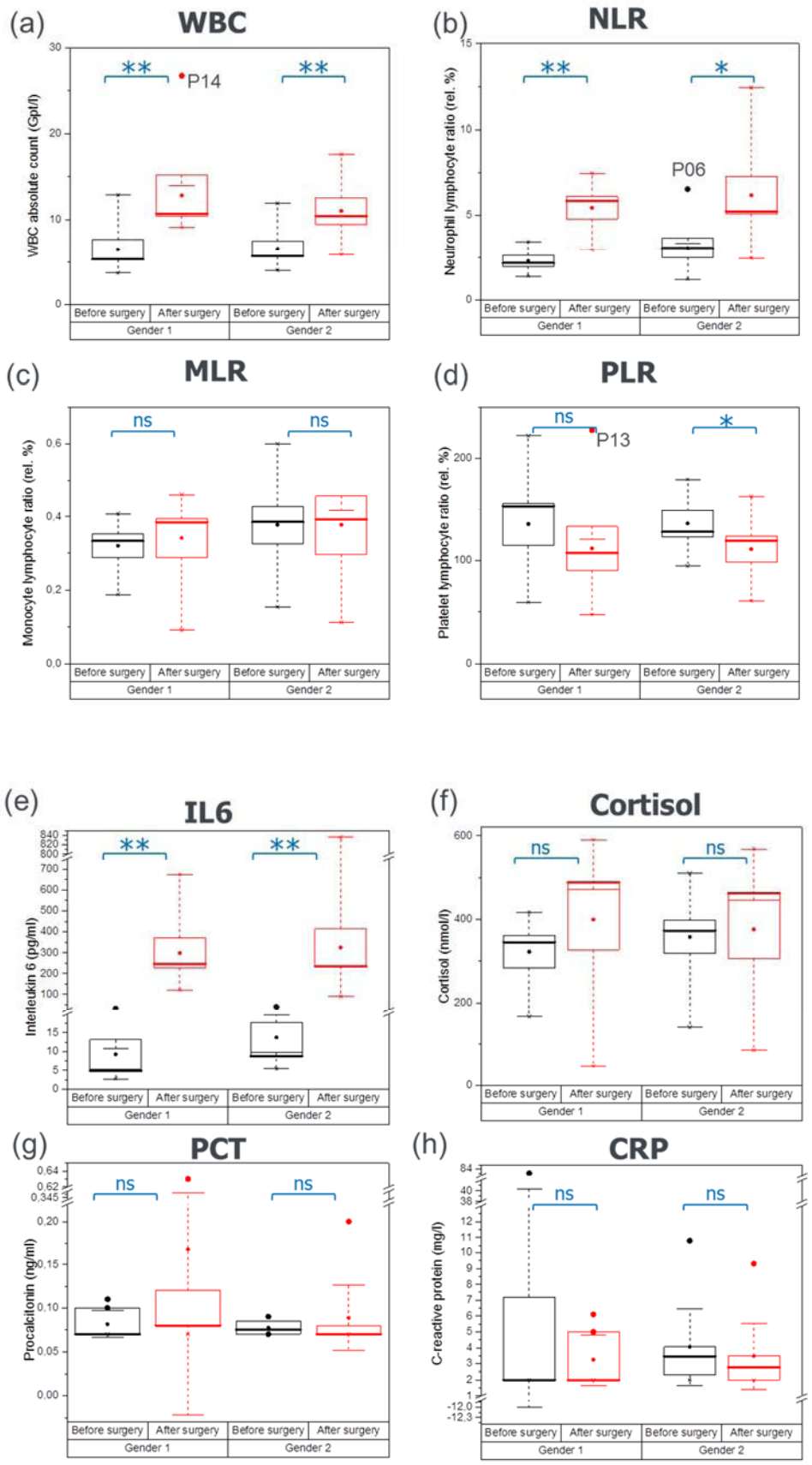

Figure 43 Impact of coronary artery bypass graft surgery on leukocytes (a, b, c, d) and on plasma (e, f, g, h) biomarker. P-value was calculated based on Mann-Whitney test. * -- p-value < 0.05, ** -- p-value < 0.01, ns -- no significance.

Pearson's correlation between clinical biomarkers and vibrational spectra. Pearson's correlation was performed to better understand the correlations between vibrational spectral data and leukocytes or plasma biomarkers. Figure 44 shows the correlation between Raman bands and neutrophils. The Raman peak around $412cm^{-1}$ correlates strongly with gender, hint for the Raman fingerprints of different hormone substances. Peaks around $1166cm^{-1}$, $630cm^{-1}$, $1304cm^{-1}$ ($1698cm^{-1}$), $1684cm^{-1}$ and $888cm^{-1}$ have a significant negative correlation with BMI, PCT, RBC, Hb and HCT respectively. While Raman fingerprint at $1604cm^{-1}$ is significantly positively correlated with monocytes. The negative correlation means that when the intensity of the chosen vibrational band is increased, there will be a decrease of the corresponding parameter or biomarker. For those positive correlations, the increases of vibrational peaks accompany with higher biomarkers values.

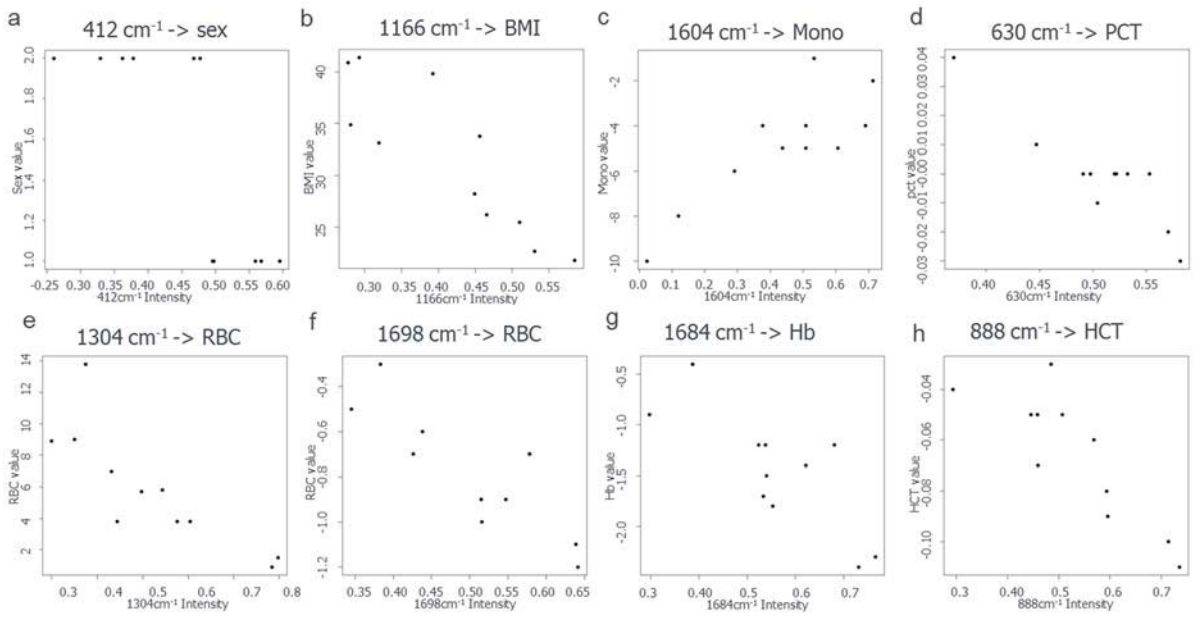

Figure 44 Pearson's correlation analysis for major subtype of leukocytes: neutrophils.

Total correlations between biomarker from blood samples (leukocytes and plasma) and vibrational spectra (Raman and FT-IR spectra) are calculated and shown in Table 9. Gender also correlated with $976cm^{-1}$ based on WBCs. Body mass index (BMI) is positively correlated with $1421cm^{-1}$ and $922cm^{-1}$ of the Raman bands from plasma sample. IL-6 has negative correlation with Raman peaks around $1062cm^{-1}$ and $922cm^{-1}$ from WBCs and plasma respectively. Whereas cortisol is positively correlated with Raman peaks and FT-IR bands based on plasma sample.

Table 9 Pearson's correlation analysis for leukocytes and plasma

Clinical markers	WBC Raman peaks		Plasma Raman peaks			Plasma FTIR peaks		
	All cells	Neutrophils	Whole droplet	Inner ring	Outer ring	Whole droplet	Inner ring	Outer ring
Gender	976	412						
BMI index		Negative 1166	Positive 1421	Positive 922				
IL6	Negative 1062		Negative 922					
PCT		Negative 630						
Cortisol				Positive 1466	Positive 771	Positive 3608		
RBC		Negative 1304 & 1698					Negative 1506	
Hb		Negative 1684						
HCT		Negative 888					Negative 1506	
NLR					Negative 1105			
Mono		Positive 1604			Negative 1005 & Positive 1127			
Eos	Positive 912					Positive 3573		

Summary and discussion. Our results show that CABG with and without the use of HLM share similar influence on the spectra of WBCs and plasma from the patients. It can be due to the improvements of on-pump CABG including warm surgery techniques, the improved biological compatibility of HLM, anti-fibrinolytic and anti-inflammatory drugs. [100] The PCA analysis based on difference spectra groups the patients into different clusters according to different patterns, showing high potential of vibrational spectroscopy for patient stratification. Vibrational spectra of leukocytes and plasma correlates well with clinical biomarkers, however larger patient cohorts will be needed to obtain further information.

3.3 Application of Raman spectroscopy to diabetes mellitus: HbA1c characterization and diagnostics

This section will focus on using Raman spectroscopy to characterize glycated haemoglobin in diabetes mellitus.

Sample cohort. After consent informed(Ethic number: 3558-08/12; 3558-09/12), EDTA blood was collected from 65 people (23 healthy donors and 42 diabetic patients). For healthy donors, $200\mu l$ EDTA blood was collected via lancet method from finger. And $2.7ml$ peripheral blood collected through BD vacutainer was obtained from diabetic patients. Summary of the clinical information for the sample cohort are shown in Table 10 and Figure 45.

Table 10 Summary of the clinical information for the sample cohorts

	Healthy cohort	Diabetic cohort
Number	23	42
Gender (Female / male)	12 / 11	9 / 33
Ages (mean ± SD)	33.60 ± 8.34	67.08 ± 11.78
HbA1c (mean ± SD) / %	5.05 ± 0.26	7.99 ±1.75

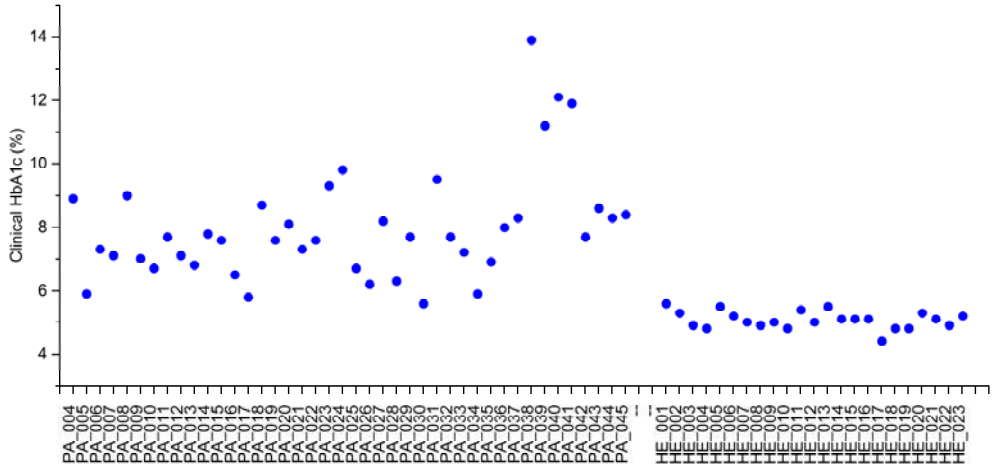

Figure 45 Overview of clinical HbA1c values from the sample cohort.

To get the reference HbA1c values from the recruited cohort, $10\mu l$ EDTA blood was hemolysed and measured by HPLC (TOSOH G8) in clinical routine diagnostic laboratory. $20\mu l$ EDTA blood was used for recording blood hemogram in clinical chemistry laboratory. For Raman spectroscopy measurements, $7ml$ EDTA blood was prepared through blood smear method on CaF_2 slide to get single RBC layer. After blood smear, the sample slide was dried under sterile hood for about 30min. The remaining EDTA blood from diabetic patients was centrifuge, after plasma was obtained it was stored at $-80°C$ for further use. Preparations for the blood sample are shown in Figure 46.

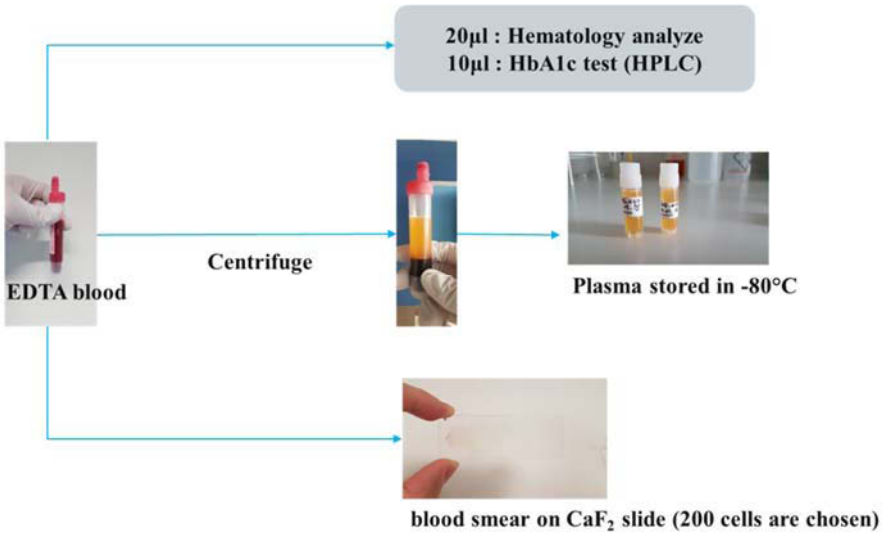

Figure 46 Sample preparations for EDTA blood.

Raman spectra of RBCs. Figure 47 shows typical Raman spectra of dried RBCs with predominant peaks around $676cm^{-1}$, $747cm^{-1}$, $993cm^{-1}$, $1085cm^{-1}$, $1128cm^{-1}$, $1171cm^{-1}$, $1222cm^{-1}$, $1302cm^{-1}$, $1337cm^{-1}$, $1359cm^{-1}$, $1394cm^{-1}$, $1430cm^{-1}$, $1555cm^{-1}$, $1584cm^{-1}$ and $1637cm^{-1}$. The peak assignments are given in Table 11. Most of the fingerprints can be assigned to porphyrin, correlating to the structures of hemoglobin A (HbA). Dried RBCs have more than 96% hemoglobin (Hb), and HbA is the most abundant (>90%) hemoglobin component within Hb family. Hb is metalloprotein in the RBCs, containing four globin protein subunits. These subunit chains are consisted of a protein chain associated with a heme group. The protein chain consists of two types: α- and non-α-chain, they have similar length but are different in amino acid sequence. The α-chain is the same in all human hemoglobins, while the non-α-chain can be β-chain of normal adult hemoglobin, γ-chain of fetal hemoglobin and δ-chain of HbA_2. Each protein chain is globin fold arranged into a set of α-helix structure, which contains a pocket binding to the heme group strongly. The prosthetic heme group iron protoporphyrin IX is the same in all hemoglobins. Each heme group contains iron ion held in the middle of a heterocyclic ring - porphyrin. The iron ion is linked to the N-terminal of a histidine, and the porphyrin ring is wedged into its pocket by a phenylalanine of α- and non-α- chain. [188, 189] Hb has many variants in adults that are formed by different globins and heme. More information about Hb in adults is shown in Table 12. Hence the signal contributions in Figure 47 are mostly from HbA and partly from RBC membrane.

Since glucose binds irreversible to N-terminal valines residues in ß-chains of HbA, it can be an indicator to monitor long term blood glucose. In clinical, HbA1c is used to evaluate the extent of blood glucose. Our idea is to measure RBCs directly and predict the HbA1c value from Raman signal. In this study, we use three approaches for test our idea. Firstly, we done in-vitro glycation of isolated RBCs from healthy donor to understand HbA1c related changes in the Raman spectra of RBCs, different concentration glucose were added into the isolated RBCs. Secondly, we evaluated ex-vivo glycation of RBCs from healthy donors. Finally, we validated ex-vivo glycation of RBCs in diabetic patients.

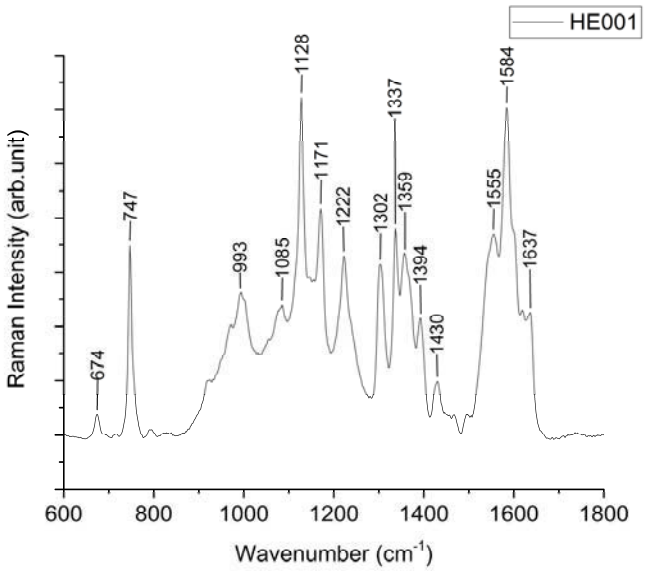

Figure 47 Mean Raman spectra of RBCs (λ_{ex} = 532nm) from healthy donor. (n=1)

Table 11 Tentative Raman assignments for RBCs [190-192]

Raman peak / cm^{-1}	Tentative assignments
674	$\delta(\text{pyr deform})_{sym}$
747	ν(pyr breathing)
993	$\nu(C_\beta C_I)_{asym}$
1085	$\delta(=C_bH_2)_4$
1128	$\nu(C_\beta\text{-methyl})$
1171	$\nu(\text{pyr half-ring})_{asym}$
1222	$\delta(C_mH)$
1302	$\delta(C_mH)$
1337	$\nu(\text{pyr half-ring})_{asym}$
1359	$\nu(\text{pyr half-ring})_{asym}$
1394	ν(pyr quarter-ring)
1430	$\nu(C_\alpha C_m)_{asym}$
1584	$\nu(C_\alpha C_m)_{asym}$
1637	$\nu(C_\alpha C_m)_{asym}$

Table 12 Summary of main hemoglobins in adult [115, 193]

Hemoglobin	Structure	Percentage
A	$\alpha_2\beta_2$	> 90%
$A1_c$	$\alpha_2(\beta\text{- NH-glucose})_2$	3%
A_2	$\alpha_2\delta_2$	2.5%
F	$\alpha_2\gamma_2$	0.2%

In-vitro glycation assay of haemoglobin in isolated RBCs. Mean Raman spectra of incubated RBCs with different concentrations ($0mM$, $5mM$, $30mM$, $50mM$, $60mM$, $70mM$, $90mM$) of glucose are shown in Figure 48. Most of the fingerprints are assigned to porphyrin as the assignments given in Table 11.

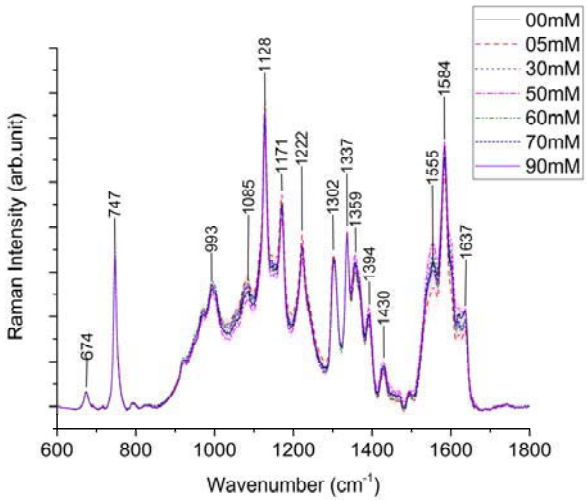

Figure 48 Mean spectra of in-vitro incubated RBCs with glucose of different concentrations.

The added glucose concentration and measured HbA1c values has a linear regression correlation [113], and this regression relationship can be confirmed in our data shown as Figure 49. Glucose concentration and HbA1c value has a Pearson correlation of 98.4%, and R^2 for this regression is about 96.8%.

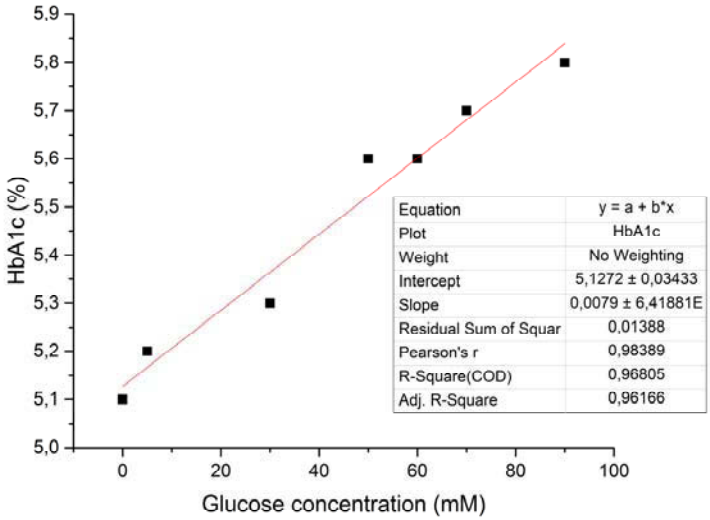

Figure 49 Linear regression between added-glucose and in-vitro incubated HbA1 (determined by Pearson correlation).

According to the previous discussion, the added glucose has a positive correlation with the incubated HbA1c value. When incubating RBCs with glucose of different concentrations, the

HbA will be affected differently by glucose, thus HbA1c will change in the vibrations. These variations are confirmed by the difference spectra between the control RBCs ($0mM$) and those added glucose cases shown in Figure 50. The difference spectra show that the changes are mainly delivered by the same porphyrin fingerprints around $676cm^{-1}$, $747cm^{-1}$, $1174cm^{-1}$, $1355cm^{-1}$, and $1397cm^{-1}$ as presented in mean Raman spectra. These bands change in intensity, indicating that they get affected by glucose binding. Raman vibrations from RBCs are mainly contributions from HbA (>90% composition). HbA is rich of porphyrin and ß-chains proteins, when glucose binds to ß-chain, it alters the valine molecules (see Figure 51), thus changes the structures and varies the vibrational bands. To verify this, healthy volunteers and diabetic patients are recruited, and the results will be discussed later.

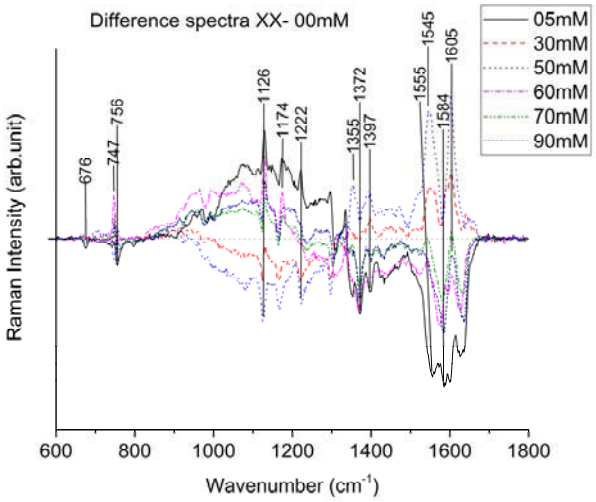

Figure 50 Difference spectra of in-vitro incubated RBCs between control (no glucose added, HbA1c from reference method 5.1%) and glucose added ones (5mM, 30mM, 50mM, 60mM, 70mM, 90mM).

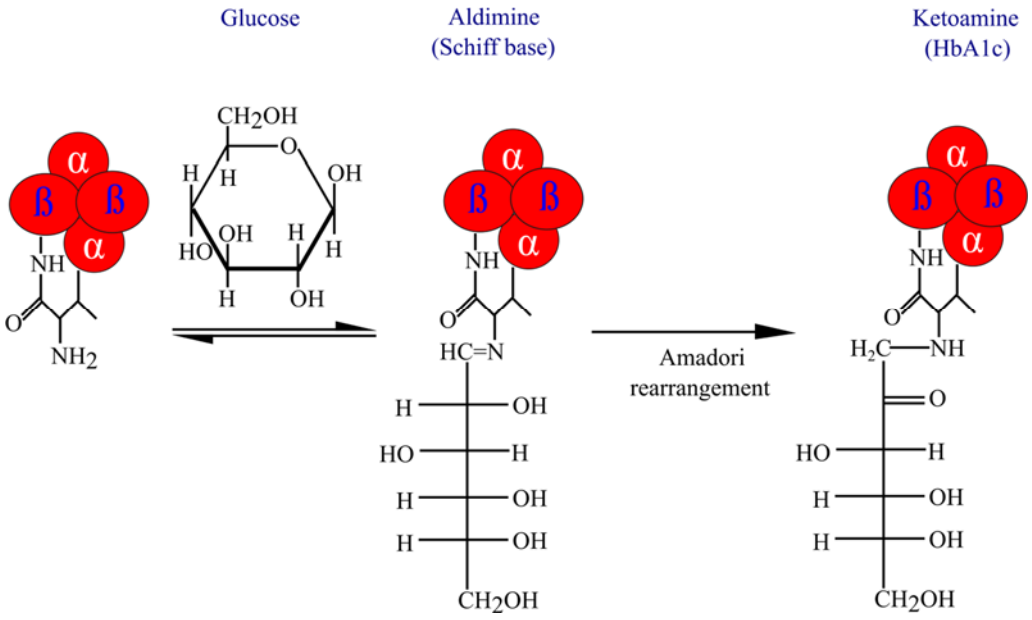

Figure 51 Formation of glycated hemoglobin (HbA1c) via the Amadori rearrangement. [111, 115, 194, 195]

In order to predict HbA1c values from Raman spectra, PLSR regression model was built via 2-layer cross-validation. Once PLSR model was built, the model was applied to predict the HbA1c values on every collected RBC from the remaining test sample. When the $30mM$ glucose was chosen as the test sample, optimal PLSR model can be obtained with R^2 of 91.2% (Figure 52). For this model, 9 components are chosen once the RMSEP has the first lowest value, in other words when the model has lowest cross validation (CV) error.

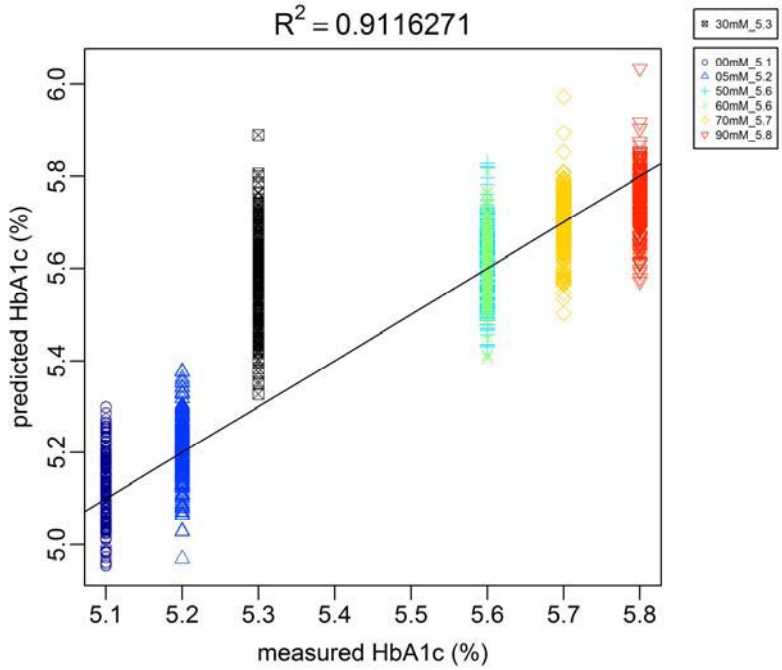

Figure 52 PLSR model with leave-one-sample-out CV, data from glucose of 30mM was used as test dataset, 9 components was chosen to build this PLSR model.

Ex-vivo glycation determination of RBCs from healthy donors. Mean spectra for the healthy cohort are presented in Figure 53, Raman profiles for these donors are similar as Figure 47 and can be mainly assigned to porphyrin. However, slight differences are visible, for example HE018 around $1635cm^{-1}$, HE017 for the spectral range from $900cm^{-1}$ to $1630cm^{-1}$.

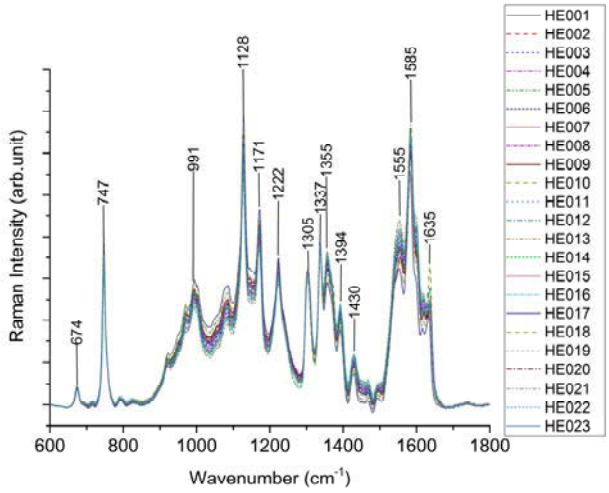

Figure 53 Mean spectra of healthy cohorts (n=23).

To better interpret the variations and to understand the difference present in RBCs for healthy donors, difference spectra between healthy donor with lowest HbA1c value (HE017, HbA1c =4.4%) and other healthy donors are calculated and shown in Figure 54. The variation patterns between these healthy donors are similar, with most predominant peaks assigning to porphyrin which are observed in the mean spectra. The intensity changes in these bands can result from the different glucose binding to the ß-chain in different individuals, thus changing the molecular structures.

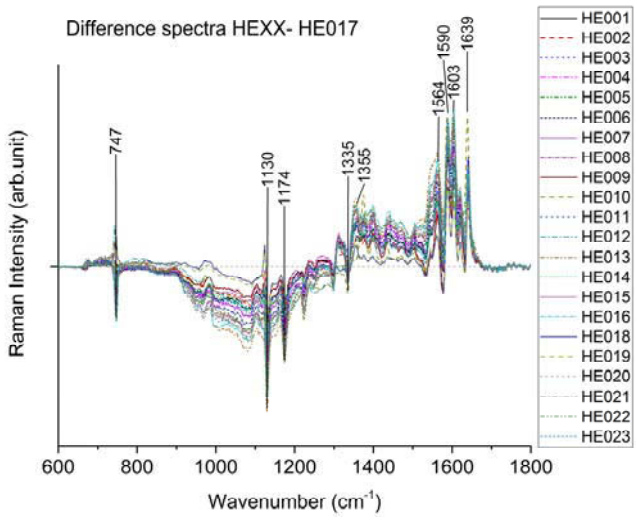

Figure 54 Difference spectra between healthy donor with lowest HbA1c value (HE017, HbA1c=4.4%) and other healthy donors.

PLSR model based on the data from 22 healthy donors was built and shown in Figure 55. Data from HE005 was used as test dataset, and the PLSR model was built based on Raman data from other 22 healthy donors. This PLSR model was applied to predict the HbA1c value for HE005. The PLSR model has a R^2 of 76.4%, and 12 components was chosen to build this model. The prediction ability of PLSR model from healthy donors is weaker than the PLSR model from in-vitro incubation RBCs. This difference can be from the individual variation between the healthy cohorts, where only one healthy donor is included in the in-vitro incubation. Other factors can also influence HbA1c values, including genetic factors, age, environment, deficiency or high doses of vitamins (B12, C, E), aspirin, alcoholism, and so on. [196]

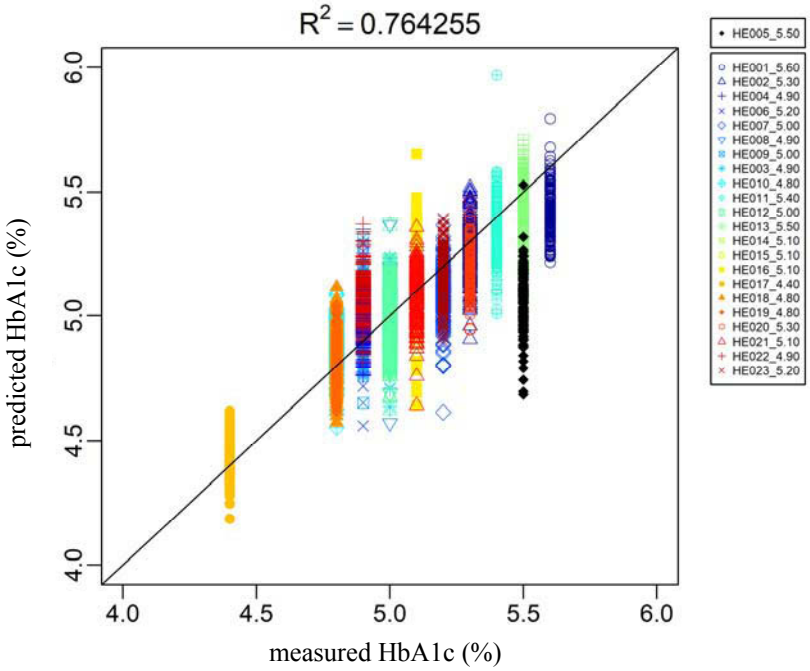

Figure 55 PLSR model with leave-one-sampe-out CV for dataset from healthy donors. Data from HE005 was used as test dataset, 12 components was chosen to build this PLSR model.

Ex-vivo glycation determination from RBCs of diabetic patients. Regarding patient cohort, their mean spectra are quite similar, albeit some differences are observed, see Figure 56. These differences can be better visualized in difference spectra between PA030 with lowest HbA1c value and other patients, see Figure 57. Similar as Figure 50 and Figure 54, the variation between the diabetic patients are dominated by porphyrin, giving hint to the structure changes of porphyrin in HbA when bound by glucose of different concentrations. The difference spectra between diabetic patients are more heterogeneous than the difference spectra between healthy donors, the heterogeneity in patients can be due to co-morbidities which influence the RBCs.

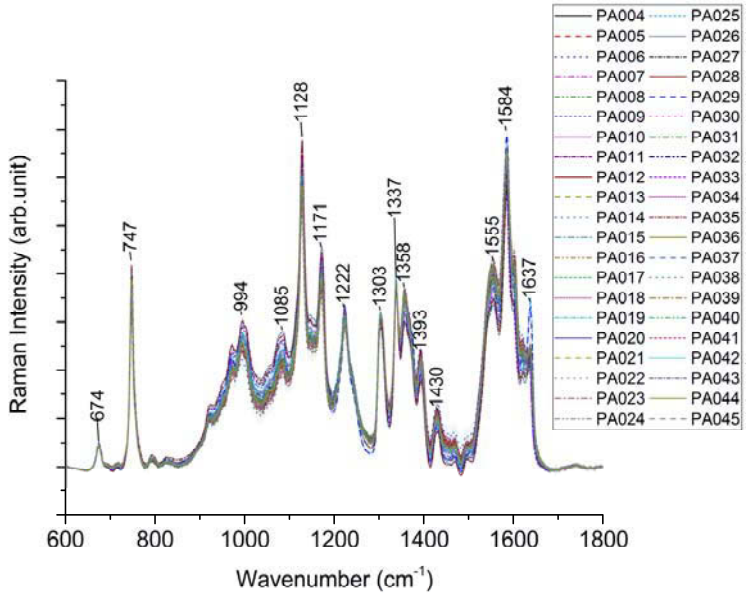

Figure 56 Mean spectra of diabetic patients (n=42).

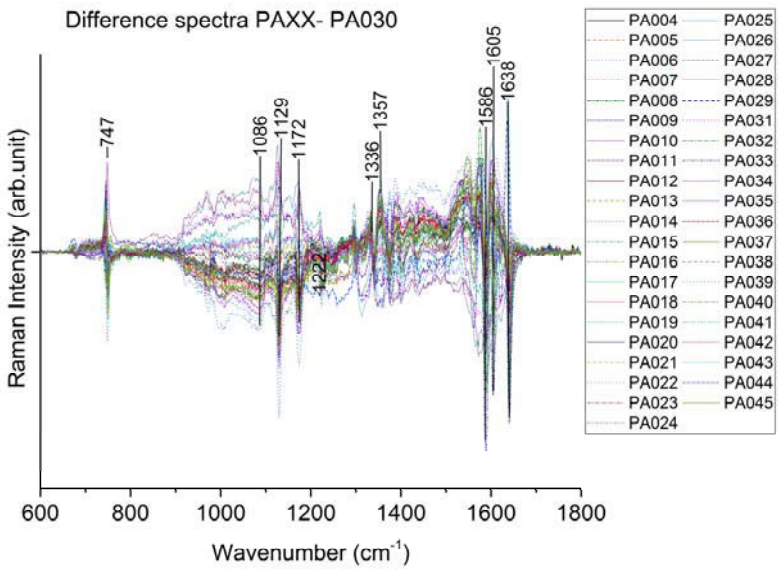

Figure 57 Difference spectra between diabetic patient with lowest HbA1c value (PA030, HbA1c=5.6%) and other patients.

The Raman data from 42 diabetic donors are used to build a PLSR model. The PLSR model is built based on the data from 41 patients, while PA037 was chosen as test sample. Figure 58 shows that the PLSR model has a R^2 of 52.2%, and 17 components were chosen to build the model. The PLSR model did not have very robust prediction ability, this can be due to the fact that other factors instead of only HbA1c are also taking into account when building this model. These factors can be individual heterogeneity, presence of hemoglobin variants, deficiency or high doses of vitamin B12, vitamin C, vitamin E or conditions affecting RBC such as hemolytic anemias, glucose-6-phosphate dehydrogenase deficiency, pregnancy, end-stage kidney disease, alcoholism, iron, use of antiretroviral drugs, rheumatoid arthritis, splenectomy, hemoglobinopathies, administration of erythropoietin.[111, 116, 196-198].

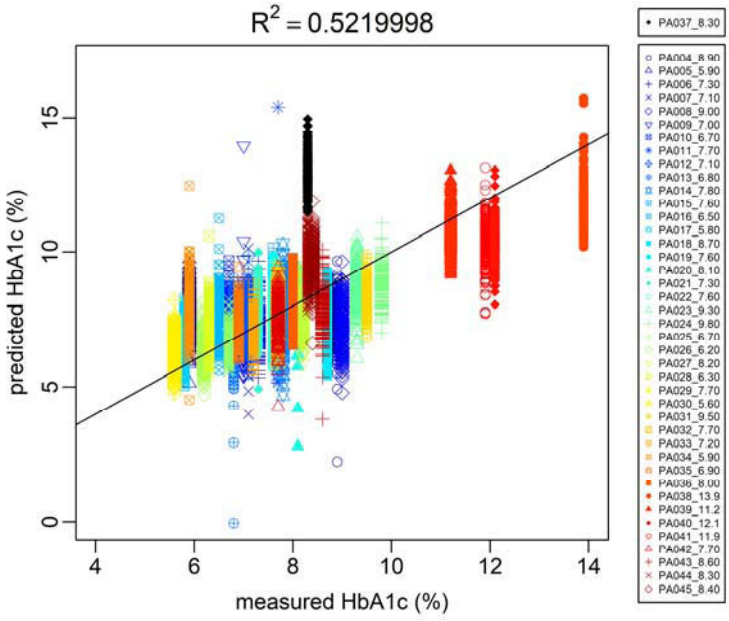

Figure 58 PLSR model with leave-one-sample-out CV for dataset from diabetic patients. Data from PA037 was used as test dataset, 17 components was chosen to build this PLSR model.

Summary and discussion. Mean spectra for the measured RBCs show that the Raman profiles are similar and can be mainly assigned to porphyrin, albeit slight differences are also visible. To dig out more information on the differences, difference spectra between sample with lowest HbA1c value and other samples are calculated. The difference spectra share similar profiles, delivering the porphyrin structure changes when glucose of different concentrations binds to β-globin in HbA. The in-vitro incubation confirms the linear correlation between glucose concentration and measured HbA1c values, with Pearson correlation of 98.4%, and R^2 about 96.8%. In order to interpret HbA1c values from Raman spectra, PLSR regression model was built via leave-one-sample-out-cross-validation. Data from one sample was chosen as test dataset whereas other samples were used as training dataset. Optimal components will be chosen automatically when the model has lowest CV error, determined by first lowest RMSEP value. Once PLSR model was built, HbA1c values on every collected RBC from the test sample can be predicted. PLSR model have best performance for the in-vitro incubation experiment with R^2 of 91.2%, and lowest prediction ability when considering diabetic patients with only 52.2% R^2.

The results above show the potential of combining Raman spectroscopy with advanced chemometric methods to quantify HbA1c values on single RBC level. The different performance on the PLSR models can be due to many factors instead of HbA1c solely. Individual variation has been reported in many clinical studies, which is unavoidable. 69% interindividual HbA1c variance is suggested from genetic factors. [199] Besides, the measured RBCs have a range of ages which have different exposure degrees to hyperglycemia. Older RBCs expose more to hyperglycemia but contribute less to HbA1c, younger RBCs have less exposure to hyperglycemia but have more contribution to HbA1c. Increasing RBC mean age will increase HbA1c. [200, 201] Deficiency of iron, vitamin B12, erythropoietin in renal failure, and bone marrow suppression in alcoholism and pregnancy will all decrease erythropoiesis, thus increase HbA1c by increasing mean age of RBCs. [202-207] RBC lifespan can be increased due to splenectomy. [208] In contrast, the RBC mean age will be decreased by increasing reticulocytes, thus decrease HbA1c. Moreover, rheumatoid arthritis, splenomegaly, antiretrovirals, ribavirin, and dapsone will increase hemolysis rate thus decrease RBC lifespan, hence will result in decreased HbA1c. [209-212] Hemoglobin variants will also influence HbA1c value. [196]

Outlook. The measured RBCs have different lifespan which affect HbA1c extent, thus HbA1c from single RBC will be more interesting and needed to be further investigated in the future. Moreover, multiple diagnostic methods or multiple biomarkers are more attractive and robust since they can provide more compensate information for the same clinical condition. Actually, HbA1c has several limitations to diagnose DM as abovementioned. Another early stage glycated protein - glycated albumin (GA), now is attracting more and more attention to become an alternative for HbA1c, especially as a mid-term glycemic indicator. Albumin is the most abundant protein in blood plasma, it has a half-life of 12-21 days [198]. GA presents a more intermediate glycemic marker compared to HbA1c, which helps to control diabetic condition earlier before HbA1c variation. GA in normal health is about 1% - 10%, where the value can be two to five fold higher in diabetic patients [197, 213]. IR absorption spectroscopy and Raman spectroscopy has been shown to investigate GA of different

concentrations successfully. GA determination via vibrational spectroscopy on donor cohorts can be considered in the future.

4 Summary and Outlook

In the current aging society, more and more people will suffer from age-related diseases such as cardiovascular diseases or diabetes mellitus. To better diagnose and treat these diseases, individual characterisation of the patient's unique condition is needed. Vibrational spectroscopy, including Raman spectroscopy and Fourier transform infrared spectroscopy (FTIR), is one of the favourite techniques being developed to enable personalized medicine. Vibrational spectroscopic techniques have the advantages of being non-destructive, rapid, and label-free, can be ultimately performed in high-throughput and provide biochemical fingerprint information on molecular level. Among the samples measured by vibrational spectroscopy, blood is a very popular and important specimen for personalized medicine.

In daily clinical routine, there can be a time delay between blood collection and blood processing. During this time delay, individual biomolecules in the blood can disintegrate, which could influence the medical diagnosis. Within the scope of this work, serum samples from five healthy donors were collected by centrifugation after a delay time of $30min$, $60min$, $120min$ and $240min$ after blood collection, respectively, and temporarily stored at $-80°C$ until Raman spectroscopic characterization. The Raman spectroscopic characterization of the serum was performed in the dried droplet. As expected, the Raman spectra were dominated by the abundant albumin and immunoglobulin G. Some smaller spectral differences were observed due to time delay prior processing. However, with the small cohort (n=5) the difference pattern was not identical for all individuals. For Raman spectroscopic measurements of blood samples, a time delay of up to 4 hours can probably be tolerated in most analysis cases.

For the vibrational spectroscopic characterization of blood plasma and serum for biomedical analysis, the measurement of blood samples in dried droplets is a suitable method because high quality spectra can be collected quickly. However, the drying of the plasma or serum samples in the droplet leads to an inhomogeneous coffee ring effect: a center characterized by crystal patterns and a homogeneous ring. Within the scope of this work, an equal number of spectra from the center and ring were recorded and a statistically comparison between these two regions was carried out. The spectral intensity in the ring zone is significantly higher than in the middle. This work has shown examples in which optimal results were obtained exclusively with spectra only from the centre or only from the ring zone, but also examples in which it is advisable to characterise the entire droplet. The measurement scheme proposed in this thesis offers the greatest flexibility for systematic plasma and serum analyses, which can be transferred to different cases.

The potential of spectroscopic analysis of blood for clinical application is demonstrated in this thesis for typical age-related diseases, in particular cardiovascular diseases and diabetes mellitus. Cardiovascular diseases are very heterogeneous and can lead to different clinical presentations. It is of great interest for the physicians to have a fast and simple method to differentiate the different clinical presentations. In this work, the blood plasma and serum of 18 cardiac patients of the Jena University Hospital as well as of 7 (plasma) and 10 (serum) healthy donors were characterized by vibrational spectroscopy (Raman and FTIR).

Chemometric analysis of the spectra shows a clear grouping of the patients into different clusters, which probably contain important information on the disease pattern. A more in-depth analysis can be performed after the clinical information is released by the cooperating physician. Plasma and serum samples from healthy donors can be very well distinguished from cardiac patients. Spectroscopic signatures of carotenoids play a decisive role, as can be clearly seen in the difference spectra and in the principal component analysis. Carotenoids are found with lower concentrations in cardiac patients, which is consistent with other clinical studies.

After the cardiovascular patients were well distinguished from the healthy volunteers, two different treatment strategies for cardiac disease were followed by vibrational spectroscopy. This includes the follow-up of immunoadsorption therapy in dilated cardiomyopathy and spectroscopic changes of peripheral leukocytes and blood plasma during coronary artery bypass surgery.

For dilated cardiomyopathy, immunoadsorption therapy has been shown to remove circulating antibodies and to improve cardiac function. In this study, the spectroscopic fingerprint of blood plasma and serum during immunoadsorption therapy was monitored over a period of about 1 year. With the help of chemometric methods, the respective immunoadsorption treatment stages can be well differentiated based on the collected spectra. Difference spectra between different treatment stages show characteristic changes which can be easily explained by the biological changes caused by the therapy. The variations in immunoglobulin G values during therapy show excellent agreement between immunoturbidimetry analysis and the spectral data. The study shows a promising potential to follow variations during immunoadsorption therapy based on blood samples by using vibrational spectroscopy.

During coronary artery bypass grafting surgery, a coronary bypass grafting restores normal blood flow to the obstructed coronary artery. The operation can be performed with or without a heart-lung machine. Spectroscopic characterization of the peripheral leukocytes and blood plasma of 15 patients before and after surgery showed small changes in both leukocytes and plasma, but these varied from patient to patient. Significant changes of leukocyte and plasma biomarkers can be correlated well with vibrational spectra.

In diabetes mellitus, the value of glycated hemoglobin (Hb1Ac) is an important diagnostic parameter for the average blood sugar. Currently, this value is determined by high-performance liquid chromatography (HPLC) for the mean value of all measured erythrocytes, but not at the level of individual erythrocyte. This work investigated the potential of Raman spectroscopy in combination with chemometric methods to quantify glycated hemoglobin on individual erythrocytes. For in-vitro glycation experiment and healthy young volunteers (including diabetes patients), an excellent correlation of the spectroscopic markers with the Hb1Ac value was found. However, studies on individual erythrocytes of older diabetes mellitus patients with further comorbidities showed some limitations.

In summary, vibrational spectroscopy in combination with chemometric methods has a high potential to become a diagnostic method for personalized medicine. This technique requires

only very small amounts of blood ($7\mu l$ blood for HbA1c analysis, or $1\mu l$ plasma and serum for other studies) and minimal sample preparation, providing specific information on the clinical picture and course of therapy.

5 Zusammenfassung

In der heutigen alternden Gesellschaft werden immer mehr Menschen an altersbedingten Krankheiten wie Herz-Kreislauf-Erkrankungen oder Diabetes mellitus leiden. Um diese Krankheiten besser diagnostizieren und behandeln zu können, ist eine individuelle Charakterisierung des Zustands des Patienten erforderlich. Die Schwingungsspektroskopie, einschließlich der Raman-Spektroskopie und Fourier-Transformations-Infrarotspektroskopie (FTIR), ist eine leistungsstarke Technik, die für eine personalisierte Medizin entwickelt wird. Schwingungsspektroskopische Techniken haben den Vorteil, dass sie zerstörungsfrei, schnell und markierungsfrei sind, letztlich im Hochdurchsatz durchgeführt werden können und biochemische Informationen auf molekularer Ebene liefern. Eine ideale Probe für die personalisierte Medizin ist Blut, bzw. daraus gewonnenes Serum und Plasma.

Im klinischen Alltag kann es zu einer zeitlichen Verzögerung zwischen Blutabnahme und Blutverarbeitung kommen. Während dieser Zeitverzögerung können sich einzelne Biomoleküle im Blut zersetzen, was die medizinische Diagnose beeinflussen könnte. Im Rahmen dieser Arbeit wurden Serumproben von fünf gesunden Spendern nach einer Lagerzeit von $30min$, $60min$, $120min$ bzw. $240min$ nach der Blutentnahme durch Zentrifugation entnommen und bei $-80°C$ bis zur spektroskopischen Charakterisierung von Raman zwischengelagert. Die Raman-spektroskopische Charakterisierung des Serums wurde im getrockneten Tropfen durchgeführt. Wie erwartet, wurden die Raman-Spektren von dem reichlich vorhandenen Albumin und Immunglobulinen dominiert. Einige kleinere spektrale Unterschiede aufgrund der Lagerzeit konnten beobachtet werden. Bei der kleinen Kohorte (n=5) war das Differenzmuster jedoch nicht für alle Individuen identisch. Für eine allgemeine Raman-spektroskopische Untersuchung der Blutproben kann wahrscheinlich eine Zeitverzögerung von bis zu 4 Stunden in den meisten Analysenfällen toleriert werden

Für die schwingungsspektroskopische Charakterisierung von Blutplasma und Serum für die biomedizinische Analyse ist die Messung von Blutproben im getrockneten Tropfen eine geeignete Methode, da qualitativ hochwertige Spektren in kurzer Zeit gemessen werden können. Die Trocknung der Plasma- oder Serumproben im Tropfen führt jedoch zum Kaffeering-Effekt: ein Zentrum, das durch Kristallmuster und einen homogenen Ring gekennzeichnet ist. Im Rahmen dieser Arbeit wurde eine gleiche Anzahl von Spektren aus dem Zentrum und dem Ring aufgenommen und ein statistischer Vergleich zwischen diesen beiden Regionen durchgeführt. Die spektrale Intensität in der Ringzone ist deutlich höher als in der Mitte. In dieser Arbeit werden Beispiele gezeigt, in denen optimale Ergebnisse mit Spektren nur aus dem Zentrum oder nur aus der Ringzone erzielt wurden, aber auch Beispiele, in denen es ratsam ist, den gesamten Tropfen zu charakterisieren. Das in dieser Arbeit vorgeschlagene Messschema bietet die größte Flexibilität für systematische Plasma- und Serumanalysen, die auf verschiedene Anwendungsfälle übertragen werden können.

Das Potenzial der spektroskopischen Analyse von Blut für die klinische Anwendung wird in dieser Arbeit für typische altersbedingte Erkrankungen, insbesondere Herz-Kreislauf-Erkrankungen und Diabetes mellitus, aufgezeigt. Herz-Kreislauf-Erkrankungen sind sehr heterogen und können zu unterschiedlichen Krankheitsbildern führen. Für die Ärzte ist es von großem Interesse, eine schnelle und einfache Methode zur Unterscheidung der verschiedenen Krankheitsbilder zu haben. In dieser Arbeit wurden das Blutplasma und Serum von 18

Herzpatienten des Universitätsklinikums Jena sowie von 7 (Plasma) und 10 (Serum) gesunden Spendern durch Vibrationsspektroskopie (Raman und FTIR) charakterisiert. Die chemometrische Analyse der Spektren zeigt eine klare Gruppierung der Patienten in verschiedene Cluster, die wahrscheinlich wichtige Informationen über das Krankheitsbild enthalten. Eine vertiefte Analyse kann durchgeführt werden, nachdem die klinischen Informationen vom kooperierenden Arzt freigegeben wurden. Plasma- und Serumproben von gesunden Spendern lassen sich sehr gut von Herzpatienten unterscheiden. Spektroskopische Signaturen von Karotinoiden spielen eine entscheidende Rolle, wie man in den Differenzspektren und in der Hauptkomponentenanalyse deutlich erkennen kann. Karotinoide werden mit niedrigeren Konzentrationen bei Herzpatienten gefunden, was mit anderen klinischen Studien übereinstimmt.

Nachdem die Herz-Kreislauf-Patienten gut von den gesunden Probanden unterschieden werden konnten, wurden zwei verschiedene Behandlungsstrategien schwingungsspektroskopisch verfolgt. Dies umfasst das Follow-up der Immunadsorptionstherapie bei dilatativer Kardiomyopathie sowie die Untersuchung der Veränderung der spektroskopischen Signatur von peripheren Leukozyten und Blutplasma während einer Koronararterien-Bypass-Operation.

Bei der dilatativen Kardiomyopathie hat sich gezeigt, dass die Immunadsorptionstherapie zirku-lierende Antikörper entfernt und die Herzfunktion verbessert. In dieser Studie wurde der spektros-kopische Fingerabdruck von Blutplasma und Serum während der Immunadsorptionstherapie über einen Zeitraum von etwa einem Jahr beobachtet. Mit Hilfe chemometrischer Verfahren können die jeweiligen Immunadsorptionsbehandlungsstufen anhand der Spektren gut differenziert werden. Errechnete Differenzspektren zwischen verschiedenen Behandlungsstadien zeigen charakteristische Veränderungen, die mit den biologischen Veränderungen durch die Therapie gut erklärbar sind. Unter anderem zeigt sich eine ausgezeichnete Übereinstimmung der Variationen der Immunglobulin-G-Werte während der Therapie aus etablierter immunoturbidimetry-Analyse der klinischen Chemie und den Spektraldaten.

Während einer Koronararterien-Bypass-Operation wird durch ein koronares Bypass-Transplantat der normale Blutfluss zur verstopften Koronararterie wiederhergestellt. Die spektroskopische Charakterisierung der peripheren Leukozyten und des Blutplasmas von 15 Patienten vor und nach der Operation zeigte kleine Veränderungen sowohl bei den Leukozyten als auch beim Plasma, die jedoch von Patient zu Patient variierten. Signifikante Veränderungen von Leukozyten- und Plasmabiomarkern lassen sich gut mit Schwingungsspektren korrelieren.

Bei Diabetes mellitus ist der Wert von glykiertem Hämoglobin (Hb1Ac) ein wichtiger diagnostischer Parameter für den durchschnittlichen Blutzucker. Derzeit wird dieser Wert durch die Hochleistungsflüssigkeitschromatographie (HPLC) für den Mittelwert aller gemessenen Erythrozyten bestimmt, jedoch nicht auf der Ebene der einzelnen Erythrozyten. Diese Arbeit untersuchte das Potenzial der Raman-Spektroskopie in Kombination mit chemometrischen Methoden zur Quantifizierung von glykiertem Hämoglobin an einzelnen Erythrozyten. Für In-vitro-Glykosierungsexperimente und gesunde junge Probanden (inkl. Diabetiker) wurde eine ausgezeichnete Korrelation der spektroskopischen Marker mit dem

Hb1Ac-Wert gefunden. Studien an einzelnen roten Blutkörperchen von älteren Diabetes mellitus-Patienten mit weiteren Begleiterkrankungen zeigten noch Einschränkungen.

Zusammenfassend lässt sich sagen, dass die Schwingungsspektroskopie in Kombination mit chemometrischen Auswertemethoden ein hohes Potenzial hat, zu einer Diagnosemethode für die personalisierte Medizin zu werden. Diese Technik erfordert nur sehr geringe Blutmengen ($7\mu l$ Blut für die HbA1c-Analyse, oder $1\mu l$ Plasma und Serum für andere Studien) und eine minimale Probenvorbereitung, und kann spezifische Informationen zum Krankheitsbild und Therapieverlauf liefern.

6 References

1. Organization, W.H., *World report on ageing and health*. 2015: World Health Organization.
2. Organization, W.H., *World health statistics 2016: monitoring health for the SDGs sustainable development goals*. 2016: World Health Organization.
3. Organization, W.H., *Global report on diabetes.* 2016.
4. Roth, G.A., et al., *Demographic and epidemiologic drivers of global cardiovascular mortality.* New England Journal of Medicine, 2015. **372**(14): p. 1333-1341.
5. federation, W.h. *The costs of CVD*. Available from: http://www.championadvocates.org/en/champion-advocates-programme/the-costs-of-cvd.
6. England, N., *Improving outcomes through personalised medicine*. 2016.
7. Food, U. and D. Administration, *Paving the way for personalized medicine: FDA's role in a new era of medical product development.* Silver Spring, MD: US Food and Drug Administration, 2013.
8. Ginsburg, G.S. and H.F. Willard, *Genomic and personalized medicine: foundations and applications.* Translational research, 2009. **154**(6): p. 277-287.
9. Mann, D.L., et al., *Braunwald's Heart Disease E-Book: A Textbook of Cardiovascular Medicine*. 2014: Elsevier Health Sciences.
10. Popp, J., et al., *Handbook of biophotonics. 1. Basics and techniques*. 2011: Wiley-VCH. Verlag GmbH.
11. Johann Schaller, S.G., Urs Kämpfer, Sofia Lejon, Christian Trachsel, *Blood components*, in *Human blood plasma proteins: structure and function*. 2008, John Wiley & Sons. p. 7-16.
12. Coombes, K.R., et al., *Serum proteomics profiling—a young technology begins to mature.* Nature biotechnology, 2005. **23**(3): p. 291.
13. Geyer, P.E., et al., *Revisiting biomarker discovery by plasma proteomics.* Molecular systems biology, 2017. **13**(9): p. 942.
14. Geyer, P.E., et al., *Plasma proteome profiling to assess human health and disease.* Cell systems, 2016. **2**(3): p. 185-195.
15. Anderson, N.L. and N.G. Anderson, *The human plasma proteome: history, character, and diagnostic prospects.* Molecular & cellular proteomics, 2002. **1**(11): p. 845-867.
16. Beck, H.C., M. Overgaard, and L.M. Rasmussen, *Plasma proteomics to identify biomarkers–application to cardiovascular diseases.* Translational Proteomics, 2015. **7**: p. 40-48.
17. Mateos-Cáceres, P.J., et al., *Proteomic analysis of plasma from patients during an acute coronary syndrome.* Journal of the American College of Cardiology, 2004. **44**(8): p. 1578-1583.
18. Monteiro, M., et al., *Metabolomics analysis for biomarker discovery: advances and challenges.* Current medicinal chemistry, 2013. **20**(2): p. 257-271.
19. Psychogios, N., et al., *The human serum metabolome.* PloS one, 2011. **6**(2): p. e16957.
20. Johnson, C.H., J. Ivanisevic, and G. Siuzdak, *Metabolomics: beyond biomarkers and towards mechanisms.* Nature reviews Molecular cell biology, 2016. **17**(7): p. 451.
21. Bernini, P., et al., *Standard operating procedures for pre-analytical handling of blood and urine for metabolomic studies and biobanks.* Journal of biomolecular NMR, 2011. **49**(3-4): p. 231-243.
22. Barelli, S., et al., *Plasma/serum proteomics: pre-analytical issues.* Expert Review of Proteomics, 2007. **4**(3): p. 363-370.
23. Hsieh, S.Y., et al., *Systematical evaluation of the effects of sample collection procedures on low‐molecular‐weight serum/plasma proteome profiling.* Proteomics, 2006. **6**(10): p. 3189-3198.
24. Vaught, J.B., *Blood collection, shipment, processing, and storage.* Cancer Epidemiology and Prevention Biomarkers, 2006. **15**(9): p. 1582-1584.
25. Rai, A.J., et al., *HUPO Plasma Proteome Project specimen collection and handling: towards the standardization of parameters for plasma proteome samples.* Proteomics, 2005. **5**(13): p. 3262-3277.

26. Hassis, M.E., et al., *Evaluating the effects of preanalytical variables on the stability of the human plasma proteome.* Analytical biochemistry, 2015. **478**: p. 14-22.
27. Mateos, J., et al., *Multicentric study of the effect of pre-analytical variables in the quality of plasma samples stored in biobanks using different complementary proteomic methods.* Journal of proteomics, 2017. **150**: p. 109-120.
28. Kang, H.J., et al., *Identification of clinical biomarkers for pre-analytical quality control of blood samples.* Biopreservation and biobanking, 2013. **11**(2): p. 94-100.
29. Zhao, L., et al., *Ensuring sample quality for blood biomarker studies in clinical trials: a multicenter international study for plasma and serum sample preparation.* Translational lung cancer research, 2017. **6**(6): p. 625.
30. Teahan, O., et al., *Impact of analytical bias in metabonomic studies of human blood serum and plasma.* Analytical chemistry, 2006. **78**(13): p. 4307-4318.
31. Yin, P., et al., *Preanalytical aspects and sample quality assessment in metabolomics studies of human blood.* Clinical chemistry, 2013. **59**(5): p. 833-845.
32. Tuck, M.K., et al., *Standard operating procedures for serum and plasma collection: early detection research network consensus statement standard operating procedure integration working group.* Journal of proteome research, 2008. **8**(1): p. 113-117.
33. Jobard, E., et al., *A systematic evaluation of blood serum and plasma pre-analytics for metabolomics cohort studies.* International journal of molecular sciences, 2016. **17**(12): p. 2035.
34. Oddoze, C., E. Lombard, and H. Portugal, *Stability study of 81 analytes in human whole blood, in serum and in plasma.* Clinical biochemistry, 2012. **45**(6): p. 464-469.
35. Ayache, S., et al., *Effects of storage time and exogenous protease inhibitors on plasma protein levels.* American journal of clinical pathology, 2006. **126**(2): p. 174-184.
36. Zhang, D., et al., *Raman detection of proteomic analytes.* Analytical chemistry, 2003. **75**(21): p. 5703-5709.
37. Chen, R., et al., *Blood drop patterns: Formation and applications.* Advances in Colloid and Interface Science, 2016. **231**: p. 1-14.
38. Deegan, R.D., et al., *Capillary flow as the cause of ring stains from dried liquid drops.* Nature, 1997. **389**(6653): p. 827.
39. Deegan, R.D., *Pattern formation in drying drops.* Physical review E, 2000. **61**(1): p. 475.
40. Deegan, R.D., et al., *Contact line deposits in an evaporating drop.* Physical review E, 2000. **62**(1): p. 756.
41. Hu, H. and R.G. Larson, *Analysis of the effects of Marangoni stresses on the microflow in an evaporating sessile droplet.* Langmuir, 2005. **21**(9): p. 3972-3980.
42. Hu, H. and R.G. Larson, *Marangoni effect reverses coffee-ring depositions.* The Journal of Physical Chemistry B, 2006. **110**(14): p. 7090-7094.
43. Beaglehole, R., et al., *Measuring progress on NCDs: one goal and five targets.* The Lancet, 2012. **380**(9850): p. 1283-1285.
44. Organization, W.H., *A comprehensive global monitoring framework including indicators and a set of voluntary global targets for the prevention and control of noncommunicable diseases.* Geneva: World Health Organization, 2012.
45. Fuster, V., R. Walsh, and R. Harrington, *Hurst's the Heart: Two Volume Set*. 2011: New York, USA: McGraw Hill Professional.
46. Nabel, E.G. and E. Braunwald, *A tale of coronary artery disease and myocardial infarction.* New England Journal of Medicine, 2012. **366**(1): p. 54-63.
47. Nabel, E.G., *Cardiovascular disease.* New England Journal of Medicine, 2003. **349**(1): p. 60-72.
48. Mudd, J.O. and D.A. Kass, *Tackling heart failure in the twenty-first century.* Nature, 2008. **451**(7181): p. 919.
49. Segers, V.F. and R.T. Lee, *Stem-cell therapy for cardiac disease.* Nature, 2008. **451**(7181): p. 937.

50. Mendis, S., et al., *Global atlas on cardiovascular disease prevention and control*. 2011: Geneva: World Health Organization.
51. Cooper, R., et al., *Trends and disparities in coronary heart disease, stroke, and other cardiovascular diseases in the United States: findings of the national conference on cardiovascular disease prevention.* Circulation, 2000. **102**(25): p. 3137-3147.
52. Ford, E.S., et al., *Explaining the decrease in US deaths from coronary disease, 1980–2000.* New England Journal of Medicine, 2007. **356**(23): p. 2388-2398.
53. Richardson, P., *Report of the 1995 World Health Organization/International Society and Federation of Cardiology Task Force on the definition and classification of cardiomyopathies.* Circulation, 1996. **93**: p. 841-842.
54. Cooper Jr, L.T., *Myocarditis.* New England Journal of Medicine, 2009. **360**(15): p. 1526-1538.
55. Tubaro, M., et al., *The ESC Textbook of Intensive and Acute Cardiovascular Care*. 2015.
56. Mason, J.W., et al., *A clinical trial of immunosuppressive therapy for myocarditis.* New England Journal of Medicine, 1995. **333**(5): p. 269-275.
57. Caforio, A.L., et al., *A prospective study of biopsy-proven myocarditis: prognostic relevance of clinical and aetiopathogenetic features at diagnosis.* European heart journal, 2007. **28**(11): p. 1326-1333.
58. Magnani, J.W., et al., *Survival in biopsy-proven myocarditis: a long-term retrospective analysis of the histopathologic, clinical, and hemodynamic predictors.* American heart journal, 2006. **151**(2): p. 463-470.
59. Schwartz, J., D. Sartini, and S. Huber, *Myocarditis susceptibility in female mice depends upon ovarian cycle phase at infection.* Virology, 2004. **330**(1): p. 16-23.
60. Jefferies, J.L. and J.A. Towbin, *Dilated cardiomyopathy.* The Lancet, 2010. **375**(9716): p. 752-762.
61. Weintraub, R.G., C. Semsarian, and P. Macdonald, *Dilated cardiomyopathy.* The Lancet, 2017. **390**(10092): p. 400-414.
62. Maron, B.J., et al., *Contemporary definitions and classification of the cardiomyopathies: an American Heart Association scientific statement from the council on clinical cardiology, heart failure and transplantation committee; quality of care and outcomes research and functional genomics and translational biology interdisciplinary working groups; and council on epidemiology and prevention.* Circulation, 2006. **113**(14): p. 1807-1816.
63. Elliott, P., et al., *Classification of the cardiomyopathies: a position statement from the European Society Of Cardiology Working Group on Myocardial and Pericardial Diseases.* European heart journal, 2007. **29**(2): p. 270-276.
64. Taylor, D.O., et al., *Registry of the International Society for Heart and Lung Transplantation: twenty-sixth official adult heart transplant report—2009.* The Journal of Heart and Lung Transplantation, 2009. **28**(10): p. 1007-1022.
65. Noutsias, M., et al., *Expression of cell adhesion molecules in dilated cardiomyopathy: evidence for endothelial activation in inflammatory cardiomyopathy.* Circulation, 1999. **99**(16): p. 2124-2131.
66. Felix, S.B., et al., *Removal of cardiodepressant antibodies in dilated cardiomyopathy by immunoadsorption.* Journal of the American College of Cardiology, 2002. **39**(4): p. 646-652.
67. Staudt, A., et al., *Potential role of humoral immunity in cardiac dysfunction of patients suffering from dilated cardiomyopathy.* Journal of the American College of Cardiology, 2004. **44**(4): p. 829-836.
68. Felix, S.B. and A. Staudt, *Non-specific immunoadsorption in patients with dilated cardiomyopathy: mechanisms and clinical effects.* International journal of cardiology, 2006. **112**(1): p. 30-33.
69. Sharkey, S.W., J.R. Lesser, and B.J. Maron, *Takotsubo (stress) cardiomyopathy.* Circulation, 2011. **124**(18): p. e460-e462.

70. Ono, R. and L.M. Falcao, *Takotsubo cardiomyopathy systematic review: pathophysiologic process, clinical presentation and diagnostic approach to Takotsubo cardiomyopathy.* International journal of cardiology, 2016. **209**: p. 196-205.
71. Templin, C., et al., *Clinical features and outcomes of Takotsubo (stress) cardiomyopathy.* New England Journal of Medicine, 2015. **373**(10): p. 929-938.
72. Nef, H.M., et al., *Mechanisms of stress (Takotsubo) cardiomyopathy.* Nature Reviews Cardiology, 2010. **7**(4): p. 187.
73. Pelliccia, F., et al., *Pathophysiology of Takotsubo syndrome.* Circulation, 2017. **135**(24): p. 2426-2441.
74. Braunwald, E., *Heart Failure.* JACC: Heart Failure, 2013. **1**(1): p. 1-20.
75. Metra, M. and J.R. Teerlink, *Heart failure.* The Lancet, 2017. **390**(10106): p. 1981-1995.
76. Braunwald, E., *Biomarkers in heart failure.* New England Journal of Medicine, 2008. **358**(20): p. 2148-2159.
77. van Kimmenade, R.R. and J.L. Januzzi, *Emerging biomarkers in heart failure.* Clinical chemistry, 2012. **58**(1): p. 127-138.
78. Kumar, V., et al., *Robbins and Cotran pathologic basis of disease, professional edition e-book*. 2014: Elsevier health sciences.
79. Burke, A.P. and F. Tavora, *Practical cardiovascular pathology*. 2010: Lippincott Williams & Wilkins.
80. Staudt, A., et al., *Effects of immunoadsorption on the nt‐BNP and nt‐ANP plasma levels of patients suffering from dilated cardiomyopathy.* Therapeutic Apheresis and Dialysis, 2006. **10**(1): p. 42-48.
81. Staudt, A., et al., *Role of immunoglobulin G3 subclass in dilated cardiomyopathy: results from protein A immunoadsorption.* American heart journal, 2005. **150**(4): p. 729-736.
82. Felix, S.B., et al., *Hemodynamic effects of immunoadsorption and subsequent immunoglobulin substitution in dilated cardiomyopathy: three-month results from a randomized study.* Journal of the American College of Cardiology, 2000. **35**(6): p. 1590-1598.
83. Müller, J., et al., *Immunoglobulin adsorption in patients with idiopathic dilated cardiomyopathy.* Circulation, 2000. **101**(4): p. 385-391.
84. Baker, M.J., et al., *Developing and understanding biofluid vibrational spectroscopy: a critical review.* Chemical Society Reviews, 2016. **45**(7): p. 1803-1818.
85. Baker, M.J., et al., *Clinical applications of infrared and Raman spectroscopy: state of play and future challenges.* Analyst, 2018. **143**(8): p. 1735-1757.
86. Lovergne, L., et al., *Biofluid infrared spectro-diagnostics: pre-analytical considerations for clinical applications.* Faraday discussions, 2016. **187**: p. 521-537.
87. Mitchell, A.L., et al., *Vibrational spectroscopy of biofluids for disease screening or diagnosis: translation from the laboratory to a clinical setting.* Journal of biophotonics, 2014. **7**(3‐4): p. 153-165.
88. Bocklitz, T., et al., *How to pre-process Raman spectra for reliable and stable models?* Analytica chimica acta, 2011. **704**(1-2): p. 47-56.
89. Beebe, K.R., R.J. Pell, and M.B. Seasholtz, *Chemometrics: a practical guide*. 1998: Wiley.
90. Poon, K.W., et al., *Quantitative reagent-free detection of fibrinogen levels in human blood plasma using Raman spectroscopy.* Analyst, 2012. **137**(8): p. 1807-1814.
91. Neugebauer, U., et al., *Fast differentiation of SIRS and sepsis from blood plasma of ICU patients using Raman spectroscopy.* Journal of biophotonics, 2014. **7**(3‐4): p. 232-240.
92. Wesełucha-Birczyńska, A., et al., *Raman micro-spectroscopy tracing human lymphocyte activation.* Analyst, 2013. **138**(23): p. 7157-7163.
93. Hands, J.R., et al., *Attenuated total reflection Fourier transform infrared (ATR‐FTIR) spectral discrimination of brain tumour severity from serum samples.* Journal of biophotonics, 2014. **7**(3‐4): p. 189-199.

94. Bonnier, F., M.J. Baker, and H.J. Byrne, *Vibrational spectroscopic analysis of body fluids: avoiding molecular contamination using centrifugal filtration.* Analytical Methods, 2014. **6**(14): p. 5155-5160.
95. Petrich, W., et al., *Potential of mid-infrared spectroscopy to aid the triage of patients with acute chest pain.* Analyst, 2009. **134**(6): p. 1092-1098.
96. Owens, G.L., et al., *Vibrational biospectroscopy coupled with multivariate analysis extracts potentially diagnostic features in blood plasma/serum of ovarian cancer patients.* Journal of biophotonics, 2014. **7**(3‐4): p. 200-209.
97. Libby, P. and P. Theroux, *Pathophysiology of coronary artery disease.* Circulation, 2005. **111**(25): p. 3481-3488.
98. Hansson, G.K., *Inflammation, atherosclerosis, and coronary artery disease.* New England Journal of Medicine, 2005. **352**(16): p. 1685-1695.
99. Alexander, J.H. and P.K. Smith, *Coronary-artery bypass grafting.* New England Journal of Medicine, 2016. **374**(20): p. 1954-1964.
100. Biglioli, P., et al., *Biological effects of off-pump vs. on-pump coronary artery surgery: focus on inflammation, hemostasis and oxidative stress.* European Journal of Cardio-Thoracic Surgery, 2003. **24**(2): p. 260-269.
101. Shroyer, A.L., et al., *On-pump versus off-pump coronary-artery bypass surgery.* New England Journal of Medicine, 2009. **361**(19): p. 1827-1837.
102. Khan, N.E., et al., *A randomized comparison of off-pump and on-pump multivessel coronary-artery bypass surgery.* New England Journal of Medicine, 2004. **350**(1): p. 21-28.
103. Puskas, J.D., et al., *Off-pump vs conventional coronary artery bypass grafting: early and 1-year graft patency, cost, and quality-of-life outcomes: a randomized trial.* Jama, 2004. **291**(15): p. 1841-1849.
104. Nader, N.D., et al., *Blood product use in cardiac revascularization: comparison of on-and off-pump techniques.* The Annals of thoracic surgery, 1999. **68**(5): p. 1640-1643.
105. Møller, C.H., et al., *Clinical outcomes in randomized trials of off-vs. on-pump coronary artery bypass surgery: systematic review with meta-analyses and trial sequential analyses.* European heart journal, 2008. **29**(21): p. 2601-2616.
106. Association, A.D., *Diagnosis and classification of diabetes mellitus.* Diabetes care, 2010. **33**(Supplement 1): p. S62-S69.
107. Ta, S., *Diagnosis and classification of diabetes mellitus.* Diabetes care, 2014. **37**: p. S81.
108. *2. Classification and Diagnosis of Diabetes: Standards of Medical Care in Diabetes—2019.* Diabetes Care, 2019. **42**(Supplement 1): p. S13-S28.
109. Atlas, D., *International Diabetes Federation. IDF Diabetes Atlas, 7th edn. Brussels, Belgium: International Diabetes Federation, 2015*.
110. Sacks, D.B., et al., *Guidelines and recommendations for laboratory analysis in the diagnosis and management of diabetes mellitus.* Clinical chemistry, 2011. **57**(6): p. e1-e47.
111. Pandey, R., et al., *Emerging trends in optical sensing of glycemic markers for diabetes monitoring.* TrAC Trends in Analytical Chemistry, 2015. **64**: p. 100-108.
112. Lapolla, A., P. Traldi, and D. Fedele, *Importance of measuring products of non-enzymatic glycation of proteins.* Clinical biochemistry, 2005. **38**(2): p. 103-115.
113. Syed, I., *Glycated haemoglobin; past, present, and future are we ready for the change.* diabetes, 2011. **11**: p. 12.
114. Brownlee, M., A. Cerami, and H. Vlassara, *Advanced glycosylation end products in tissue and the biochemical basis of diabetic complications.* New England Journal of Medicine, 1988. **318**(20): p. 1315-1321.
115. Bunn, H.F., K.H. Gabbay, and P.M. Gallop, *The glycosylation of hemoglobin: relevance to diabetes mellitus.* Science, 1978. **200**(4337): p. 21-27.
116. *6. Glycemic Targets: Standards of Medical Care in Diabetes—2019.* Diabetes Care, 2019. **42**(Supplement 1): p. S61-S70.

117. Syamala Kiran, M., et al., *Selective detection of HbA1c using surface enhanced resonance Raman spectroscopy.* Analytical chemistry, 2010. **82**(4): p. 1342-1348.
118. Barman, I., et al., *Raman spectroscopy-based sensitive and specific detection of glycated hemoglobin.* Analytical chemistry, 2012. **84**(5): p. 2474-2482.
119. Pandey, R., et al., *Label‐free spectrochemical probe for determination of hemoglobin glycation in clinical blood samples.* Journal of biophotonics, 2018. **11**(10): p. e201700397.
120. Johann Schaller, S.G., Urs Kämpfer, Sofia Lejon, Christian Trachsel, *blood plasma proteins*, in *Human blood plasma proteins: structure and function*. 2008, John Wiley & Sons, Ltd p. 17-20.
121. Tu, A.T., *Raman Spectroscopy in Biology: Principles and Applications*. 1982: Wiley.
122. Svanberg, S., *Atomic and Molecular Spectroscopy: Basic Aspects and Practical Applications*. 4 ed. 2004: Springer-Verlag Berlin Heidelberg. 580.
123. Schrader, B., *Infrared and Raman Spectroscopy: Methods and Applications*. 1995: Wiley.
124. Mantsch, H.H., *The road to medical vibrational spectroscopy–a history.* Analyst, 2013. **138**(14): p. 3863-3870.
125. Lasch, P. and J. Kneipp, *Biomedical vibrational spectroscopy*. 2008: John Wiley & Sons.
126. Krafft, C. and J. Popp, *The many facets of Raman spectroscopy for biomedical analysis.* Analytical and bioanalytical chemistry, 2015. **407**(3): p. 699-717.
127. Krafft, C., et al., *Disease recognition by infrared and Raman spectroscopy.* Journal of biophotonics, 2009. **2**(1‐2): p. 13-28.
128. Petrich, W., *Mid-infrared and Raman spectroscopy for medical diagnostics.* Applied Spectroscopy Reviews, 2001. **36**(2-3): p. 181-237.
129. Ellis, D.I. and R. Goodacre, *Metabolic fingerprinting in disease diagnosis: biomedical applications of infrared and Raman spectroscopy.* Analyst, 2006. **131**(8): p. 875-885.
130. Kendall, C., et al., *Exploiting the diagnostic potential of biomolecular fingerprinting with vibrational spectroscopy.* Faraday discussions, 2011. **149**(1): p. 279-290.
131. Barker, K., *At the bench.* A Laboratory navigator. Cold spring Laboratory, 1998.
132. Douglas B. Murphy, M.W.D., *Confocal Laser Scanning Microscopy*, in *Fundamentals of Light Microscopy and Electronic Imaging*. 2012, John Wiley & Sons, Inc. p. 265-270.
133. WITec, *Raman Auto and Manual*.
134. Renishaw, *inVia Manual*.
135. Svanberg, S., *The Fourier Transform Spectrometer*, in *Atomic and Molecular Spectroscopy: Basic Aspects and Practical Applications*. 2004, Springer-Verlag Berlin Heidelberg. p. 126-8.
136. scientific, T., *Advantages of a Fourier Transform Infrared Spectrometer*.
137. Technologies, A., *Agilent Cary 600 Series FTIR Site Preparation Guide*.
138. Team, R.C., *R: A language and environment for statistical computing.* 2013.
139. Beebe, K.R., R.J. Pell, and M.B. Seasholtz, *Chemometrics: a practical guide*. Vol. 4. 1998: Wiley-Interscience.
140. Guo, S., T. Bocklitz, and J. Popp, *Optimization of Raman-spectrum baseline correction in biological application.* Analyst, 2016. **141**(8): p. 2396-2404.
141. Butler, H.J., et al., *Using Raman spectroscopy to characterize biological materials.* Nature protocols, 2016. **11**(4): p. 664.
142. Byrne, H.J., et al., *Spectral pre and post processing for infrared and Raman spectroscopy of biological tissues and cells.* Chemical Society Reviews, 2016. **45**(7): p. 1865-1878.
143. Lasch, P., *Spectral pre-processing for biomedical vibrational spectroscopy and microspectroscopic imaging.* Chemometrics and Intelligent Laboratory Systems, 2012. **117**: p. 100-114.
144. Afseth, N.K., V.H. Segtnan, and J.P. Wold, *Raman spectra of biological samples: A study of preprocessing methods.* Applied spectroscopy, 2006. **60**(12): p. 1358-1367.
145. Ryabchykov, O., J. Popp, and T. Bocklitz, *Fusion of MALDI Spectrometric Imaging and Raman Spectroscopic Data for the Analysis of Biological Samples.* Frontiers in Chemistry, 2018. **6**: p. 257.

146. Wold, S., K. Esbensen, and P. Geladi, *Principal component analysis.* Chemometrics and intelligent laboratory systems, 1987. **2**(1-3): p. 37-52.
147. Savitzky, A. and M.J. Golay, *Smoothing and differentiation of data by simplified least squares procedures.* Analytical chemistry, 1964. **36**(8): p. 1627-1639.
148. Trevisan, J., et al., *Extracting biological information with computational analysis of Fourier-transform infrared (FTIR) biospectroscopy datasets: current practices to future perspectives.* Analyst, 2012. **137**(14): p. 3202-3215.
149. Bhargava, R., S.-Q. Wang, and J.L. Koenig, *Route to higher fidelity FT-IR imaging.* Applied Spectroscopy, 2000. **54**(4): p. 486-495.
150. Martens, H. and E. Stark, *Extended multiplicative signal correction and spectral interference subtraction: new preprocessing methods for near infrared spectroscopy.* Journal of pharmaceutical and biomedical analysis, 1991. **9**(8): p. 625-635.
151. Eilers, P.H. and H.F. Boelens, *Baseline correction with asymmetric least squares smoothing.* 2005: p. 24.
152. Baker, M.J., et al., *Using Fourier transform IR spectroscopy to analyze biological materials.* Nature protocols, 2014. **9**(8): p. 1771.
153. Ryan, C., et al., *SNIP, a statistics-sensitive background treatment for the quantitative analysis of PIXE spectra in geoscience applications.* Nuclear Instruments and Methods in Physics Research Section B: Beam Interactions with Materials and Atoms, 1988. **34**(3): p. 396-402.
154. Copas, J.B., *Regression, prediction and shrinkage.* Journal of the Royal Statistical Society: Series B (Methodological), 1983. **45**(3): p. 311-335.
155. Guo, S., et al., *Model transfer for Raman‐spectroscopy‐based bacterial classification.* Journal of Raman Spectroscopy, 2018. **49**(4): p. 627-637.
156. Rinnan, Å., F. Van Den Berg, and S.B. Engelsen, *Review of the most common pre-processing techniques for near-infrared spectra.* TrAC Trends in Analytical Chemistry, 2009. **28**(10): p. 1201-1222.
157. Udelhoven, T., M. Novozhilov, and J. Schmitt, *The NeuroDeveloper®: a tool for modular neural classification of spectroscopic data.* Chemometrics and Intelligent laboratory systems, 2003. **66**(2): p. 219-226.
158. Guyon, I., et al., *Feature extraction: foundations and applications*. Vol. 207. 2008: Springer.
159. Shlens, J., *A tutorial on principal component analysis.* arXiv preprint arXiv:1404.1100, 2014.
160. Bonnier, F. and H. Byrne, *Understanding the molecular information contained in principal component analysis of vibrational spectra of biological systems.* Analyst, 2012. **137**(2): p. 322-332.
161. Beleites, C., et al., *Sample size planning for classification models.* Analytica chimica acta, 2013. **760**: p. 25-33.
162. Guo, S., et al., *Common mistakes in cross-validating classification models.* Analytical Methods, 2017. **9**(30): p. 4410-4417.
163. Filik, J. and N. Stone, *Drop coating deposition Raman spectroscopy of protein mixtures.* Analyst, 2007. **132**(6): p. 544-550.
164. Kopecký Jr, V. and V. Baumruk, *Structure of the ring in drop coating deposited proteins and its implication for Raman spectroscopy of biomolecules.* Vibrational spectroscopy, 2006. **42**(2): p. 184-187.
165. Yakhno, T., *Salt-induced protein phase transitions in drying drops.* Journal of colloid and interface science, 2008. **318**(2): p. 225-230.
166. Chen, G. and G.J. Mohamed, *Complex protein patterns formation via salt-induced self-assembly and droplet evaporation.* The European Physical Journal E, 2010. **33**(1): p. 19-26.
167. Pauchard, L., F. Parisse, and C. Allain, *Influence of salt content on crack patterns formed through colloidal suspension desiccation.* Physical Review E, 1999. **59**(3): p. 3737.
168. Leckband, D. and S. Sivasankar, *Forces controlling protein interactions: theory and experiment.* Colloids and surfaces B: Biointerfaces, 1999. **14**(1-4): p. 83-97.

169. Yakhno, T.A., *Complex pattern formation in sessile droplets of protein-salt solutions with low protein content. What substance fabricates these patterns?* Phys. Chem, 2011. **1**(1): p. 10-13.
170. Zang, D., et al., *Evaporation of a Droplet: From physics to applications.* Physics Reports, 2019.
171. Pully, V., A.T. Lenferink, and C. Otto, *Time‐lapse Raman imaging of single live lymphocytes.* Journal of Raman spectroscopy, 2011. **42**(2): p. 167-173.
172. Ramoji, A., et al., *Toward a spectroscopic hemogram: Raman spectroscopic differentiation of the two most abundant leukocytes from peripheral blood.* Analytical chemistry, 2012. **84**(12): p. 5335-5342.
173. Rao, A.V. and L.G. Rao, *Carotenoids and human health.* Pharmacological research, 2007. **55**(3): p. 207-216.
174. Voutilainen, S., et al., *Carotenoids and cardiovascular health.* The American journal of clinical nutrition, 2006. **83**(6): p. 1265-1271.
175. Di Pietro, N., P. Di Tomo, and A. Pandolfi, *Carotenoids in cardiovascular disease prevention.* JSM Atheroscler, 2016. **1**: p. 1-13.
176. Buijs, J., W. Norde, and J.W.T. Lichtenbelt, *Changes in the secondary structure of adsorbed IgG and F (ab ') 2 studied by FTIR spectroscopy.* Langmuir, 1996. **12**(6): p. 1605-1613.
177. Thumanu, K., et al., *Diagnosis of liver cancer from blood sera using FTIR microspectroscopy: a preliminary study.* Journal of biophotonics, 2014. **7**(3‐4): p. 222-231.
178. Al-Delaimy, W., et al., *Plasma carotenoids as biomarkers of intake of fruits and vegetables: ecological-level correlations in the European Prospective Investigation into Cancer and Nutrition (EPIC).* European journal of clinical nutrition, 2005. **59**(12): p. 1397.
179. Leng, S., et al., *Total and differential white blood cell counts and their associations with circulating interleukin-6 levels in community-dwelling older women.* The Journals of Gerontology Series A: Biological Sciences and Medical Sciences, 2005. **60**(2): p. 195-199.
180. Roth‐Isigkeit, A., et al., *Inter‐individual differences in cytokine release in patients undergoing cardiac surgery with cardiopulmonary bypass.* Clinical & Experimental Immunology, 2001. **125**(1): p. 80-88.
181. Wehlin, L., et al., *Activation of complement and leukocyte receptors during on-and off pump coronary artery bypass surgery.* European journal of cardio-thoracic surgery, 2004. **25**(1): p. 35-42.
182. Busti, A.J. *A General Review of the Mechanisms for Steroid or Glucocorticoid Induced Increases in the White Blood Cell (WBC) Count*. 2015; Available from: https://www.ebmconsult.com/articles/steroids-glucocorticoids-wbc-neutrophiles-increase.
183. Yuan, S.-M. and H.-Z. Lin, *Interleukin-6 in cardiac surgery.* Periodicum biologorum, 2017. **119**(2): p. 93-99.
184. Mu, D.-L., et al., *High serum cortisol level is associated with increased risk of delirium after coronary artery bypass graft surgery: a prospective cohort study.* Critical Care, 2010. **14**(6): p. R238.
185. Roth-Isigkeit, A.K. and P. Schmucker, *Postoperative dissociation of blood levels of cortisol and adrenocorticotropin after coronary artery bypass grafting surgery.* Steroids, 1997. **62**(11): p. 695-699.
186. Aouifi, A., et al., *Effect of cardiopulmonary bypass on serum procalcitonin and C-reactive protein concentrations.* British journal of anaesthesia, 1999. **83**(4): p. 602-607.
187. Sponholz, C., et al., *Diagnostic value and prognostic implications of serum procalcitonin after cardiac surgery: a systematic review of the literature.* Critical Care, 2006. **10**(5): p. R145.
188. Mader, S., *32.4 Blood, a transport medium* in *Biology*. 2010, McGraw-Hill Publishing Company. p. 606-10.
189. Marengo-Rowe, A.J. *Structure-function relations of human hemoglobins*. in *Baylor University Medical Center Proceedings*. 2006. Taylor & Francis.
190. Atkins, C.G., et al., *Raman spectroscopy of blood and blood components.* Applied spectroscopy, 2017. **71**(5): p. 767-793.

191. Wood, B.R., et al., *Resonance Raman spectroscopy of red blood cells using near-infrared laser excitation.* Analytical and bioanalytical chemistry, 2007. **387**(5): p. 1691-1703.
192. Lemler, P., et al., *NIR Raman spectra of whole human blood: effects of laser-induced and in vitro hemoglobin denaturation.* Analytical and bioanalytical chemistry, 2014. **406**(1): p. 193-200.
193. Bunn, H.F., *Hemoglobin I. Structure and Function*, in *Hematology*, W.S. Beck, Editor. 1991, The MIT Press. p. 173-86.
194. Adamczyk, M., et al., *Chemiluminescent acridinium-9-carboxamide boronic acid probes: Application to a homogeneous glycated hemoglobin assay.* Bioorganic & medicinal chemistry letters, 2006. **16**(5): p. 1324-1328.
195. Park, J.-Y., et al., *Selective electrochemical sensing of glycated hemoglobin (HbA1c) on thiophene-3-boronic acid self-assembled monolayer covered gold electrodes.* Analytical chemistry, 2008. **80**(21): p. 8035-8044.
196. Gallagher, E.J., D. Le Roith, and Z. Bloomgarden, *Review of hemoglobin A1c in the management of diabetes.* Journal of diabetes, 2009. **1**(1): p. 9-17.
197. Freitas, P.A.C., L.R. Ehlert, and J.L. Camargo, *Glycated albumin: a potential biomarker in diabetes.* Archives of endocrinology and metabolism, 2017. **61**(3): p. 296-304.
198. Anguizola, J., et al., *Glycation of human serum albumin.* Clinica Chimica Acta, 2013. **425**: p. 64-76.
199. Snieder, H., et al., *HbA1c levels are genetically determined even in type 1 diabetes: evidence from healthy and diabetic twins.* Diabetes, 2001. **50**(12): p. 2858-2863.
200. Jeffcoate, S., *Diabetes control and complications: the role of glycated haemoglobin, 25 years on.* Diabetic Medicine, 2004. **21**(7): p. 657-665.
201. Goldstein, D.E., et al., *Tests of glycemia in diabetes.* Diabetes care, 2004. **27**(7): p. 1761-1773.
202. Coban, E., M. Ozdogan, and A. Timuragaoglu, *Effect of iron deficiency anemia on the levels of hemoglobin A1c in nondiabetic patients.* Acta haematologica, 2004. **112**(3): p. 126-128.
203. Tarim, Ö., et al., *Effects of iron deficiency anemia on hemoglobin A1c in type 1 diabetes mellitus.* Pediatrics international, 1999. **41**(4): p. 357-362.
204. Gram‐Hansen, P., et al., *Glycosylated haemoglobin (HbA1c) in iron‐and vitamin B12 deficiency.* Journal of internal medicine, 1990. **227**(2): p. 133-136.
205. Ng, J., et al., *Erythropoetin treatment significantly alters measured glycated haemoglobin (HbA1c).* Diabetic Medicine, 2008. **25**(2): p. 239-240.
206. Hashimoto, K., et al., *A1C but not serum glycated albumin is elevated in late pregnancy owing to iron deficiency.* Diabetes care, 2008. **31**(10): p. 1945-1948.
207. Proto, G., S.M. De, and E. Cecchin, *Glycosylated hemoglobin in chronic alcoholics.* Drug and alcohol dependence, 1983. **12**(3): p. 299-302.
208. Willekens, F.L., et al., *Hemoglobin loss from erythrocytes in vivo results from spleen-facilitated vesiculation.* Blood, 2003. **101**(2): p. 747-751.
209. Robertson, M., *Artificially low HbA1c associated with treatment with ribavirin.* Bmj, 2008. **336**(7642): p. 505-505.
210. Bernstein, R., et al., *Glycosylated haemoglobin in rheumatoid arthritis.* Annals of the rheumatic diseases, 1982. **41**(6): p. 604-606.
211. Diop, M.-E., et al., *Inappropriately low glycated hemoglobin values and hemolysis in HIV-infected patients.* AIDS Research & Human Retroviruses, 2006. **22**(12): p. 1242-1247.
212. Albright, E.S., F. Ovalle, and D.S. Bell, *Artifactually low hemoglobin A1c caused by use of dapsone.* Endocrine Practice, 2002. **8**(5): p. 370-372.
213. Rondeau, P. and E. Bourdon, *The glycation of albumin: structural and functional impacts.* Biochimie, 2011. **93**(4): p. 645-658.

Curriculum Vitae

Personal information

Name	**Jing Huang, M.S. of Optics**
Adress	**Hans-Berger-Str. 22**
Date and place of birth	**04. 03. 1990 in Guangdong, China**
Marial Status	**single**

Education

Sep. 2015 –	**Doctoral Candidate in Physical Chemistry, in Biophotonics** Doctoral project under supervision of Prof. Dr. Jürgen Popp and Prof. Dr. Ute Neugebauer **Topic:** "Vibrational Spectroscopy as a Powerful Tool for Stratifying Patients Using Minimal Amounts of Blood" Friedrich-Schiller University Jena, Jena, Germany
Sep. 2012 – Jun. 2015	**M.S. in Optics** Master project under supervision of Prof. Dr. Katarina Svanberg and Prof. Dr. Sune Svanberg **Topic:** "Non-invasive Optical Diagnostics for Biomedical Applications" South China Normal University, Guangzhou, China
Sep. 2008 – Jun. 2012	**B.S. in Optical Information Science and Technology** Guangdong University of Technology, Guangzhou, China

Publications and Conference Contributions

Journal publications

1. **Jing Huang,** Anuradha Ramoji, Shuxia Guo, Thomas Bocklitz, Valérie Boivin-Jahns, Jan Möller, Michael Kiehntop, Michel Noutsias, Jürgen Popp and Ute Neugebauer. "Vibrational spectroscopy as a powerful tool for follow-up immunoadsorption therapy treatment of dilated cardiomyopathy – a case report", Analyst, DOI: 10.1039/c9an01696a (2019).
2. **Jing Huang,** Anuradha Ramoji, Michael Kiehntopf, Michel Noutsias, Shuxia Guo, Thomas Bocklitz, Jürgen Popp, Ute Neugebauer. "Raman Spectroscopic Investigation of Plasma by Drop Coating Deposition for Clinical Application", Proc. SPIE 11073, Clinical and Preclinical Optical Diagnostics II, 1107306 (2019).

3. **Jing Huang,** Hao Zhang H., Huiying Lin, Tianqi Li, Liang Mei, Katarina Svanberg, Sune Svanberg. "Gas Exchange in Fruits Related to Skin Condition and Fruit Ripening", Journal of Biomedical Optics **21**(12), 127007 (2016).

4. Sune savnberg, Guangyu Zhao, Hao Zhang H., **Jing Huang,** Ming Lian, Tianqi Li, Shiming Zhu, Yiyun Li, Zheng Duan, Huiying Lin, Katarina Svanberg. "Laser Spectroscopy Applied to Environmental, Ecological, Food Safety, and Biomedical Research", Opt. Express **24**, A515-A527 (2016).

5. **Jing Huang**, Hao Zhang, Tianqi Li, Huiying Lin, Sune Svanberg, Katarina Svanberg. "Assessment of Human Sinus Cavity Air Volume using Tunable Diode Laser Spectroscopy, with application to Sinusitis Diagnostics", Journal of Biophotonics **8**, No. 11-12, 985-992 (2015).

6. Hao Zhang, **Jing Huang**, Tianqi Li, Sune Svanberg, Katarina Svanberg. "Optical Detection of Middle Ear Infection using Spectroscopic Techniques - Phantom Experiments", Journal of Biomedical Optics **20**(5), 057001 (2015).

7. Hao Zhang, **Jing Huang**, Tianqi Li, Xiuxiang Wu, Sune Svanberg, Katarina Svanberg. "Studies of Tropical Fruit Ripening using Three Different Spectroscopic Techniques", Journal of Biomedical Optics **19**(6), 067001 (2014).

Publication in preparation

1. **Jing Huang,** Anuradha Ramoji, Shuxia Guo, Thomas Bocklitz, Michel Noutsias, Jürgen Popp and Ute Neugebauer. "Vibrational spectroscopy as a powerful tool to diagnose cardiomyopathy patients".

2. Anuradha Ramoji, **Jing Huang,** Oleg Ryabchykov, Thomas Bocklitz, Michael Kiehntopf, Michael Bauer, Juergen Popp, Ute Neugebauer. "Influence of Cardiac bypass graft surgery on spectroscopic signature of leukocytes and plasma".

3. **Jing Huang,** Michael Bauer, Michel Noutsias, Shuxia Guo, Thomas Bocklitz, Jürgen Popp, Anuradha Ramoji, Ute Neugebauer. "Vibrational Spectroscopic Investigation of Blood Plasma and Serum by Drop Coating Deposition for Clinical Application".

4. **Jing Huang,** Xiaoxun Chen, Nicolle Müller, Ute Neugebauer, Jürgen Popp, Anuradha Ramoji. "Characterization and diagnostics of HbA1c in diabetes mellitus via Raman spectroscopy".

Conference contributions

1. **Invited talk. Jing Huang,** Anuradha Ramoji, Ute Neugebauer, Jürgen Popp. " Raman spectroscopy as a powerful tool for blood-based diagnostics ", Inside Raman 2019, Pliezhausen, Germany.

2. ***Presentation.*** **Jing Huang,** Anuradha Ramoji, Michael Kiehntopf, Michel Noutsias, Shuxia Guo, Thomas Bocklitz, Jürgen Popp, Ute Neugebauer. "Raman Spectroscopic Investigation of Plasma by Drop Coating Deposition for Clinical Application", European Conferences on Biomedical Optics 2019, Munich, Germany.

3. ***Presentation.*** **Jing Huang,** Anuradha Ramoji, Michel Noutsias, Jürgen Popp, Ute Neugebauer. "Immunoadsorption Therapy Follow-up for Dilated Cardiomyopathy Using Vibrational Spectroscopies", XXVI International Conference on Raman Spectroscopy 2018, Jeju, Korea.

4. ***Poster.*** **Jing Huang,** Anuradha Ramoji, Michel Noutsias, Jürgen Popp, Ute Neugebauer. "Vibrational Spectroscopic Follow-up for Immunoadsorption Therapy in Dilated Cardiomyopathy", Tag der Nachwuchswissenschaftler des FZL 2018, Jena, Germany.

5. ***Poster.*** **Jing Huang,** Anuradha Ramoji, Shuxia Guo, Thomas Bocklitz, Michael Schmitt, Michel Noutsias, Jürgen Popp and Ute Neugebauer. "Changes of plasma and serum readouts by Raman spectroscopy and Fourier transform infrared spectroscopy in a dilated cardiomyopathy patient under immunoadsorption treatment", Fraunhofer Life Science Symposium 2017, Leipzig, Germany.

6. ***Poster.*** **Jing Huang,** Anuradha Ramoji, Shuxia Guo, Thomas Bocklitz, Michael Schmitt, Michel Noutsias, Jürgen Popp and Ute Neugebauer. "Raman Spectroscopic Analysis of Blood Serum and Plasma", Leibniz-Doktorandenforum, Berlin, Germany.

7. ***Presentation.*** **Jing Huang,** Hao Zhang, Tianqi Li, Guangyu Zhao, Sune Svanberg, and Katarina Svanberg. "Studies of Oxygen and Oxygen Exchange in Fruits using Gas in Scattering Media Absorption Spectroscopy", Progress in Electromagnetics Research Symposium 2014, Guangzhou, China.

8. ***Presentation.*** Hao Zhang, **Jing Huang,** Tianqi Li, Sune Svanberg, Katarina Svanberg. "Optical Diagnostics of Middle Ear Infection using Spectroscopic Techniques - Phantom Experiments", Progress in Electromagnetics Research Symposium 2014, Guangzhou, China.

9. ***Poster,*** Hao Zhang, **Jing Huang,** Guangyu Zhao, Sune Svanberg and Katarina Svanberg. "Studies on Fruit Ageing by Fluorescence Spectroscopy and Diode Laser Absorption Spectroscopy", Asia Communications and Photonics Conference 2013, Beijing, China.

Acknowledgments

My Ph.D study abroad at Jena, Germany shows a more different world and new life to me. During this almost four year Ph.D experience, I have learned a lot, for academics and for life. As a child, I never thought to become a person who will work on scientific research, because that should be for those very talent people. But after my Ph.D, I come to realize that scientists, professors are those people who work very very hard firstly, not those with extremely high talent. My Ph.D training gives me the confidence to continue my academic path. After Ph.D, I come to know more clearly how a real academic life should be.

Too many words I would like to say about my Ph.D life. And too many people I would like to thank for my Ph.D study and life.

First of all, I would like to thank my funding: China Scholarship Council (CSC) for funding my Ph.D study in Germany, other funding from the German Federal Ministry of Education and Research (BMBF), from European Union and from Friedrich-Schiller Jena University is also highly appreciated. Secondly, I would like to thank the people. My previous master supervisors Prof. Katarina Svanberg and Prof. Sune Svanberg, who open the door of science for me and help for my CSC funding opportunity. With the funding, I am so lucky to have Prof. Jürgen Popp, Prof. Ute Neugebauer and Dr. Anuradha Ramoji as my supervisors. They show me how a real scientist should be. Dare to doubt anything, anyone, most importantly, try the best to find out the answers for questioning doubts. One cannot do perfectly at the beginning; but keep improving all the time. Particular thanks to Dr. Anuradha Ramoji, who also helps me a lot for my abroad life. Prof. Michael Schmidt helpd a lot for me to settle down and started my Ph.D study, and also for the study reports to my scholarship. P.D. Dr. Michel Noutsias, Dr. Michael Kiehntopf, Prof. Dr. Michael Bauer and Dr. Nicolle Müller, who provided me the clinical samples for my study. The blood donors, who donated the important blood for my study. Cora Richert, who measured clinical information at clinical chemistry lab. P.D. Thomas Bocklitz, Dr. Shuxia Guo, and Nairveen Ali, thank you for patient guidance and fruitful discussion on data analysis by using R programming language. Especially Shuxia Guo, who provided me the code for my data analysis at the beginning. Xiaoxun Chen, who measured the samples for glycated haemoglobin characterization. Colleges of our group at clinic, who provide a comfortable working environment and willing to help me whenever is needed. Administration people from IPHT, CSCC, and IPC, for your help with those complicated administrate work.

Dr. Xiaoshan Zheng, Dr. Yunxia Ma, You Zi, Fengjiao Ma, Jinlu Ji and other friends at Jena, thanks a lot for the enjoying experiences with you together.

Jinxia Zhu, a close friend who helps to comfort me when I am down and provides me the accommodation every time when I am back in Guangzhou.

My dear family, my parents, my elder sister, her husband, and their two cutie babies, for the warm and harmonic family we build together and for your support for my Ph.D life abroad.

Words will be too plain to express my deepest respect and greatest gratitude to all of you. Wish you and myself all the best for the future.